UNIVERSITY OF OKLAHOMA

GRADUATE COLLEGE

# ANALYSIS AND CONTROL OF STICK-SLIP USING A SCALED EXPERIMENTAL DRILLING RIG

A DISSERTATION

SUBMITTED TO THE GRADUATE FACULTY

in partial fulfillment of the requirements for the

Degree of

DOCTOR OF PHILOSOPHY

By

ADITYA SHARMA
Norman, Oklahoma
2023

ANALYSIS AND CONTROL OF STICK-SLIP USING A SCALED EXPERIMENTAL DRILLING RIG

A DISSERTATION APPROVED FOR THE
MEWBOURNE SCHOOL OF PETROLEUM AND GEOLOGICAL ENGINEERING

BY THE COMMITTEE CONSISTING OF

Dr. Catalin Teodoriu, Chair

Dr. Choon Yik Tang

Dr. Ramadan Ahmed

Dr. Deepak Devegowda

# Dedication

*This dissertation is dedicated to my beloved family,*

*my grandparents,*

*Krishna Devi & Dayakrishan Sharma, Kamlesh Mishra & Mohan Lal Mishra,*

*my parents,*

*Preeti Sharma & Gopal Mohan Sharma*

*and my brother*

*Hemant Sharma*

# Acknowledgements

First and foremost, I would like to extend my deepest gratitude and appreciation to my advisor, Dr. Catalin Teodoriu. His immense knowledge, enthusiasm and dedication towards my research has been instrumental for me in achieving this academic milestone. The unwavering support and confidence he has shown in me has helped me explore my potential. I am forever grateful for his mentorship, guidance, and constructive feedback. I am also grateful to Dr. Catalin and his wife Lavinia, for all their help outside of school and for always making me feel at home.

I would like to thank Dr. Choon Yik Tang for sharing his expert knowledge in Control Systems, for his valued advice and feedback and for always being available for meetings and discussions. Without his help I would not have been able to accomplish my research goals. I am grateful to Dr. Ramadan Ahmed and Dr. Deepak Devegowda for their suggestions, insightful comments and feedback, and for their critical evaluation as this has significantly enriched the quality of my dissertation. I am also thankful to Katie Shapiro for all her help and guidance over the last few years and for making sure that I submit all the academic paperwork on time. I also want to acknowledge Helmerich & Payne for their continuous support in funding our research and for their valuable feedback.

Furthermore, I would like to thank my friends and colleagues for their camaraderie and support. I would especially like to thank my dear friend Jack Borer for always pushing me to have faith and confidence in my work and for always supporting me. I would also like to thank Khizar Abid, Saket Srivastava and Hussain Al Ramis for their help and advice through my PhD journey, and to my lab mates Miguel Romero and Andres Felipe Baena Velasquez for making my time in the lab fun and productive.

I would like to extend my gratitude to my cousin sister Surabhi Sharma, my brother-in-law Dr. Gautam Gupta and my nephew Shivansh Gupta for all their love, care, and support throughout my time in grad school. To Sara, I would like to express my appreciation for her encouragement and support during the crucial final stages of my PhD journey.

Lastly, but most importantly, I would like to express my heartfelt appreciation to my parents and my brother. I am immensely thankful for their unconditional love, encouragement, sacrifices and most importantly for their belief in me. Without their constant support and motivation, I would not have been able to complete this challenging journey.

To everyone mentioned here and to the others who in some way helped in my academic pursuit, please accept my sincere gratitude.

-Aditya Sharma

## Table of Contents

# List of Tables

# List of Figures

# Abstract

Drilling is one of the most challenging and expensive processes involved in oil and gas production. Due to the destructive nature of the drilling process, dysfunctions are common during drilling. These dysfunctions can increase the non-productive time (NPT) greatly, cause loss of revenue and pose a safety concern. Avoiding and controlling these dysfunctions is essential for safe and efficient drilling.

Friction from the wellbore and the rock formation induces vibrations in the drillstring. The drillstring vibrations can be classified into three modes: axial, lateral and torsional. Stick-slip vibrations are a type of torsional vibrations which occur very frequently during drilling. These vibrations are responsible for decreasing the rate of penetration (ROP), causing damage to the drilling equipment and greatly reducing the life of a drill bit. Different control algorithms have been proposed in the last few decades but only one of them (Shell Soft Torque) has seen industry-wide adoption. Now, with the increase in the complexity of well design and increasing depths, the limitations of Soft Torque have been highlighted. Therefore, extensive research is still underway to design a new stick-slip control/mitigation approach.

The main aim of this study was to analyze and control stick-slip vibrations in a drillstring using a downscaled experimental drilling rig setup. To achieve this, an experimental setup was designed and constructed. Thereafter, strategies to control/mitigate stick-slip were devised and tested on the constructed setup.

The results showed that surface parameters alone may not be sufficient to design a robust stick-slip mitigation system. Access to downhole data, even at low frequency, can significantly help in the development of a stick-slip mitigation system.

# Chapter 1: Introduction

## 1.1 Overview

The world we live in has an insatiable demand for energy, which increases with every passing day. Oil and gas has been and still is the most dominant source of energy. Due to decades of hydrocarbon extraction, there is a decline in the conventional oil and gas resources available. Although oil and gas is still being produced from conventional sources, unconventional sources present at deep to ultra-deep depths onshore and offshore are also being tapped into (Zou, et al., 2014) (Han, et al., 2013). Extracting hydrocarbons from the unconventional wells poses many challenges. Drilling techniques like managed pressure drilling (MWD), directional drilling, rotary steerable systems (RSS) etc. have been developed to help address these challenges. One of the biggest challenges faced during drilling is vibrations. Vibrations are unavoidable drilling dynamic phenomena that occur in conditions such as: aggressive drilling bit used in low drill ability rocks, long drilling string used for deep and ultra-deep wells, vortex-induced vibration caused by the slender offshore structures used for drilling in deep and ultra-deep water, instability of borehole during drilling in shale and coal formation and increasing the trajectory of the borehole during directional drilling (Rector & Marion, 1991). One commonly occurring vibration during drilling is stick-slip which is a type of torsional vibration.

In the rotary drilling process, the rotation to the drillstring is provided by a top drive system, or rotary table, at a constant speed. However, the rotary speed at the lower end of the drillstring, the drill bit, fluctuates because of oscillation that occurs due to the low torsional stiffness of the drilling pipes. The magnitude of these oscillations depends on three parameters: (1) the properties of the driving system at the surface, (2) the friction that exists between the wellbore and drillstring, (3) bit/rock interaction (Robnett, et al., 1999). Stick-slip is caused by the torsional vibration in the drillstring that happens when the dynamic friction coefficient becomes much smaller than the static friction coefficient (Brett, 1992). This drillstring vibration is characterized by low-frequency fluctuation, usually in the order of 2-10 sec of the oscillation period (Kriesels, et al., 1999). When stick-slip is fully developed, the bottom hole assembly (BHA) periodically stops rotating which results in the torque build-up followed by a release of the energy. This leads to an alternating rotation of the bit and the BHA which might be faster or slower than the RPM provided at the surface. The situation worsens when the difference between dynamic and static friction increases. In this case, BHA tends to over-rotate and create a reverse torque. As a result, the BHA/bit rotates in the opposite direction. This phenomenon is damaging to the PDC bit in particular (Brett, 1992). Moreover, torsional stick-slip also decreases the rate of penetration, causes twist-off, is harmful to the rotary table/top drive system, wears off the connection, and damages the drilling component due to the propagation of the cracks caused by fatigue which happens when the frequency of torsional vibration goes above 50 Hz (Robnett, et al., 1999). It was reported by (Dufeyte & Henneuse, 1991) that during 3500 hours of drilling in four different fields, stick-slip occurred almost 50% of the drilling time.

(Cunningham, 1968) was the first to describe this phenomenon by analyzing data gathered from downhole equipment. Since then, extensive research has been carried out to study and analyze stick-slip. Different numerical approaches have been used to model the drillstring vibrations. These models are used to analyze the harmful effects of vibrations on a drillstring and also to help design control techniques to control/mitigate stick-slip and other modes of vibration. Although various control systems/algorithms have been proposed, only one such system, Shell Soft Torque, has been successfully adopted in the field. Now, after over four decades since Soft Torque (Jansen & van den Steen, 1995) was introduced, the limitations of the system have surfaced when being used in wells with complex geometries and greater depths. With recent technological advancements new downhole tools, capable of acquiring downhole data at high sampling rates, have been designed. This has helped in painting a clearer picture of the downhole drilling dynamics. Research efforts to design a robust control system for vibration prevention and mitigation are still underway.

### 1.2 Objectives

The principle objective of this study is to analyze and control stick-slip vibrations in a drill-string. The work undertaken to achieve this objective was divided into four phases each with their individual objective as listed below:

- Design and construct an experimental setup to mimic dynamics of a vertical and a directional well (with torsional oscillations, specifically stick-slip, being the main focus).
- Develop software code to monitor and control the setup and integrate the hardware components. Additionally, develop a user interface/human-machine interface for the setup.
- Develop a control algorithm to mitigate stick-slip.
- Conduct experimental testing to validate the control system design.

### 1.3 Problem statement

Drilling vibrations, as mentioned earlier, are an unavoidable drilling phenomenon. Among the different types of vibrations, stick-slip vibrations are very common while drilling. They lead to many drilling dysfunctions which ultimately result in an increase in non-productive time (NPT) and loss of revenue. Control and mitigation of stick-slip can greatly help in increasing the efficiency of the drilling process. Because of this reason vibration control is an active area of research.

Research on drilling vibration has been ongoing for over half a century. During this time, many numerical models have been proposed. Since drilling is a dynamic process with multiple parametric variables, numerical modeling of this system is a very difficult task. Numerical models proposed often have multiple assumptions, simplifications, and limitations. Different control techniques to mitigate stick-slip have been proposed, but out of these only one, Shell Soft Torque, has been widely adopted in the field. Soft Torque has been around since the 1980's and its limitations are apparent in modern well configurations.

### 1.4 Significance

Stick-slip is one of the most commonly occurring drilling dysfunction. A robust control system design which is capable of controlling and mitigating stick-slip will significantly reduce the non-productive time (NPT) and increase revenues.

# Chapter 2: Literature Review

## 2.1 Drilling Vibrations

The process of drilling involves creating a borehole to access the hydrocarbon or geothermal resource present under the surface of the earth. To achieve this, rotational mechanical energy from an electric motor is transmitted through the drillstring to a drill bit which chips/crushes the rock formation and creates the borehole. The drillstring, which is composed of a series of slender tubes called drill pipes and the bottom hole assembly, can be thousands of feet in length, thus making it elastic. Non-linear friction is experienced throughout the length of the drillstring and at the interface between the drill bit and the rock formation. The elastic nature of the drillstring and the disturbance introduced in the system, due to the friction, leads to vibrations. Other factors like bent drill pipes and misaligned drillstring can induce or increase the severity of the vibration (Sotomayor, et al., 1997). Vibrations experienced during drilling result in substantial loss of drilling energy and are a major concern as they have the tendency to damage drilling tools and equipment (Abbassian & Dunayevsky, 1998) (Reckmann, et al., 2010), severely impacts the well bore integrity (Macpherson, et al., 1993), increase Non-Productive Time (NPT), and lower the rate of penetration. It is reported that about 25% of the NPT is caused by the vibrations and shocks every year which reduces the overall drilling efficiency (Dong & Chen, 2016) and increases the drilling cost by 10% (Jardine, et al., 1994).

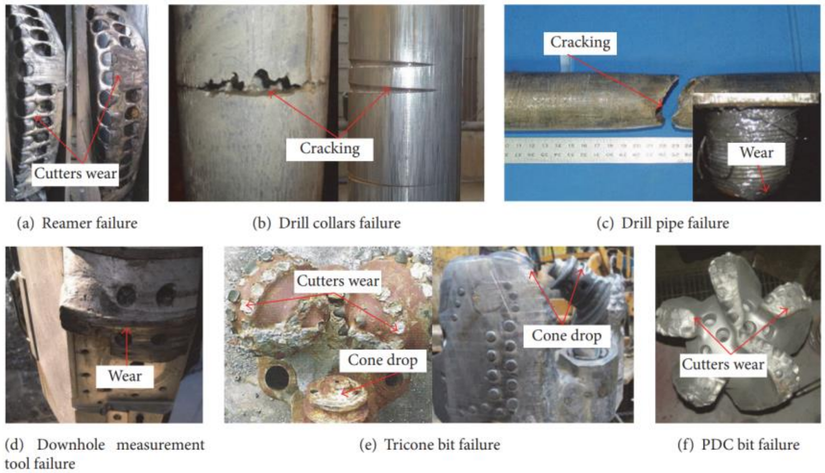


**Figure 1. Drilling tool damage due to drillstring vibrations (Dong & Chen, 2016)**

### 2.1.1 Modes of Drilling Vibrations

Drilling vibrations can be categorized into three modes: axial, lateral and torsional, which have been described in the following sub-sections.

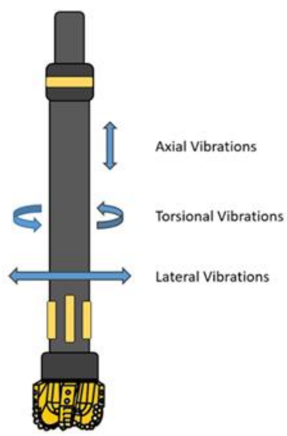


**Figure 2. Modes of drillstring vibration (Srivastava, et al., 2023)**

- *Axial Vibrations*: This mode of vibration causes irregular motion of the drillstring in the longitudinal/rotational axis leading to a phenomenon known as bit bounce. It can result in periodic fluctuations of the weight-on-bit (WOB) and can destroy the drill bit and damage the bottom hole assembly (BHA). This type of vibration is more common in roller-cone bits and in shallow vertical well can be detected at the surface from the changes in the hook load. In deep and directional wells, it is dampened before it reaches the surface, thus requiring a vibration detection system to register it.

- *Lateral Vibrations*: Lateral vibrations are a result of off-centered rotation of the drill-string, i.e., when the center of rotation of the drillstring does not coincide with the center of the well. This is commonly known as whirl and can lead to an eccentric hole and can damage the BHA because of collision with the borehole wall (Mitchell & Allen, 1987). The quality of the borehole can be severely affected and deviation from the well path can occur. Whirl can be forward or backward. In the forward whirl the center of rotation moves in the direction of the rotation of the drillstring whereas the center of rotation moves in the direction opposite to the direction of the drillstring rotation in backward whirl. This vibration may not be detected on the surface and therefore requires downhole instruments to be identified. Bailey et al. reported that out of the approximately 4 million feet drilled each year by an operator, 40% is adversely affected by whirl (Bailey, et al., 2008).

- *Torsional Vibrations*: These vibrations are characterized by irregular rotation of the drill bit. A constant surface RPM does not always translate to a smooth rotational motion at the bit, in fact, the bit RPM undergoes large amplitude fluctuations most of the drilling time. Stick-slip is a type of self-excited torsional vibration in which even though the surface RPM is constant, the bit periodically stops to rotate followed a sudden spike in the bottom hole RPM which can be 10 to 15 times the surface RPM (Dufeyte & Henneuse, 1991) (Sharma, et al., 2020).

Another commonly encountered torsional oscillation is the high frequency torsional oscillation (HFTO) which has a frequency range of up-to 700Hz (Sugiura & Jones, 2019). These oscillations are normally not detectable at the surface as they are localized in the bottom hole assembly (BHA) and decay as they move up the drillstring. In the past the downhole measurement tools lacked the bandwidth to detect HFTO but with recent advances in sensor technology and high-frequency downhole data acquisition the detection and analysis of HFTO has been made possible.

It also must be mentioned here that when drilling in the field, the three modes of vibration rarely exist independently. Usually coupling between the vibration modes is observed, for example: axial-torsional, axial-lateral and axial-lateral-torsional.

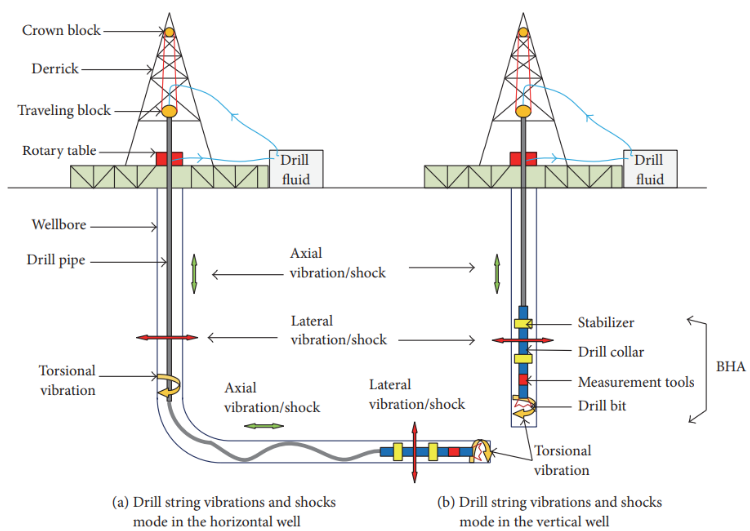


**Figure 3. A standard drilling system and drillstring vibrations (Dong & Chen, 2016)**

### 2.1.2 Mechanisms of failures due to drilling vibrations

The drillstring constantly undergoes bending and twisting stresses, compression and tension while drilling specially in complex lithological formations. The heavy and complex dynamic loading results in excessive vibration and shocks (V&S) which have the tendency to damage drilling tools like drill bits (Abbassian & Dunayevsky, 1998), drill collars, and drill pipes. Monitoring and logging tools used during drilling are also susceptible to damage due to vibrations (Reckmann, et al., 2010). Moreover, V&S severely impacts the well bore integrity (Macpherson, et al., 1993), increase Non-Productive Time (NPT), and due to energy dissipation, lower the rate of penetration. This section discusses the mechanisms of failure due to drilling vibrations.

Plácido, et al. (2002), analyzed drilling abnormalities in three wells to demonstrate the effect of vibrations on drillstring failure. Table 1, 2 and 3 list the abnormalities and the corresponding possible causes for the three wells. Most of the abnormal occurrences were caused due to washouts and other drillstring failures related to vibration induced fatigue or wellbore instability. The authors found a correlation between wellbore enlargement and drillstring vibration and concluded that typical vibration related problems like drill pipe washouts were observed in wells with enlarged wellbores.

**Table 1. Well 1 abnormal occurrences (Plácido, et al., 2002)**

| Depth (m) | Abnormality | Possible Cause |
|---|---|---|
| 503 | Lost Circulation | Excessive ECD |
| 790 | Drill collar failure | Fatigue due to vibration |
| | Annulus obstructed | Wellbore instability |
| 830 | Shock-sub failure | Fatigue due to vibration |
| 1205 | Re-drilling | Well closed in |
| | Drag when pulling out | Wellbore instability |
| 1878 | Re-drilling | Cave-in of diabase |

**Table 2. Well 2 abnormal occurrences (Plácido, et al., 2002)**

| Depth (m) | Abnormality | Possible Cause |
|---|---|---|
| 1200 | Fishing drillstring | Fatigue due to vibration |
| 1442 | Stuck pipe | Cave-in of diabase |
| 1451 | Stuck pipe | Cave-in of diabase |
| 1735 | Fall in pressure | Washout |
| 2040 | Unable to advance | Stabilizer working the wellbore |
| 3658 | Fall in pressure | Washout |
| | Stabilizer failure | Fatigue due to vibration |

**Table 3. Well 3 abnormal occurrences (Plácido, et al., 2002)**

| Depth (m) | Abnormality | Possible Cause |
|---|---|---|
| 768 | Logging tool did not reach the bottom | Edges due to differential hole enlargement |
| 2009 | Reduced penetration rate | Loss of three cones |
| 2089 | Fall in pump pressure | Washout |
| 2012 | Bit worn and missed nozzle | Abrasion |
| | Drilling jar failure | Washout |
| | Fall in pressure | Washout in the thread of the sub |
| 2263 | Fall in pressure | Washout in the thread of the sub |
| 2922 | Logging tool did not reach the bottom | Edges due to differential hole enlargement |

Ghasemloonia, et al. (2014), modeled the axial-transverse dynamics of a drillstring that consisted of drill pipes, multi-span BHA, shock sub and a force generator tool near the bit. The effects of driving torque, mud damping, spatially varying axial load along with nonlinearities due to geometry, axial stiffening, strain energy and Hertzian contact forces were also included. Their results showed that damage to the drillstring and drilling tools can be caused as a result of non-linear axial-transverse vibrations and lateral instabilities.

Drillstring vibrations cause premature failure of the drillstring components and the drill bit (Macpherson, et al., 1993). Drillstring failure means a complete separation of the drill pipe or separation of a part of the BHA which can often occur in complex deep wells. Fatigue, which is a fracture arising from cyclic stresses, is a major cause of drillstring failure. Failure due to fatigue is intensified specifically at curved well trajectories or in buckled drillstring sections with high vibrational loads, where high bending stresses occur. The most critical fatigue damage happens when the drillstring is in resonance with one of its natural frequencies (Rivas, et al., 2021). Fatigue fractures originate from highly localized stress concentration points. A high concentration of stress in the thread roots and the upset transition area of the drill pipe is one of the causes of fatigue failure (Knight & Brennan, 1999; Lin, et al., 2013). Moreover, bending, torsion and surface defects can induce high stresses leading to drillstring failure (Moradi & Ranjbar, 2009). The destructive nature of drillstring vibration is even more evident in gas drilling when compared to mud drilling (Jianhong , et al., 2012). Wash outs and twist-offs are another type of failures that can occur due to mechanical fatigue resulting from vibrations or corrosion. A wash out is a hole or a crack in the drill pipe and it can lead to a twist-off which is the breaking of the drillstring due to fatigue or excessive torque. It was reported that 65% of these failures occur around the slips area and 22% occur around the drill collar (Albdiry & Almensoury, 2016).

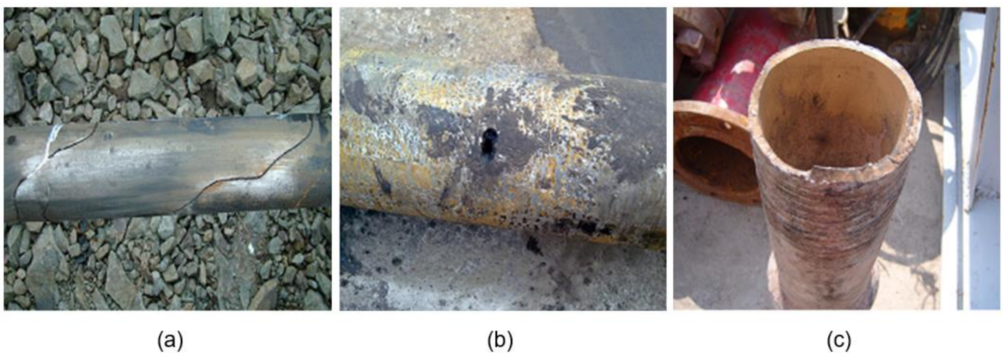


**Figure 4. (a) Fatigue failure, (b) wash out, (c) twist off (Wang, et al., 2011)**

Drilling vibrations have a severe effect on the drill bit. The impact force that acts on the bit as a result of the interaction with the rock can lead to failures like tooth/cutter loss, wear, or fracture. This can make the drilling inefficient and can greatly reduce the life of the drill bit. PDC (polycrystalline diamond compact) bits, which are commonly used bits today are severely affected by stick-slip vibrations (Fear, et al., 1997). Ledgerwood et al. (2010) used downhole vibration measurements and modeling to show that stick-slip, which is a common type of torsional drillstring vibration, is the cause of PDC bit damage. Lateral vibrations can be induced during the slip phase of the stick-slip vibrations leading to bit damage. They highlight stick-slip as the root cause of PDC bit damage and suggest eliminating stick-slip to extend the life of the bit. A comprehensive review of bit wear can be found in (Abbas, 2018). Since vibrations are unavoidable and bit wear is considered an intrinsic cost, it is crucial to minimize bit wear to increase the efficiency and life span of a bit.

### 2.1.3 Vibration severity

Quantifying the severity of vibration is essential for risk management and to make parametric changes while drilling to reduce the adverse effects of drilling vibrations. The vibrations are not always detectable at the surface therefore, downhole measurements are required to detect vibrations and measure their severity. One commonly used vibration severity metric is the stick slip index (SSI) which is used to measure the severity of torsional oscillations. The SSI can be calculated using the following equation:

$$SSI = \frac{bit\ RPM_{max} - \ bit\ RPM_{min}}{2 \cdot RPM_{avg}} \quad \ldots\ldots\ldots\ldots\ldots\ldots (1)$$

where:

$1 \leq$ SSI is pure stick – slip,

0.5 <SSI<1 is torsional oscillation,

$0 \leq$ SSI $\leq 0.5$ is weak torsional oscillations.

Arevalo and Fernandes (2012) proposed a risk quantification technique to calculate a risk index that can be used to evaluate the ongoing risk due to drilling vibrations in real time. They used seismic ground-motion-intensity indices to estimate the risk of a vibration-related drillstring-integrity failure. The following indices were used:

- Vibrations Intensity (Arias Intensity): It represents the square root of the energy per mass, having units of meters per second and can be denoted by the following equation:

$$I_A = \frac{\pi}{2g}\int_0^{\infty} a(t)^2 dt \quad \ldots\ldots\ldots\ldots\ldots\ldots (2)$$

It was used to calculate the intensity related to lateral vibrations by use of the RMS measurement available from the downhole vibration measurement tool.

- Acceleration Root Square: calculates the square-root value of the vibration intensity and is represented by the following equation:

$$a_{rs} = \sqrt{\int_0^{T_d} a(t)^2 dt} \quad \ldots\ldots\ldots\ldots\ldots\ldots (3)$$

where $T_d$ is the total time of the bit run.

- RMS acceleration: It helps to understand what sort of vibration level was recorded on average. It does not reflect the cumulative risk along a bit run since it will also depend on the duration of the run. RMS acceleration is denoted by:

$$a_{rms} = \sqrt{\frac{1}{T_d}\int_0^{T_d} a(t)^2 dt} \quad \ldots\ldots\ldots\ldots\ldots\ldots (4)$$

- Power Index: provides an estimation of the average intensity of vibrations.

$$P_a = \frac{1}{T_d}\int_0^{T_d} a(t)^2 dt \quad \ldots\ldots\ldots\ldots\ldots\ldots (5)$$

Characteristic Intensity: It suggests that the damage created by drillstring vibrations correlates to the acceleration RMS to the power of 1.5 and is also to the duration of the exposure to vibration. The authors found this approach to be the best correlation with drillstring-integrity failures.

$$I_c = a_{rms}^{1.5} - t_d^{0.5} \quad \ldots\ldots\ldots\ldots\ldots\ldots (6)$$

- Peak Acceleration: This index refers to the maximum value of acceleration along the movement interval. The relevance of this index is due to the fact that damage to drillstring can be related to singular events or peak values or that may not correlate with accumulative measures.

The study concluded that the use of seismic ground-motion-intensity indices to evaluate downhole vibration provides a practical and accurate representation of the actual integrity-failure risks. Using the proposed risk-quantification solution approximately 80% of drill-string-integrity failures analyzed were shown to be identified and prevented.

## 2.2 Control Systems

A control system is an arrangement of different components, devices and algorithms that is used to regulate the behavior of a dynamic system and to achieve a desired output. Control systems can be found all around us, they can be as simple as a bread toaster which pops out the bread slice after a set amount of time interval to an auto-pilot system controlling an aircraft. Figure 5 shows a simplified block diagram of a control system. The rectangle in the center represents the control system with a single input and a single output. The output of this system changes as a response to a change in the input.

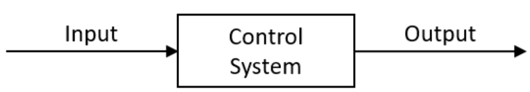


**Figure 5. Simplified block diagram of a control system**

Control System can be classified into different categories: (i) linear and non-linear control systems and, (ii) open-loop and closed-loop control systems.

### 2.2.1 Linear and non-linear control systems

Systems can be categorized as linear or non-linear depending on if they satisfy the principle of superposition or not. The principle of superposition can be defined by the following two properties:

i. Additive Property: $F(x_1 + x_2) = F(x_1) + F(x_2)$ .................*(7)*

*ii.* Homogeneity Property: $F(ax) = aF(x)$ .................*(8)*

- *Linear control systems*: These are systems where the input and the output have a linear relationship, i.e., the relationship between the input and the output is proportional and can be represented mathematically with a linear equation. Such systems follow the principle of superposition and are easier to design and analyze. Some examples of linear control systems are: speed control, temperature control and position control.

- *Non-linear control system:* When the inputs and the outputs of the system cannot be represented using a linear relationship the control system is said to be non-linear control system. These systems do not obey the principle of superposition and are often governed by non-linear differential equations. Unlike linear control systems these systems are much more complex to design and analyze and may require significant computational resources.

It is worth mentioning here that most of the real-word systems are inherently non-linear. Linearization techniques are often used to linearize such non-linear systems and to approximate their behavior making the design and analysis phase easier. Sometimes the non- linearities of the system are neglected to make the analysis simpler but this comes at the cost of decreasing the accuracy of the designed system.

### 2.2.2 Open-loop and Closed-loop Systems

Another basis of classifying control systems is based on the relationship of the control action with the output where the system can be classified as an open-loop system or a closed-loop system.

- *Open-loop Control System:* A system in which the control action is independent of the system output is called an open-loop system. In other words, the input to the system is not influenced by the system output. These control systems operate on a fixed set of predefined instructions. An example of such a system is a bread toaster where the quality of the bread toast is dependent on the time (preset by the user) for which it is heated inside the toaster. Another example is traffic light system which suns on a fixed schedule independent of the traffic conditions. Figure 6 shows an open-loop control system.

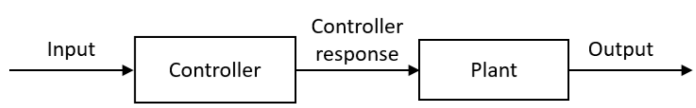


**Figure 6. Open-loop control system**

- *Closed-loop Control System:* In closed-loop control systems the control action is dependent on the output. A feedback signal is incorporated in these control system which is basically used to compare the actual output of the system with the desired output to generate an error signal. The controller input is then adjusted in response to this error signal to produce the desired output. Closed loop control systems are used in situations where the input parameters have to be adjusted in response to system dynamics thus making them adaptive to the changes and disturbance in the environment. This control scheme is more complex and expensive compared to open-loop control but offers more accuracy and adaptability. A simple example of a closed-loop system is a thermostat which measures the present room temperature and adjusts the cooling/heating system to match the desired room temperature. A closed loop system block diagram is shown in figure 7.

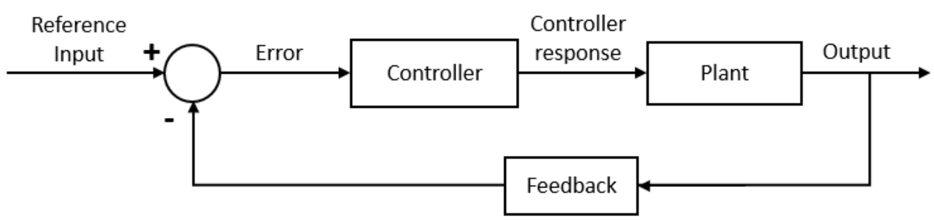


**Figure 7. Closed-loop control system**

### 2.2.3 Modeling of Control Systems

*………I asked Fermi whether he was not impressed by the agreement between our calculated numbers and his measured numbers. He replied, "How many arbitrary parameters did you use for your calculations?" I thought for a moment about our cut-off procedures and said, "Four." He said, "I remember my friend Johnny von Neumann used to say, with four parameters I can fit an elephant, and with five I can make him wiggle his trunk."*

Freeman Dyson on describing the predictions of his model for meson-proton scattering to Enrico Fermi in 1953 (Dyson, 2004).

An arrangement or combination of physical objects that serve an objective is called a physical system. When studying and analyzing such systems it is important to describe the different components/objects of the system and their relationships. In studying control systems, it is essential to model the system dynamics in mathematical equations or physical models. Once a model is developed it can be used to design control strategies and algorithms that can be used to regulate the system as desired. As mentioned before, control systems can be modeled mathematically or physically.

- *Mathematical Modeling:* As the name suggests, this modeling technique involves the use of mathematical equations to represent the system behavior. A mathematical model is not unique to a given system, i.e., a system can be represented in numerous ways and may have a number of mathematical models. This technique is used when the system has a clear input-output mathematical relationship and is well understood. A compromise between the simplicity of the model and the accuracy of the results has to be made when modeling the system mathematically. Certain physical properties inherent to the system are ignored when simplicity of the model is chosen over accuracy. On the other hand, choosing accuracy over simplicity comes at the cost of higher computational requirements. Lumped parameter modeling and distributed parameter modeling are two popular types of mathematical modeling techniques which are discussed later in this report.

- *Physical Modeling:* In this modeling approach a physical model of the system is created. A combination of sensors, actuators and controllers is put together, and up-scaling or down-scaling is performed if needed, to from a physical system that behaves in a way similar to the real system. Physical modeling of the system can come in handy when the system under study is very complex and challenging to model mathematically. Once the physical model is ready different control strategies can be tested on it before they are implemented in the real system.

### 2.2.4 Controllers

Controllers are one of the most important component of a control system. These can be physical devices and/or software algorithms that regulate the system by minimizing the difference between the actual output of the system (process variable) and the desired value (setpoint). The role of a controller is to regulate the behavior of the system in presences of changes in the system parameters and other external disturbances. Controllers reduce the steady state error of the system thus improving stability.

- *Bang-Bang Controller:* Bang-bang controller, also known as 2-step controller or on-off controller, is a type of binary controller that switches abruptly between two states depending on a threshold value. The system input is on or off depending on whether the measured feedback is above or below the set threshold value. An example of this controller is a common household thermostat which turns on the heating if the room temperature is below the set temperature and turns off if the temperature rises above the setpoint.

- *PID controller:* PID stands for proportional-integral-derivative, which are the three coefficients of this controller. It is the most commonly used control algorithm used in the industry which can be attributed to its simplicity and robust performance in a wide range of applications. The three coefficients: proportional (P), integral (I) and derivative (D) are varied to get the optimal response.

- The ‘P’ term uses the error signal (difference between the actual and the desired value) and produces an output proportional to it.
- The ‘I’ term removes the steady-state error that may exist based in past errors.
- Finally, the ‘D’ term reduces the oscillations and overshoots using the rate of change of the error. By tuning these three coefficients, the PID controller an achieve robust and stable control of a wide range of dynamic systems.

- *Sliding mode controller:* Sliding mode control is a control method used to control the behavior of non-linear systems. In this method a discontinuous control signal is applied that forces the system state to slide along a predefined trajectory in the state space. A sliding surface in the state space is defined which represents the desired behavior of the system. The control input brings the system state to the sliding surface and keeps it there. This control technique is robust to modeling uncertainties and external disturbances.

- *Fuzzy Logic Controller:* Fuzzy logic is a multi-valued logic where the truth value is a matter of degree (any real number between 0 and1) rather than a strict true or false. It is used in situations of partial truth, where the true value may range between completely true and completely false. This is in contrast to Boolean logic where only the integer values 1 (true) and 0 (false) are allowed. Fuzzy logic controllers use fuzzy logic to regulate the behavior of a dynamic system. This control method consists of three stages:

    - Fuzzification: the crisp inputs are converted into fuzzy sets which can be processed in accordance with the fuzzy logic rules.

- Rule Evaluation: Expert knowledge or data-driven methods based fuzzy logic rules are used to determine appropriate control action. The rules can take up the form of ‘if-then’ logic statements.
- Defuzzification: Finally, the fuzzy control output is converted back to crisp output that is used to control the system.

Fuzzy logic controllers are useful in situations where a precise mathematical model of the system is not available and in systems with uncertainty and non-linear behavior.

- *State feedback control coupled with an observer:* A state feedback controller can be combined with an observer/estimator to regulate a system. The observer/estimator, designed using a mathematical model, estimates the states of the system based on the inputs and outputs. These estimated states can then be used to help generate the control actions. This approach is useful in scenarios where the actual parameters of the system cannot be measured directly and/or have a limited sensor feedback ability. However, the design of such a controller can be challenging and the mathematical model of the system can be sensitive to uncertainties and modeling errors.

- *Model Predictive Controller (MPC):* In model predictive control (MPC) a mathematical model of the system is used to calculate the optimal control action over a finite time horizon. At each individual step the controller estimates or receives the current state of the system and generates control actions that minimize the cost function, subject to the input and output constraints of the system. This method is useful in complex non-linear systems with constraints. The models used in MPC can be derived from first principles or can be obtained by empirical data obtained by system identification. Compared to traditional control techniques like PID control, the MPC can handle system constraints and can perform optimization over a finite time horizon resulting in noise rejection and better reference tracking.

### 2.3 Drilling Vibrations Modeling

The drilling system, as described in section 3, consists of several sub-systems and is a complex system to model. When modeling the drilling process two types of models are considered. The first one is the drillstring model which accounts for the dynamics of the drillstring and, the second is bit-rock-interaction model which represents the friction forces between the drill bit and the rock formation. Figure 8 shows a block diagram of a basic drilling system model which includes the drillstring model and the friction model. Various modeling techniques have been used to model the dynamics of the drilling system, especially to study the drillstring vibrational dynamics. This section provides a concise summary of the various existing models. A detailed review of the different modeling techniques can be found in (Saldivar, et al., 2014; 2016).

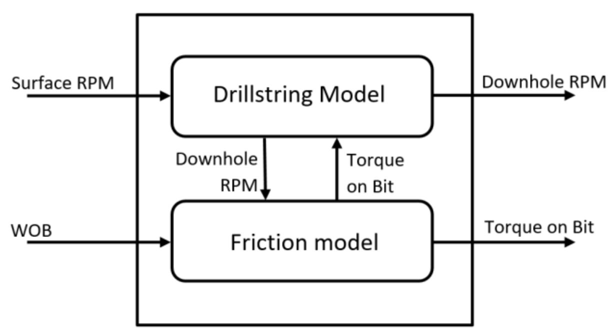


**Figure 8. Drilling system model**

### 2.3.1 Drillstring Model

The two most widely used drillstring models are the lumped parameter model and the distributed parameter model. The lumped parameter modeling techniques involve representing the drillstring as a mass-spring-damper system. In a lumped system the dependent variables of interest are a function of time only, making it possible to describe the system mathematically using ordinary differential equations thus making the analysis simpler. Lumped parameter models with one or multiple degrees-of-freedom (DOF) have been developed (Brett, 1992; Lin & Wang, 1991; Jansen & van den Steen, 1995; Abdulgalil & Siguerdidjane, 2005; Navarro-López & Cortés, 2007). Models with higher DOF have higher accuracy.

Although the lumped parameter models can make the analysis simpler, they do not account for the distributed nature of the system. A distributed parameter model of the drillstring describes the system more accurately especially when an oscillatory system behavior is involved (Aarrestad, et al., 1986; Tucker & Wang, 1999; Challamel, 2000; Sagert, et al., 2013; Bresch-Pietri & Krstic, 2014). The dependent variables of interest are a function of time and one or more spatial variables in a distributed system. A beam subjected to torsional and/or axial forces represents the drillstring and partial differential equations are used to describe the system. This modeling approach is more accurate but has a higher level of analysis and simulation complexity.

Figure 9 shows mass-spring-damper system models of a drillstring with different DOF. A 1-DOF model is shown in Figure 9(a), the BHA is represented by a mass element with a moment of inertia ‘J’, ‘k’ is the spring constant which represents the stiffness of the drillstring, ‘c’ is the damping constant of the drilling fluid, and the RPM at the surface and the bottom are represented by $\omega_s$ and $\omega_b$ respectively. The schematic in figure 9(b) is for a 2-DOF model.

In this case, there are two inertial masses, one at the top, to represent the rotary system and the other at the bottom to represent the BHA. '$J_1$' and '$J_2$' are the moment of inertia of the rotary table or topdrive and BHA respectively, 'k' is the stiffness of the drillstring, and 'c' is the damping constant. Finally, in figure 9(c) a multi-DOF drillstring model is depicted. In this model system multiple inertial masses can be used to represent different sections of the drillstring. For example, in figure 9(c) 'n' number of masses are used to represent multiple sections of the drill pipe, one mass for the rotary table/top drive, one for BHA and one for the bit, making it a 'n+3'-DOF drillstring model. Different values of stiffness 'k' and damping constant 'c' can be assigned. Models with higher DOF have higher accuracy but on the other hand require more computation.

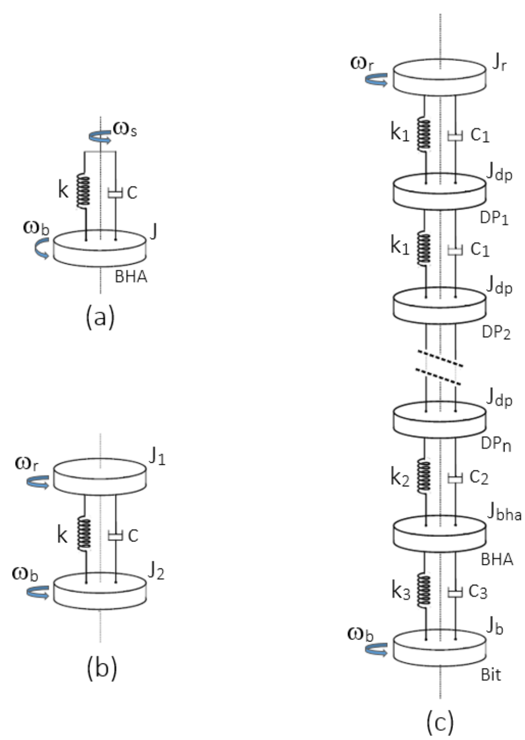


**Figure 9. Drillstring model with: (a) 1DOF, (b) 2DOF and (c) multiple-DOF**

In this section the analytical approaches to model the drillstring vibrations are discussed. Firstly, a lumped parameter modeling approach is presented followed by distributed parameter modeling of the drillstring vibrations.

**Lumped Parameter Approach**

In this section the lumped parameter modeling approach is used to model the drillstring. The drillstring consisting of the drill pipes and the BHA is represented by a torsional pendulum with two degrees-of-freedom as shown in figure 10.

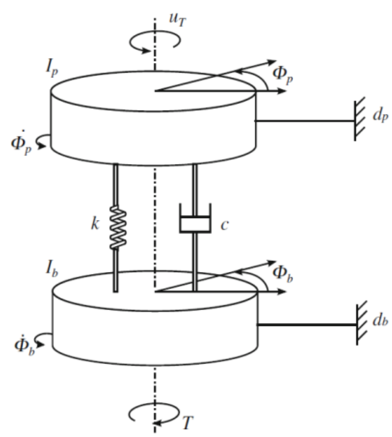


**Figure 10. Lumped parameter mode with 2 DOF (Márquez, et al., 2015)**

$I_p$ and $I_b$ are the inertial masses representing the rotary table and the BHA respectively, $d_p$ and $d_b$ is the damping and the drillstring is represented by stiffness $k$ and torsional damping $c$. The equations of motion for this system are as follows:

$$I_p\ddot{\phi}_p + c(\dot{\phi}_p - \dot{\phi}_b) + \mathrm{k}(\phi_\mathrm{p} - \phi_\mathrm{b}) + d_p\dot{\phi}_p = \mu_T \quad \text{.................}(9)$$
$$I_b\ddot{\phi}_b - c(\dot{\phi}_p - \dot{\phi}_b) - \mathrm{k}(\phi_\mathrm{p} - \phi_\mathrm{b}) + d_b\dot{\phi}_b = -T(\dot{\phi}_b) \quad \text{.................}(10)$$

where,

$\phi_\mathrm{p}$ is the angular displacement of the rotary table,
$\phi_\mathrm{b}$ is the angular displacement of the BHA,
$\mu_T$ is the drive torque from the rotary table,
$\dot{\phi}_b$ is the rotary angular velocity at the bit,
$T$ is the torque at the bit.

**Distributed Parameter Approach**

Bailey and Finnie (1960) were one of the first to model drilling vibrations. They developed a distributed model based on wave theory to model the axial and torsional vibrations. The model is described in this section.

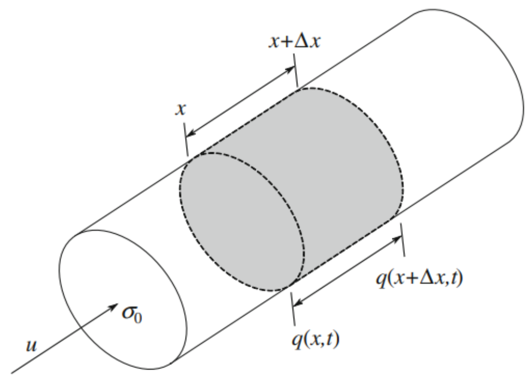


**Figure 11. Flexible metal bar (Márquez, et al., 2015)**

Consider a flexible metal bar of length *L*, cross-section $\sigma_0$ and linear density $\rho_0$ (figure 11). The displacement of a point *x* on the bar w.r.t. its equilibrium position is denoted by *q(x,t)* and, tension *T(x,t)* is applied to the point *x* at time *t*.

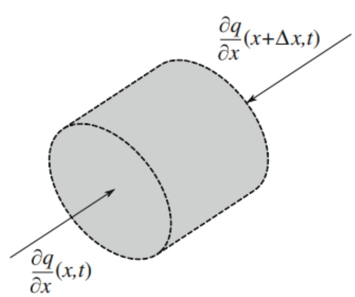


**Figure 12. Short segment of the bar (Márquez, et al., 2015)**

Now assume a tension $T_0$ is applied to a short segment of the bar (figure 12), let the length of this short segment be $l_0$. According to the fundamental law of elasticity:

$$\frac{dT}{\sigma_0} = E_0 \frac{dl}{l_0} \quad \dots\dots\dots\dots\dots\dots (11)$$

where:

*dl* is the elongation $(dl = l - l_0)$,
*dT* is an infinitesimal tension $(dT = T - T_0)$,
$E_0$ is the Young modulus or elasticity factor under the tension $T_0$

The segment $(x,x+\Delta x)$, with static length $l_0$, takes the position $(x+q(x,t)\ ,\ x+\Delta x+q(x+\Delta x,t))$.

When the tension is applied the length of the segment increases from $l_0 = \Delta x$ to $l = l_0 + dl$.

$$l = l_0 + dl$$
$$l = \Delta x + \left(\frac{\partial q}{\partial x}\right)\Delta x$$
$$l = l_0\left(1 + \frac{\partial q}{\partial x}\right)$$
$$\frac{l - l_0}{l_0} = \frac{\partial q}{\partial x}$$
$$\frac{dl}{l_0} = \frac{\partial q}{\partial x} \quad \ldots\ldots\ldots\ldots\ldots\ldots (12)$$

Using Eq. 11 and Eq. 12:

$$dT = T - T_0 = E_0\sigma_0\frac{\partial q}{\partial x} \quad \ldots\ldots\ldots\ldots\ldots\ldots (13)$$

From the fundamental principle of dynamics:

$$\rho_0\frac{\partial^2 q}{\partial t^2}\Delta x = \frac{\partial T}{\partial x}dx \quad \ldots\ldots\ldots\ldots\ldots\ldots (14)$$

Using Eq. 13 and Eq. 14:

$$\rho_0\frac{\partial^2 q}{\partial t^2} = E_0\sigma_0\frac{\partial^2 q}{\partial x^2}$$
$$\frac{\partial^2 q}{\partial t^2} = \left(\frac{E_0\sigma_0}{\rho_0}\right)\frac{\partial^2 q}{\partial x^2}$$
$$\frac{\partial^2 q}{\partial t^2} = c^2\frac{\partial^2 q}{\partial x^2} \quad \ldots\ldots\ldots\ldots\ldots\ldots (15)$$

Eq. 15 is the equation of wave propagation where $c = \sqrt{\left(\frac{E_0\sigma_0}{\rho_0}\right)}$ is the speed of the propagation of the wave.

$$\frac{\partial^2 q}{\partial t^2}(x,t) = c^2\frac{\partial^2 q}{\partial x^2} \quad \ldots\ldots\ldots\ldots\ldots\ldots (16)$$

$$\frac{\partial q}{\partial x}(0,t) = -u(t) \quad \frac{\partial q}{\partial x}(1,t) = 1 \quad \ldots\ldots\ldots\ldots\ldots\ldots (17)$$

$$q(x,0) = q_0(t) \quad \frac{\partial q}{\partial t}(x,0) = q_{t_0}(x) \quad \ldots\ldots\ldots\ldots\ldots\ldots (18)$$

Eq. 16 represents the normalized model and eq. 17 and 18 the boundary conditions and initial conditions respectively.

Longitudinal and torsional vibrations of the drillstring are analogous. The set of equations above describe the longitudinal vibrations but can represent torsional vibrations if the following substitutions are made (Bailey & Finnie, 1960):

- angular displacement in place of longitudinal displacement,
- speed of propagation of torsional wave in place of speed of longitudinal wave,
- polar moment of inertia of the string instead of cross-sectional area of the string,
- torque in the string in place of axial force in the string,
- shear modulus instead of Young's modulus,

Challamel (2000) modeled the propagation of torsional wave along a the drillstring using the following hyperbolic partial differential equation:

$$GJ\frac{\partial^2 \phi}{\partial s^2}(s,t) - I\frac{\partial^2 \phi}{\partial t^2}(s,t) - \gamma\frac{\partial \phi}{\partial t}(s,t) = 0 \quad \ldots\ldots\ldots\ldots\ldots (19)$$

where,

$s \in (0, L)$,
$L$ is the length of the drillstring,
$\Phi$ is the twist angle and depends on the length coordinate '$s$' and time '$t$',
$G$ is the shear modulus,
$J$ is the geometric moment of inertia,
$I$ is the inertia, $I = \rho_a J$, where $\rho_a$ is the area density,
$\gamma$ is the viscous damping

The energy dissipation while drilling takes place at the bit-rock interface, therefore the damping γ can be assumed to be null. This reduces eq. 19 to:

$$GJ\frac{\partial^2\phi}{\partial s^2}(s,t) = I\frac{\partial^2\phi}{\partial t^2}(s,t)$$
$$\frac{\partial^2\phi}{\partial s^2}(s,t) = \tilde{c}^2\frac{\partial^2\phi}{\partial t^2}(s,t) \quad \dots\dots\dots\dots\dots\dots(20)$$

where $\tilde{c}^2 = \sqrt{\frac{I}{GJ}} = \sqrt{\frac{\rho_a}{G}}$

Eq. 20 is the wave equation describing torsional vibrations in the drillstring.

**Stick-slip Control Analytical Solution**

A stick –slip suppression control by torsional rectification method was proposed by (Tucker & Wang, 1999). The wave equation describing torsional vibrations in the drillstring (eq. 20) is used with the assumption that the speed of propagation of torsional wave is one. Therefore, the equation reduces to:

$$\frac{\partial^2\phi}{\partial s^2}(s,t) = \frac{\partial^2\phi}{\partial t^2}(s,t) \quad \dots\dots\dots\dots\dots\dots(21)$$

the following boundary conditions are used:

$$\frac{\partial^2\phi}{\partial t^2}(0,t) = F_0\left(\frac{\partial q}{\partial x}(0,t), \frac{\partial q}{\partial s}(0,t), \phi(0,t), t\right)$$
$$\frac{\partial^2\phi}{\partial t^2}(1,t) = F_1\left(\frac{\partial q}{\partial x}(1,t), \frac{\partial q}{\partial s}(1,t), \phi(1,t), t\right)$$

where,

*s=0* denotes the connection between the drillstring and the rotary table,
*s=1* denotes the bottom of the drillstring,
$F_0$ is a function determined by the drive torque at the top,
$F_1$ is the friction at the bottom

The general solution of the wave equation is given by:

$$\phi(s,t) = \varphi(s,t) + \psi(s,t) \quad \dots\dots\dots\dots\dots\dots(22)$$

$\varphi$ and $\psi$ are arbitrary continuously differentiable real-valued functions that represent an up-traveling and a down traveling wave respectively.

$$\frac{\partial \phi}{\partial t}(s,t) = \dot{\varphi}(s,t) + \dot{\psi}(s,t)$$
$$\frac{\partial \phi}{\partial t}(s,t) = \dot{\varphi}(s,t) + \dot{\psi}(s,t)$$

The above two equations describe the time and spatial derivatives of $\phi(s,t)$ respectively and $\dot{\psi}$ represents the transmission of torque to the bottom hole assembly. To achieve a smooth drilling operation with a constant rotary speed $\dot{\psi}$ must be monitored

$$\Psi(t) = \frac{\partial \phi}{\partial t}(0,t) - \frac{\partial \phi}{\partial s}(0,t) = 2\dot{\psi}(t) \quad \ldots\ldots\ldots\ldots\ldots\ldots (23)$$

The boundary condition is described by the following equation:

$$\frac{\partial^2 \phi}{\partial t^2}(0,t) = G_{top}\frac{\partial \phi}{\partial s}(0,t) + u_T(t)$$

Where,

$G_{top} = \frac{GJ}{LI_T}$ and is proportional to the torsional rigidity of the drillstring,
*G* is the shear modulus,
*J* is the geometric moment of inertia,
*L* is the length of the drillstring,
$I_T$ is the moment of inertia of the top-drive,
$u_T$ is the external torque delivered by the rotary table

To maintain a constant angular velocity ($\Omega_0$), the following control law is commonly used:

$$u_T(t) = k_p\dot{\xi}(t) + k_i\xi(t) \quad \ldots\ldots\ldots\ldots\ldots\ldots (24)$$
$$\xi(t) = \Omega_0 t - \phi(o,t) + \xi_0$$
$$\dot{\xi}(t) = \Omega_0 - \frac{\partial \phi}{\partial t}(0,t)$$

where $k_p$ and $k_i$ are the proportional gain and integral gain respectively and $\xi_0$ is the displacement of the drillstring from its reference value at the top.

### 2.3.2 Friction Model

When drilling, the drillstring makes frictional contact with the borehole. The drill bit is connected with the drill pipe and comes in contact with the rock formation while the drill pipes and BHA experience multiple points of frictional contact throughout the length of the borehole. Viscous friction is also encountered by the drillstring due to the presence of drilling fluid in the wellbore. All this friction experienced by the drillstring causes instability in the drilling process therefore an appropriate friction model is essential to gain an insight into the drilling dynamics. Common friction models like the Coulomb friction, Stribeck friction and Karnoop's model are used to model friction encountered by the drillstring. A comprehensive review of mechanical friction models can be found in (Armstrong-Hélouvry, et al., 1994). Figure 13 shows the plot for the Coulomb and static friction model where $T_{sb}$ is maximum torque acting on the bit corresponding to the static friction which clamps the bit. When the bit starts to rotate, it experiences Coulomb friction and the corresponding torque $T_{cb}$. $T_{fb}$ is the friction torque on the bit and $\omega_b$ is the bit RPM. At $\omega_b$=0, i.e. when the bit is clamped, static equilibrium of the bit is maintained by the adjustment of the friction torque to the drillstring torque.

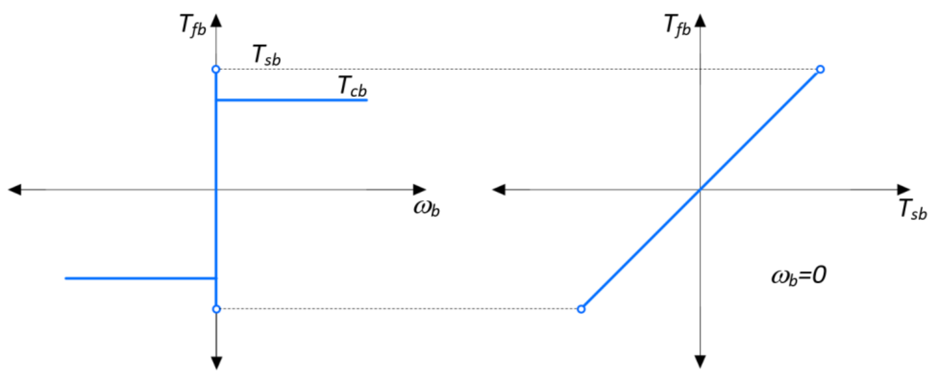


**Figure 13. Coulomb and static friction**

The Karnopp friction model is represented in figure 14. This model accounts for the nonlinear exponential decay of the dry friction torque ($T_{fb}$) with respect to bit RPM ($\omega_b$) where the friction torque leads to a decrease in torque on bit with increase in the RPM. $T_{sb}$ is the static torque, and $T_{cb}$ is the Coulomb friction torque, and the dry friction varies between these two values for $\omega_b$>0. A region of small RPM is defined between '-$d\omega$' and '$d\omega$' around $\omega_b$=0, in this region the RPM is considered to be zero and outside this region the friction is a function of the RPM.

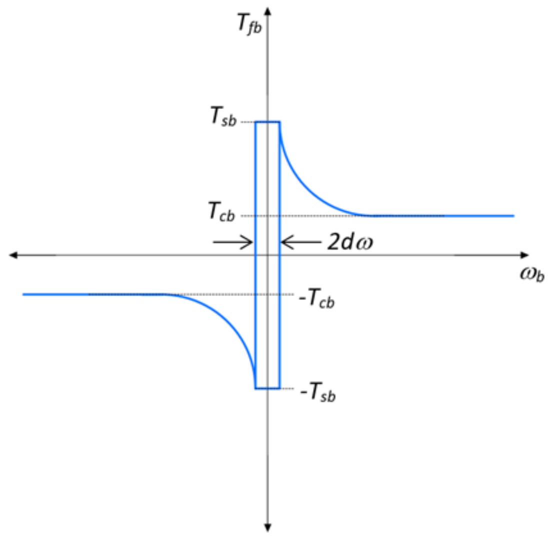


**Figure 14. Karnopp's model with a decaying friction term**

### 2.4 Experimental Analysis of Drilling Vibrations

Over the years mathematical models of the drillstring have evolved from basic models to sophisticated models. Although extensive research has been done to understand the drilling dynamics mathematical, the models still have shortcomings and are often based on assumptions and simplification. Many non-linearities involved in the drilling process are ignored to help ease the computational expense (Ghasemloonia, et al., 2015).

An alternate approach to study drillstring dynamics is the physical modeling approach in which experimental laboratory scaled rigs are developed to simulate the process of drilling. This section presents some of the laboratory scaled rigs that have been developed to study drillstring vibration. A detailed review of the experimental rigs can be found in (Patil & Teodoriu, 2013; Srivastava & Teodoriu, 2019).

In most of the experimental rigs electric motors are used to replicate the behavior of the top drive assembly. To provide rotational energy to the drillstring DC motors are commonly used as they are easy to control. In some cases, servo motor (Franca, 2010; Kovalyshen, 2014; Ullah & Bohn, 2018) and stepper motors (Patil & Teodoriu, 2013; Cayeux, et al., 2017; Marquez & Teodoriu, 2017) have also been used to provide the rotational energy. DC motors are preferred when torsional vibrations of the drillstring are being simulated and analyzed. This is because with a DC motor a smooth rotational motion and continuous torque transfer can be achieved, which is not the case in step incremented motors. Due to high power requirement for their setup Raymond, et al. (2008), used a 25 hp positive displacement motor. Stepper motors and servo motors due to their precise position control are used with a linear actuator to replicate the hoisting system. This also allows control of the weight-on-bit.

**Figure 15. Experimental setup at Sandia National Laboratories (Raymond, et al., 2008)**

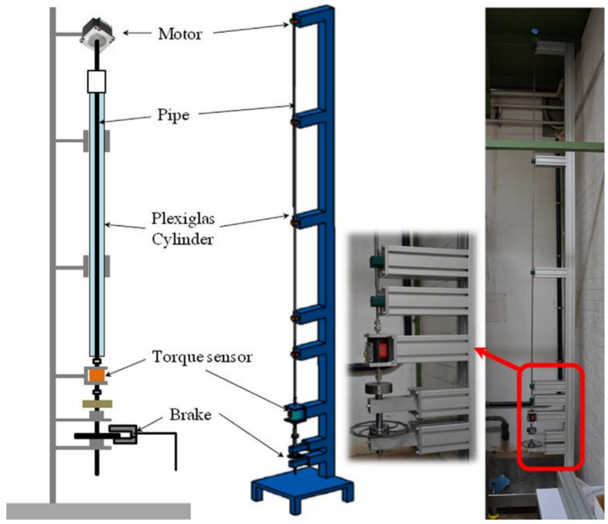


**Figure 16. Experimental rig to study torsional vibrations (Patil & Teodoriu, et al., 2013)**

The choice of material to use as the drillstring is crucial when analyzing drilling dynamics. Use of materials like steel, aluminum and PVC has been reported in literature (Srivastava & Teodoriu, et al., 2019). A rigid steel drillstring is preferred when the mechanical properties of a drill bit are in consideration. A more flexible/less stiff material should be used when studying drillstring dynamics. Some setups have the capability to interchange the drillstring to test materials with different stiffness (Kapitaniak, et al., 2015; Sharma, et al., 2020) and some have the ability to pre-tension the drillstring (Forster, 2011). Patil and Teodoriu (2013) conducted a series of tests to show the dependence of the stick-slip behavior of a drillstring on the stiffness of the drillstring. Three different materials: steel, aluminum and PVC were tested and the use of PVC was recommended for studying stick-slip in downscaled experimental rigs.

When designing an experimental setup of the drilling rig the choice of an appropriate downscaling factor is essential. With appropriate downscaling of the geometric, kinematic and dynamic properties, the behavior of the setup can be close to real scale drilling rig behavior. Although downscaling might seem straightforward, there are some constraints that must be considered. For example, downscaling the length of the drill pipe might see straightforward at first but when the diameter of the drill pipe has to be downscaled with the same factor it becomes impractical after a certain point. This is because of the slenderness of the drillstring.

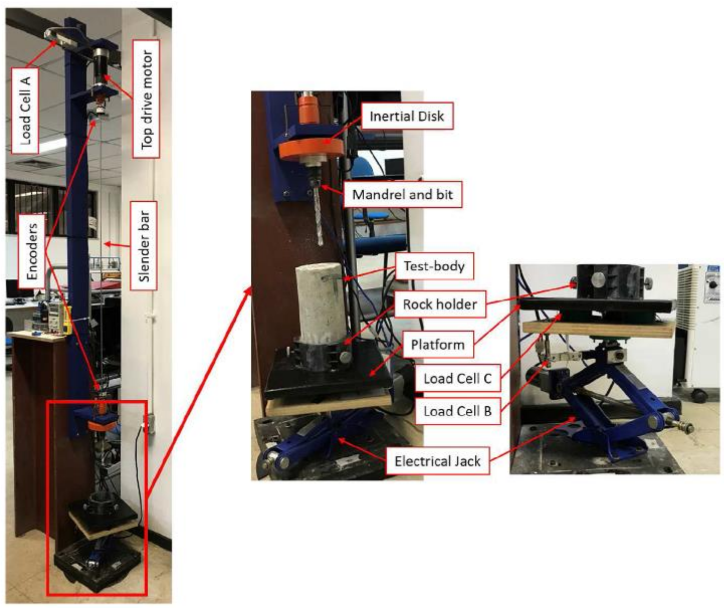


**Figure 17. Setup to analyze axial and torsional vibration of drillstring (Real, et al., 2018)**

Bit-rock interaction is simulated in the experimental setups by drilling actual rock samples or by using brakes. Raymond et al. (Raymond, et al., 2008) used e 3-1/4 in. diameter bit to drill Sierra white granite rock sample. Franca (Franca, 2010) used a roller cone bit to drill two sandstones (Castlegate and Mountain Gold) and two limestone (Savonnière and Tuffeau) samples. Bavadiya, et al. (2017) used a two cutter PDC bit to drill through sandstone rock sample. When performing drilling with the experimental setups it is easier to analyze the coupled modes of vibrations. To study individual modes of vibrations breaking mechanisms are used instead of actual drilling. Mechanical breaking (Patil & Teodoriu, 2013) systems and electromagnetic braking systems (Sharma, et al., 2020) have been used to generate torsional oscillation in the experimental drillstring. Lateral vibrations have also been generated using electro-mechanical shakers (Shyu, 1989; Antunes, et al., 1992; Khulief & Al-Sulaiman, 2009). A summary of experimental drilling rig setups is provided in table 4 (Srivastava & Teodoriu, 2019)

**Table 4. Summary of experimental drilling rig setups**

| Reference | Inclination | Drillstring Length | Drillstring OD | Measured Vibrations | Bit-Rock Interaction |
|---|---|---|---|---|---|
| Shyu 1989 | All inclinations | 1 m | 6.5 mm | Axial & lateral | A function operated mini shaker |
| Antunes, et al., 1992 | Vertical | 1.5 m | 75 mm | Axial & lateral | 200N Electro mechanical shaker |
| Berlioz, et al., 1996 | Vertical & Horizontal | 3 m | 2-7mm adjustable | Axial & lateral | Magnetic powder brake |
| Melakhessou, et al. 2003 | Vertical | 2 m | 4mm | Lateral | Powder Brake |
| Mihajlovic, et al., 2006 | Vertical | 1.47 m | | Torsional | Lubricated disc brake system |
| Raymond, et al., 2008 | Vertical | ≤ 2 m Actuator system | 76.2 mm | Axial | Drilling on white granite rock sample |
| Khulief and Al-Sulaiman 2009 | Vertical | 1-2 m | 3 -10 mm | Axial & Torsional | Magnetic tension break and Vibration shaker both |
| Lu, et al., 2009 | Vertical | ≤2 m | | Torsional | Drilling on cedar wood block |
| Forster, et al., 2010 | Vertical | 2 m | 5 mm | Lateral and torsional | |
| Franca 2010 | Vertical | Actuator system | | Axial | Sandstone and Limestone rock samples |
| Forster 2011 | Vertical | 1.25 m | 1 mm | Axial & Torsional | Steel insert as well bore |
| Liao, et al., 2011 | Vertical | 1 m | 5 mm | Torsional | |
| Esmaeili, et al., 2012 | Vertical | 0.524m Actuator system | 40 mm | Axial | Sandstone |
| Patil and Teodoriu 2013 | Vertical | 5m | 4 mm | Torsional | Torque braking system |
| Kovalyshen 2014 | Vertical | Actuator system | 49 mm | Axial & Torsional | Limestone |

| | | | | | |
|---|---|---|---|---|---|
| Cayres, et al., 2015 | Horizontal | 2.4 m | 3 mm | Torsional | Disc brake |
| Kapitaniak, et al., 2015 | Vertical | ≤ 2 m | 10 mm | Torsional | Rock sample |
| Westermann, et al., 2015 | Horizontal | 5m | 44.5 mm | Axial, Lateral & Torsional | |
| Bavadiya, et al., 2017 | Vertical | 0.9 m | 9.5 mm | Axial & Lateral | Rock sample |
| Cayeux, et al., 2017 | Horizontal | 1m | 9.5 mm | Lateral & Torsional | Rock sample |
| Marquez and Teodoriu 2017 | Vertical | 15m | 6-12mm | Torsional | Disc brake system |
| Bilgesu, et al., 2017 | Vertical | 0.9 m | 9.5 mm | Axial & Lateral | Rock sample |
| Ullah and Bohn 2018 | Vertical | 4.1 m | 6 mm | Torsional | |
| Zarate-Losoya, et al., 2018 | Vertical | 0.9 m | 9.5 mm | Axial & Lateral | Rock sample |
| Loeken, et al., 2018 | Vertical | 0.8 m | 9.5 mm | Axial & Torsional | PDC bit |
| Lin, et al., 2018 | Horizontal | 25 m | 12 mm | Axial, Lateral & Torsional | Rock sample |
| Wen, et al., 2018 | Horizontal | 11 m | | Lateral | Pressurized rock sample |
| Real , et al., 2018 | Vertical | 1.53 m | 5 mm | Axial & Torsional | Concrete Sample |
| Pires, et al., 2019 | Horizontal | ≤ 2 m | | Torsional | Disc brake |
| Sharma, et al., 2020 | Lateral, Curved & Hori-zontal | 15m | 6-12mm | Torsional | Torque braking system |

## 2.5 Drilling Vibrations Control

Drilling vibration control techniques are classified into two categories: passive and active. Passive control techniques deal with the physical manipulation of downhole tools. On the other hand, active control involves making decisions/changing drilling parameters (RPM, WOB etc.) in real-time. This section consists of a brief overview of passive control available in literature followed by a detailed review of active control techniques presented by various researchers.

### 2.5.1 Passive Control Methods

Many authors have come to the conclusion that by changing/addition of the bottom-hole stick slip can be controlled. This section gives a brief overview of the passive control presented by different authors.

Fear, et al., (1997), discuss the damage on the PDC bit that was caused by the torsional vibration and the absence of an anti-whirl stabilization tool in the BHA. They also stated that the addition of more stabilizers in the BHA can only delay the process of slip-stick vibration but cannot eliminate it. To eradicate the slip-stick vibration, anti-whirl technology (if present) should be installed to the BHA, if not then combine the PDC bit with the stabilized steerable motor. It was further concluded that slip-stick vibration is correlated with rotary speed and torque of the bit as this relationship characterizes the bit balance. Therefore, it is important to understand this correlation to minimize the damage to the PDC bit.

In another research, damage to tools and low performance in drilling were studied by Janwadkar, et al. (2006). In this paper, buckling load analysis, critical speed analysis, and torque and drag were investigated. It was found that the buckling of BHA generates stick slip which leads to bit damage. It was observed that when the WOB of 21.11 kip was applied the sinusoidal buckling started which reduced the ROP. To mitigate this issue modeling of drillstring was done and a new BHA was designed in which the number of stabilizers was increased and installed at proper position along the length of BHA assembly. As a result, the buckling that started at 21.11 kip was shifted to 33.89 kip WOB and improved the ROP The same conclusion on increasing the number of stabilizers and putting them in correct position in order to reduce the stick slip problem was given by Bailey & Remmert (2010) and Mahyari, at al. (2010).

Bit selection and stiffness are other important parameters that can avoid stick slip and BHA whirl. In that respect Jaagi, et al. (2007), analyzed the data obtained from the field and concluded that by using a bit with a proper depth of cut in a close loop rotary drilling system will give better stability and load distribution on the cutters. Furthermore, torsional energy accumulated in the bit was reduced by increasing the stiffness of the downhole tools. Whereas effect of rotary dynamic of BHA on the stick slip was discussed by Jansen (1991). Wu, et al. (2010), presented optimum zone idea (Figure 18) that can give better ROP and drilling operations.

Ortiz, et al. (1996), discussed how the bit whirl and lateral vibrations affect the PDC bit usually in hard formations due to the imbalance of forces. Based on the case study from the field and the lab it was found that with the new bit design that incorporated tracking cutting structure, impact arrestors, and a deep profile cone helped to reduce the bit whirl effect on the drilling string. The new design of the bit also reduced the cost of the project as compared to the one which did not utilize the novel bit design because the damage to the bit was reduced. While Chen, et al. (2002), focused their efforts to study how lateral and whirl vibrations affect and reduce the bit performance on a roller-cone bit. They concluded that BHA was more affected by the stick slip frequency as compared to the bit type or bit-rock interaction. There are recent studies that are focused on tool failures due to stick-slip. For instance, Huang, et al. (2018), concluded that torsional impact drilling is more efficient than non-impact drilling. To show this, mathematical model was developed and a field experiment was conducted. In both cases, a torsional oscillator was used. The fourth-fifth-order Runge-Kutta method was applied to solve the mathematical model and it was found that stick-slip vibration intensity on the PDC bit in torsional impact drilling was less than non-impact drilling with a value equal to 0. As a result, the service life of the bit was increased. While in the field experiment torsional oscillator was introduced in the test well and its results were compared with the two wells. It was found that ROP was increased in the test well as much as two times in comparison to the other two wells. Moreover, it was observed that the condition of the bit was good when it was pulled out of the hole. The same conclusion was made by Tian et al. (2020a) where it is said that the use torsional oscillator could improve the ROP. Whereas Tian et al. 2020 (2020b) develop a new composite tool to generate regular torsional vibration which helped to reduce the variation range of the torque.

### 2.5.2 Active Control

Drilling is a dynamic process, and monitoring and control of the dynamic drilling parameters is essential to increase efficiency and to prevent severe drilling dysfunctions. Changing drilling parameters actively have been proven to assist in suppression of drillstring vibrations (Sananikone, et al., 1992; Pavone & Desplans, 1994; Efteland, et al., 2015; Vogel & Creegan, 2016). Controlling parameters like the WOB and RPM can keep the drilling process in an optimal zone and maximize the ROP as shown in figure 18 (Wu, et al., 2010).

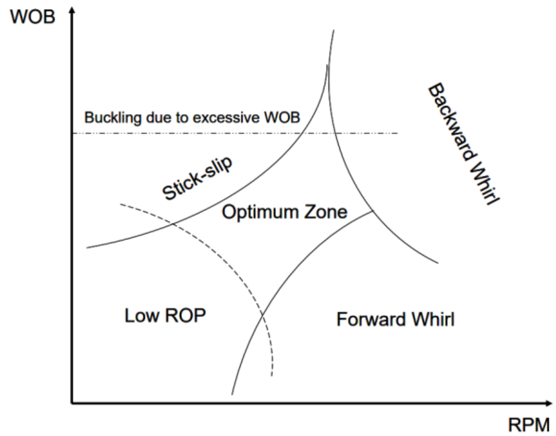


**Figure 18. Optimal drilling zone (Wu, et al., 2010)**

Active control strategies involve the use of real-time drilling parameters as feedback to control the drilling process. These control systems can be open-loop or closed-loop. In an open-loop system the driller can change the surface drilling parameter set points in response to changes in the dynamic drilling parameters which can be acquired from monitoring tools like MWD. On the other hand, in a closed-loop control a feedback loop is incorporated which tracks the drilling parameters and changes the set points for the controller. In literature many active control techniques to mitigate stick-slip vibrations have been presented and this section provides a chronological review of these active control techniques. A discussion on these control strategies is provided later in this paper.

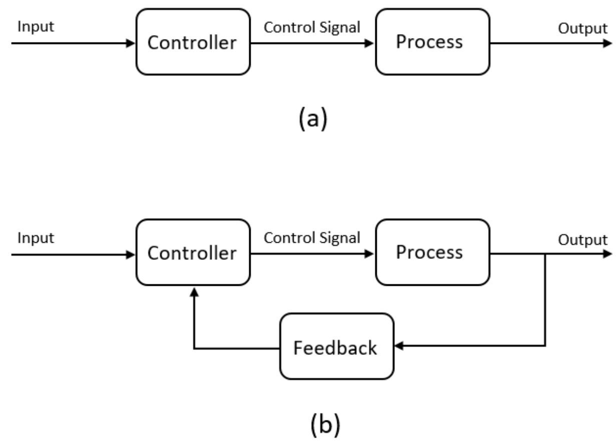


**Figure 19. (a)Open-loop control, (b) Closed-loop control**

Halsey, et al. (1988), proposed an active control technique in which torque feedback was used to control the rotary speed of the drillstring in addition to the regular tachometer signal. Field tests performed with this new control approach cured the stick-slip motion of the bottom hole assembly.

In the 1990's Shell introduced the Soft Torque Rotary System (Jansen & van den Steen, 1995; Kriesels, et al., 1999). The system reduced the risk of BHA sticking by increasing the system damping to an extent that the RPM does not drop to levels below which sticking could occur. It used the drive motor's current and voltage as feedback instead of using the motor torque, thus eliminating the need for a torque meter.

Dufeyte and Henneuse (1991), analyzed downhole and surface drilling data and characterized the drillstring behavior. They also demonstrated the possibility of suppressing and mitigating stick-slip by adjusting drilling parameters like weight on bit, rotational speed, and mud properties.

Nicholson (1994), formulated an integrated approach involving real-time monitoring and control of drilling parameters along with drilling dynamic analysis and planning to prevent and/or eliminate severe drilling dysfunctions like stick-slip, bit bouncing and BHA lateral vibrations. The method was proven effective with field examples.

Shuttleworth, et al. (1998), demonstrated the use of a downhole vibration detection MWD tool (Vibration Stick-Slip MWD) to minimize the destructive effects of downhole vibrations. The tool comprised of a triaxial accelerometer that was capable of transmitting downhole vibration data using regular MWD tools to the surface that could assist drillers to make corrective adjustments to the drilling parameters.

Serrarens, et al. (1998) used a two degree of freedom lumped parameter model and applied the $H_\infty$ control design technique to design a controller to suppress stick-slip. The controller was tested on a scaled test setup and with numerical simulation.

Yigit and Christoforou (1996) (2000), proposed models that account for fully coupled torsional, axial, and lateral drillstring vibrations. They further designed a linear quadratic regulator (LQR) controller (Christoforou & Yigit, 2001) based on linearized version of the coupled vibration models to control stick-slip vibrations. Their simulation results also showed that axial vibration has a positive effect towards suppressing stick-slip as it reduces the severity of stick-slip.

Al-Hidabbi, et al. (2003), stated that linear controllers are not effective in mitigating coupled vibrations and thus proposed a controller design based on a coupled non-linear model and a dynamic inversion approach.

Abdulgalil and Siguerdidjane (2005) also applied non-linear control theory to design a control scheme to eliminate stick-slip oscillations. They adopted the backstepping control design which involves a step-by-step coordinate transformation and virtual control design using a Lyapunov function, with the definition of a tuning function, and attaining the true control expression at the last step. This technique, unlike conventional feedback linearization, can avoid cancelation of useful nonlinearities in the system and still achieve the desired system stability and tracking. Simulations performed using this control design showed a quick response time of less than three seconds, and robustness to uncertainties of drillstring length and damping.

Yigit and Christoforou (2006), introduce a new model that was built on their previous work which examined the coupling between stick-slip vibrations and bit-bounce. Simulation results indicated that rotary control alone may not be sufficient for smooth drilling because of the changes in subsurface formations and operating conditions. Therefore, the authors proposed active control of the WOB in addition to the rotary control system to reduce the axial vibrations.

Zamanian, et al. (2007), developed a two degree-of-freedom model and an active damping system based on it. The model also accounted for coupling between torsional and axial vibration through a bit-rock interaction law. The authors stated that stick-slip oscillations can be avoided by increasing the drilling mud damping, increasing bit parameter used in the model and also by obtaining a feedback function through appropriate selection of model with certain parameters.

A sliding-mode control based on a lumped parameter discontinuous torsional model with four degrees of freedom was proposed by Navarro-Lopez and Cortes (2007). Simulation results showed that the controller could achieve the desired reference angular velocities despite the presence of dry friction and weight-on-bit variations under stick-slip conditions. The analysis was further extended and corrected in (Navarro-Lopez and Licéaga-Castro 2009).

Canudas-de-Wit, et al. (2008), proposed the use of weight-on-bit as a control variable for their stick-slip control mechanism called D-OSKIL (drilling oscillation killer). This approach does not require a redesigning of the velocity control mechanism and the simulation performed using this method eliminated the stick-slip problem.

Puebla and Alvarez-Ramirez (2008), designed a two degree of freedom model-based feedback-control approach using modeling error compensation technique, and cascade and decentralized control schemes.

Kyllingstad and NessjØen (2009), introduced a new system called SoftSpeed, for preventing and curing stick-slip oscillations. SoftSpeed, which does not require drillstring torque or motor current measurements, was launched by NOV as an alternative to other systems like Shell Soft Torque. The system is basically a proportional-integral (PI) speed controller which is tuned to dampen the torsional vibrations at the detected stick-slip frequency. Hardware-in-the-loop simulation test (Kyllingstad & Nessjøen, 2010) and field testing (Nessjøen, et al., 2011) was conducted to show the effectiveness of the control system.

In 2009, Navarro-Lopez proposed an alternate method to analyze and control stick-slip oscillations (Navarro-López E., 2009). A linear proportional-integral (PI) controller was designed and the drillstring was modeled with three degrees of freedom.

Karkoub, et al. (2010), discussed the use μ-synthesis control design technique to address the drillstring stick-slip control problem. This technique is based on the $H_\infty$ control design and D-K iterations optimization method. It accommodates system modeling imperfections in the control design process. In this study, two μ-synthesis controllers were designed, one without measurement delay and another with measurement delay. Testing was carried out and the controllers proved to be robust against the actuator uncertainties, unmolded nonlinearities, high frequency dynamics, measurement delay and noise. The authors used a three degree of freedom model and highlighted that fact that if the degrees of freedom are increased for the dynamic system the control problem will become more challenging and might not result in good performance.

Omojuwa et al. (2011a; 2011b), used a stepped shaft drillstring model to analyze the response of the drillstring to torsional vibrations. A torque rectification control system to control stick-slip was presented and simulations conducted showed the importance of WOB parameter to reduce stick-slip. The authors concluded that the stick-slip can be suppressed by decreasing the weight-on-bit control. On the other hand, a decreased weight-on-bit leads to lower ROP, therefore maintaining a balance between stick-slip and ROP is essential.

Rudat and Dashevskiy (2011), introduced a stick-slip control strategy in which stick-slip could be identified using simple drillstring and bit-rock models. It consisted of continuous identification and adjustment of the model parameters by using downhole MWD data to determine the optimal drilling parameters.

Bayliss, et al. (2012), presented an online-identification-based adaptive stick-slip control algorithm. Linear SISO (Single Input Single Output) feedback architecture was used to design the adaptive controllers, the gains of which are set recursively by pole placement utilizing drilling parameters identified on-line by RLS (Recursive Least Squares) algorithm. The algorithm requires bit RPM and torque on bit measurements to be transmitted to the surface.

Sagert, et al. (2013), used a distributed parameter wave PDE model of the drillstring torsional dynamics to derive two control laws to suppress unwanted torsional oscillations. The first control law uses the flatness property of the system to design a non-linear PI controller with distributed delays, and the second approach was to design a backstepping controller for a linearized model around a reference trajectory. Although the settling time of the backstepping controller was at least five times faster than the flatness controller and other similar controllers (Canudas-de-Wit, et al., 2008), it is not practical as it uses full-state feedback, which is not easily available.

Bresch-Pietr and Krstic (2014) used the wave PDE drillstring model with unknown anti-damping dynamic boundary to propose an adaptive output-feedback control scheme. The controller only required the knowledge of top and bottom RPM and not the entire system, but again, the authors mention the difficulty in acquiring real-time bottom RPM, which in practice is extremely noisy and noticeably delayed.

Bu and Dykstra (2014) applied the indirect adaptive robust controller (IARC) framework for rotational speed control of a drilling rig. The designed controller accounted for system uncertainties and nonlinear friction torque acting on the bit but required downhole measurements, which the authors highlighted can be updated at a low frequency (using mud pulsing) or at a high frequency but can be expensive to achieve. Simulations showed good speed tracking performance and mitigation of stick-slip.

A linear matrix inequality (LMI) approach to design a controller to control stick-slip was demonstrated by Harris, et al. (2014). A three degree of freedom model and a nonlinear bit-rock interaction model were used to represent the system. The LMI based controller was designed to minimize the output disturbance and control magnitude constraints were also implemented. Parametric uncertainties were also introduced to make the controller robust. The results indicated the design to be effective in controlling stick-slip.

Vromen, et al. (2014), modelled a jack-up drilling rig using the finite element method (FEM) with eighteen elements. Furthermore, an observer-based controller design strategy for Lur' e-type systems with discontinuities was employed to design locally stabilizing controllers for mitigating stick-slip. The benefits of this approach are that it uses a multi-modal drill-string model, accounts for sever velocity weakening in the bit-rock interaction and only uses surface measurements. Simulations in which the proposed control design was applied to the FEM model showed the design to be effective, whereas an existing industrial PI controller could not mitigate stick-slip under similar conditions.

Vromen, et al (2015) compared the frequency response of a four degree of freedom lumped parameter model of the drillstring with the FEM model proposed earlier in (Vromen, et al., 2014). It was evident that the first three resonance modes are dominant which made them use the four degree of freedom model and design an output-feedback controller based on the skewed-μ DK iteration approach. The controller was designed to have robustness when facing bit-rock interaction uncertainties, had integrated performance specifications, and used only surface measurements. Simulations conducted showed the controller to be successful in mitigating stick-slip. This controller was later tested with an eighteen degree of freedom drillstring model in Vromen, et al. (2019).

Liu (2015) studies the stick-slip phenomenon using a four degree of freedom lumped parameter model and proposed a sliding mode controller to suppress the oscillations. This controller differed from the one proposed by (Navarro-López & Cortés, 2007) as it is robust to parametric uncertainties and weight-on-bit variations.

Hong, et al. (2016), highlighted that many stick-slip control system designs require real-time downhole measurements which are not easily available. To address this, they put forward a control system design consisting of a Kalman estimator to estimate downhole states, and a linear quadratic regulator to control the vibrations. The estimator and controller design were based on a simple two degree of freedom model. To validate the controller a high-fidelity lumped parameter model of the drillstring was developed and numerical simulations were performed. Simulation results demonstrated the control scheme to be effective in controlling stick-slip.

Besselink et al. (2016), stated that stick-slip is a result of interaction between axial and torsional drillstring dynamics. They used a two degree of freedom drillstring model to model coupled axial-torsional stick-slip oscillations. As for the bit-rock interaction, a model was devised that combined the cutting and frictional boundary conditions. Using these dynamic models, they designed a state-feedback controller and an observer-based output-feedback controller to mitigate stick-slip. The observer-based output-feedback only used surface measurements.

Kabziński (2017), incorporated bit and rotary table friction torque, uncertain stiffness and damping with a two degree of freedom lumped parameter model to design a non-linear adaptive backstepping control with command control filtering. Stribeck curve-based friction model was used for this study. The control aim was to eradicate torsional vibrations by smoothly following a reference bit RPM but this stratergy assumed that downhole state variables like bit position and bit RPM are available. Numerous simulations were performed in which no malfunction was observed.

Pehlivantürk, et al. (2017), developed a thirty-five degree of freedom lumped mass drillstring experimental setup to check the performance of a feedback controller designed using frequency-domain loop shaping techniques. The controller was effective in mitigating torsional vibrations in the experimental setup.

An infinite horizon dynamic programming-based control approach was applied by Feng, et al. (2017), and the control problem of suppressing drillstring stick-slip vibrations was transformed into an optimization problem. They found that the BHA speed had a negligible influence on the control input according to the optimization policy obtained. This resulted in a dimension reduction which eliminated the dependence of the control input on BHA speed thus increasing the computational efficiency of the system. Simulations carried out indicated the proposed controller to be effective in suppressing stick-slip.

An observer-based boundary controller based on a distributed system model was developed by (Basturk, 2017). The boundary control design for a wave partial differential equation (PDE) was converted to a linear time invariant (LTI) system stabilization problem using Riemann variables. The presence of sensor and actuator delays, and unknown disturbances were also considered.

Kamel, et al. (2018), developed an integrated approach to control rotary steerable systems (RSS) and optimize drilling parameters to regulate stick-slip and bit wear in directional wells. An adaptive real-time optimal controller based on particle swarm optimization (PSO) was presented. Simulations with different drilling scenarios were performed and it was observed that the control design was able to minimize the difference between angular velocities of the rotary table and the bit which resulted in reduction of torsional vibrations.

Vaziri, et al. (2018), carried out an experimental and numerical investigation to suppress stick-slip using a sliding-mode controller. For the experimental analysis a test rig was built that uses a PDC bit to drill rock samples and for the numerical analysis a 2 degree of freedom model was used. The controller design was based on the sliding mode controller proposed by (Navarro-López & Cortés, 2007) and (Navarro-López & Licéaga-Castro, 2009), but it was redesigned for a two degree of freedom model including actuator delay. By defining a robust Lyapunov function, the stability of the proposed controller was proven in the presence of model parameter uncertainties. The controller was successful in mitigating stick-slip in both experimental and numerical simulation testing, however, a limit cycle was detected around the desired set point because of the delay and dead zone observed in the actuator. Furthermore, parametric analysis of this controller design was performed (Vaziri, et al., 2020) and it was found that the sliding mode control scheme effectively mitigates stick-slip in ideal systems with no actuator delays. The controller becomes unstable in the presence of actuator delay when the input is unconstrained. However, within a limited parameter range and with constrained inputs the controller is stable and effective.

An observer and reference governor-based control design was proposed by (Fu, et al., 2019). A two degree-of-freedom lumped parameter model and a non-linear torque-on-bit model were used to design the control strategy in which the observer estimates the downhole drilling parameter state vector and the non-linear friction torque. Further, based on the estimates, the reference governor control changes the reference inputs for the PI controller. Simulation results showed that this combination of the controller and observer was effective against the stick-slip.

Zhang and Xv (2019) proposed the use of fractional order PID (FOPID) controller to suppress stick-slip. The concept of FOPID is based on fractional calculus and adds the integral and the differential orders to the integer order PID controller (Caponetto, 2010). Better control of dynamic systems can be achieved by using FOPID controllers as compared to PID controllers. In this study, a four degree of freedom torsional model was used, and simulations were performed using a set of system parameters. The FOPID controller had a faster response time and was more stable than the PID controller.

Cheng, et al. (2020) highlighted the importance of considering the change in length of drillstring as an important dynamic parameter. They presented a linear parameter varying (LPV) model with multiple degrees of freedom to design a control technique based on gain scheduling and $H_\infty$ technique. Simulations were done, and the system suppressed the stick slip problem despite continuous variation in the drillstring length. Performed well despite variations in drillstring length and stick-slip was mitigated.

MacLean, et al. (2021) emphasized the presence of actuator delays and constraints which affect the ability of the controller to reach the required response. To address the issue a two degree of freedom drillstring model which included actuator delays and actuation constraints was used to investigate a modified integral resonant controller (MICR) with integral tracking to tackle stick-slip. The scheme was tested under varying systems parameters, actuator delays and actuation constraints and proved to be superior to sliding mode controllers which requires a complex design.

Derbal, et al. (2021) used a four degree of freedom model with drill pipe and drill collar dynamics and designed a fractional-order proportional-derivative (FOPD) controller and a fractional-order proportional-integral (FOPI) controller. The performance of these controllers was compared with the FOPID controller proposed (Zhang & Xv, 2019) and with the regular PID controller. Robustness of the four controllers was tested under varying weight-on-bit and reference velocity conditions using MATLAB/Simulink simulations and it was found that all the controllers were successful in suppressing stick-slip vibrations. The FOPD controller had the highest overshoot, most oscillations and the slowest response time and was severely affected by the changes in reference velocity. The FOPID controller had the fastest response time but higher overshoot than the FOPI and PID controllers. Among the PID and the FOPI controllers, the FOPI had a faster response and improved stability but a slightly higher overshoot.

A super-twisting sliding mode controller to cure stick-slip oscillations was proposed by Krama et al. (2021). When compared to a sliding mode controller, the super-twisting sliding mode controller has better tracking, faster convergence, improved robustness, and chatter-free implementation. The authors used a four degree of freedom model which included an induction motor with VFD and a gearbox which represented the actual drilling system. The proposed controller was tested using numerical simulations and with a HIL test infrastructure.

To mitigate the problem of stick slip Riane et al. presented an observer-based $H_\infty$ controller (Riane, et al., 2022a) and an observer-based LQG controller (Riane, et al., 2022b). The observer designed to estimate the downhole states like bit speed and torque on bit, was cascaded with the controller and a ten degree of freedom model was used in these studies. Simulation results showed the observer-based $H_\infty$ controller had better efficiency in suppressing stick-slip under unstructured perturbations and suppressed the oscillations in under 5 seconds. On the other hand, the observer-based LQG controller suppressed stick-slip within 3 seconds and had smoother response for structured perturbations.

To achieve a better controller performance for a multi-DOF drillstring system, Laib et al. (2022) proposed a hybrid fuzzy PID control structure in which an interval type-2 fuzzy logic controller (IT2FC) is combined with a conventional PID controller. To model the system, a four degree of freedom drillstring model with a non-linear bit rock interaction model including friction torque and mud damping was used. To select the optimal parameters for the controller particle swarm optimization (PSO) algorithm was utilized. For validating the controller, simulations, and experimental testing with a hardware in loop (HIL) system were performed and comparisons were made to other controllers like the sliding mode controller and the PID controller. The proposed controller had a comparatively faster response time but had small overshoots.

**Table 5. Active control strategies**

| Year | Authors | Control Technique | Drillstring Model | Bit-Rock Friction Model | Testing |
|---|---|---|---|---|---|
| 1988 | Halsey, et al., (1988) | Torque Feedback | Drillpipe section modeled as a transmission line for torsional waves. | NA | Field |
| 1995 | Jansen and van den Steen (1995) | Shell Soft Torque Rotary System | 2 and 3 DOF lumped parameter model | Coulomb friction law | Experimental and Field |
| 1998 | Serrarens, et al., (1998) | $H_\infty$ control | 2 DOF lumped parameter model | Non-linear friction model | Experimental |
| 2001 | Christoforou and Yigit (2001) | Linear Quadratic Regulator (LQR) controller | 1 DOF lumped parameter model | Coulomb friction law | Simulation |
| 2003 | Al-Hidabbi, et al., (2003) | Non-linear inverse dynamic Controller | 1 DOF Lumped parameter model | Non-linear friction model | Simulation |
| 2005 | Abdulgalil and Siguerdidjane (2005) | Non-linear Backstepping Control | 2 DOF lumped parameter model | Non-linear friction model | Simulation |
| 2007 | Navarro-López and Cortés (2007) | Sliding mode controller | 4 DOF lumped parameter model | Karnopp friction model | Simulation |
| 2008 | Canudas-de-Wit et al. (2008) | D-OSKIL, Weight-on-Bit control | 2 DOF lumped parameter model | Stribeck friction | Simulation |
| 2008 | Puebla and Alvarez-Ramirez (2008) | Modeling error compensation technique | 2 DOF lumped parameter model | NA | Simulation |
| 2009 | Kyllingstad and NessjØen (2009) | SoftSpeed, PI speed controller | NA | NA | Experimental and Field |
| 2009 | Navarro-López (2009) | Linear Proportional-Integral (PI) controller | 3 DOF lumped parameter model | Karnopp friction model | Simulation |

| | | | | | |
|---|---|---|---|---|---|
| 2010 | Karkoub, et al., (2010) | μ-Synthesis controllers | 3 DOF lumped parameter model | Non-linear friction model | Simulation |
| 2011 | Rudat and Dashevskiy (2011) | Model parameter identification using downhole MWD data to determine optimal drilling parameters | 1 DOF lumped parameter model | Non-linear friction model | Simulation and Field |
| 2012 | Bayliss, et al., (2012) | Adaptive controller design using pole placement and on-line RLS based parameter identification | 2 DOF lumped parameter model | Drag bit model (Detournay et al. 2008) | Simulation |
| 2013 | Sagert, et al., (2013) | Backstepping and Flatness approache | Wave PDE, Distributed parameter model | Karnopp friction model | Smulation |
| 2014 | Bresch-Pietri and Krstic (2014) | Adaptive Output Feedback control | Wave PDE, Distributed parameter model | Karnopp friction model | Smulation |
| 2014 | Bu and Dykstra (2014) | Indirect Adaptive Robust Controller (IARC) | 2 DOF lumped parameter model | Stribeck friction | Simulation |
| 2014 | Harris, et al., (20114) | Linear Matrix Inequality (LMI) approach | 3 DOF lumped parameter model | Karnopp friction model | Simulation |
| 2014 | Vromen, et al., (2014) | Observer-based output-feedback | FEM model with 18 elements | Bit-Rock interaction: Coulomb friction law with Stribeck curve (Drillstring-Borehole interaction: Coulomb friction law) | Simulation |
| 2015 | Vromen, et al., (2015) | Skewed-μ DK iteration approach | 4 DOF lumped parameter model | Bit-Rock interaction: Coulomb friction law with Stribeck curve (Drillstring-Borehole interaction: Coulomb friction law) | Simulation |
| 2015 | Liu (2015) | Sliding mode controller | 4 DOF lumped parameter model | Karnopp friction model | Simulation |
| 2016 | Hong, et al., (2016) | Kalman Estimator , Linear Quadratic Regulator (LQR) | 2 DOF lumped parameter model | Non-linear friction model (Borehole-drillstring friction modeled as Columb friction) | Simulation |

| | | | | | |
|---|---|---|---|---|---|
| 2016 | Besselink, et al., (2016) | State-feedback controller and Output-feedback controller | 2 DOF lumped parameter model (with coupled axial-torsional dynamics) | Model accounting for frictional contact and cutting processes (Richard et al. 2007) | Simulation |
| 2017 | Kabziński (2017) | Nonlinear adaptive backstepping controller with command control filtering | 2 DOF lumped parameter model | Stribeck friction | Simulation |
| 2017 | Pehlivantürk, et al., (2017) | Feedback controller designed using frequency-domain loop shaping techniques | 35 DOF lumped parameter model | NA | Simulation and Experimental |
| 2017 | Feng, et al., (2017) | Dynamic programming based control | 2 DOF lumped parameter model | Karnopp friction model | Simulation |
| 2017 | Basturk (2017) | Observer-Based Boundary Control | Wave PDE, Distributed parameter model | Dry friction and Viscous damping | Simulation |
| 2018 | Kamel, et al., (2018) | Adaptive real-time optimal controller based on Particle Swarm Optimization | 2 DOF lumped parameter model | Coulomb friction law | Simulation |
| 2018 | Vaziri, et al., (2018) | Sliding Mode Controller | 2 DOF lumped parameter model (with actuator delay) | Empirical torque on bit model (M. Kapitaniak, et al. 2015) | Simulation and Experimental |
| 2019 | Fu, et al., (2019) | Observer and reference governor based control | 2 DOF lumped parameter model | Karnopp friction model | Simulation |
| 2019 | Zhang and Xv (2019) | Fractional Order PID (FOPID) control | 4 DOF lumped parameter model | Non-linear friction model | Simulation |
| 2019 | Vromen, et al., (2019) | Skewed-μ DK iteration approach | FEM model with 18 elements | Stribeck friction | Simulation |
| 2020 | Cheng, et al., (2020) | Gain Scheduling and $H_\infty$ technique | Multi-DOF lumped parameter model and LPV model | Karnopp friction model | Simulation |
| 2021 | MacLean, et al., (2021) | Modified Integral Resonant Controller (MICR) with Integral Tracking | 2 DOF lumped parameter model (with actuator delays and actuation constraints ) | Karnopp friction model | Simulation |

| | | | | | |
|---|---|---|---|---|---|
| 2021 | Derbal, et al., (2021) | Fractional Order PD (FOPD) and Fractional Order PI (FOPI) control | 4 DOF lumped parameter model | Karnopp friction model | Simulation |
| 2021 | Krama, et al., (2021) | Super-twisting sliding mode controller | 4 DOF lumped parameter model | Karnopp friction model | Simulation and Experimental |
| 2022 | Riane, et al., (2022) | Observer-based $H_\infty$ control | 10 DOF lumped parameter model | NA | Simulation |
| 2022 | Laib, et al., (2022) | Interval type-2 fuzzy logic controller (IT2FC) combined with a conventional PID controller | 4 DOF lumped parameter model | Karnopp friction model | Simulation and Experimental |
| 2022 | Riane, et al., (2022) | Observer-based LQG control | 10 DOF lumped parameter model | NA | Simulation |

## 2.6 Conclusion

Although passive control techniques are a good first step specially during the well planning stage, active control schemes are more affective when tackling stick-slip as they enable to make changes to the drilling parameters in response to the drilling dynamics Numerous active control strategies, as listed in table 5, have been proposed in literature but most have not made it beyond the laboratory/research stage. One of the biggest limitations of these controller designs is the system modelling. The drillstring models and the friction models used to represent the drilling process are often simplified. Many system dynamics are ignored to help reduce the computational load and not all factors that impact the system are well understood. For example, the dynamics of the electric motors and the time delays in the system are not considered in many cases. Most of the controllers listed in table 5 are based on lumped parameter models with four or lesser degrees-of-freedom, as evident in figure 20. The lesser the degrees-of-freedom of the model, the lesser the accuracy. Furthermore, the lumped parameter models might have a satisfactory performance when considering vertical well configuration but when it comes to horizontal and directional wells their efficacy must be proven (Tang, et al., 2020). The model parameters and the system dynamics are different for vertical and horizontal wells and in an experimental study it was shown that the performance of a PID based RPM controller improves when tuned for the specific well configuration (Sharma, et al., 2021). Friction models are oversimplified in most cases as modeling the contact friction throughout the length drillstring and the bit-rock interaction accurately is extremely challenging. The dynamics predicted by the simplified drillstring and friction models can be vastly different from the actual real-world dynamics, therefore the set-points calculated by the controllers may not be optimal. Also, the models must be updated in real-time to account for the changes in the drilling conditions.

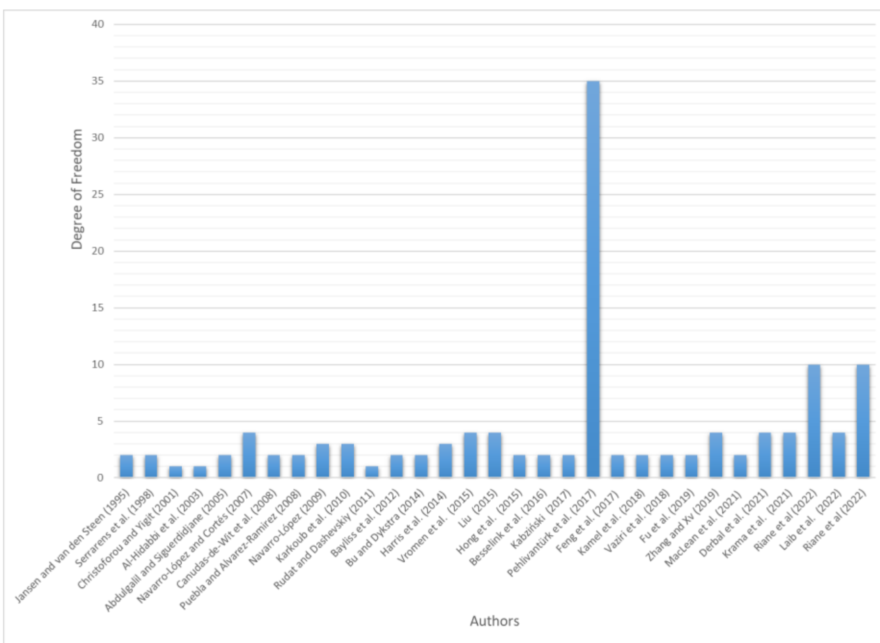


**Figure 20. Controllers designed using lumped parameter model with the corresponding DOF**

When it comes to testing the performance of the controllers, they are mostly tested using computer simulations on a predefined set of drilling conditions and therefore often have a limited band of operation. This is the reason why most of the controllers might not perform as expected when tested in the field under actual drilling conditions. Another challenge is the absence of high-frequency downhole state feedback variables like the bit RPM in most real-world drilling systems. MWD tools used to transmit downhole data to the surface operate on much lower data transmission frequencies. (Srivastava, et al., 2023) presents a review of existing downhole tools and their data acquisition sampling frequencies. Additionally, the study also highlighted the need for surface and downhole data sampled at higher frequencies($\geq$10Hz) for stick-slip vibration detection.

The industry still mostly uses a stiff PI controller or the Shell SoftTorque system which have been around since the 1980s and 1990s. The other two active control strategies that have made it to the field are the NOV SoftSpeed and the Z-Torque. Although these industrial controllers have been shown to control stick-slip, they still have limitations. The stiff PI controller manages to reduce the magnitude of the oscillations but cannot always mitigate stick-slip. SoftTorque has a narrow band of operation and is vulnerable to frequency mistuning. SoftSpeed is sensitive to time delays in the feedback loops. Z-Torque, which is also developed by Shell, performs better than the original SoftTorque system and has a wider band of operation, but is still sensitive to time delays. Comparative studies on the industrial stick-slip controllers have been done by (Kyllingstad A. , 2017) and (Aarsnes, et al., 2018).

# Chapter 3: Methodology

## 3.1 Drilling Rig Systems

Rotary drilling is the most popular and efficient drilling technique used to create a bore-hole/well in the earth's surface to access the subsurface hydrocarbon and geothermal re-sources. The set of equipment/machinery used to drill a well is called a drilling rig. It con-sists of the following sub-systems: (i) power system, (ii) hoisting system, (iii)circulating system, (iv) rotary system and, (v) blowout prevention/well control system. A drilling rig and its sub-systems are shown in figure 21.

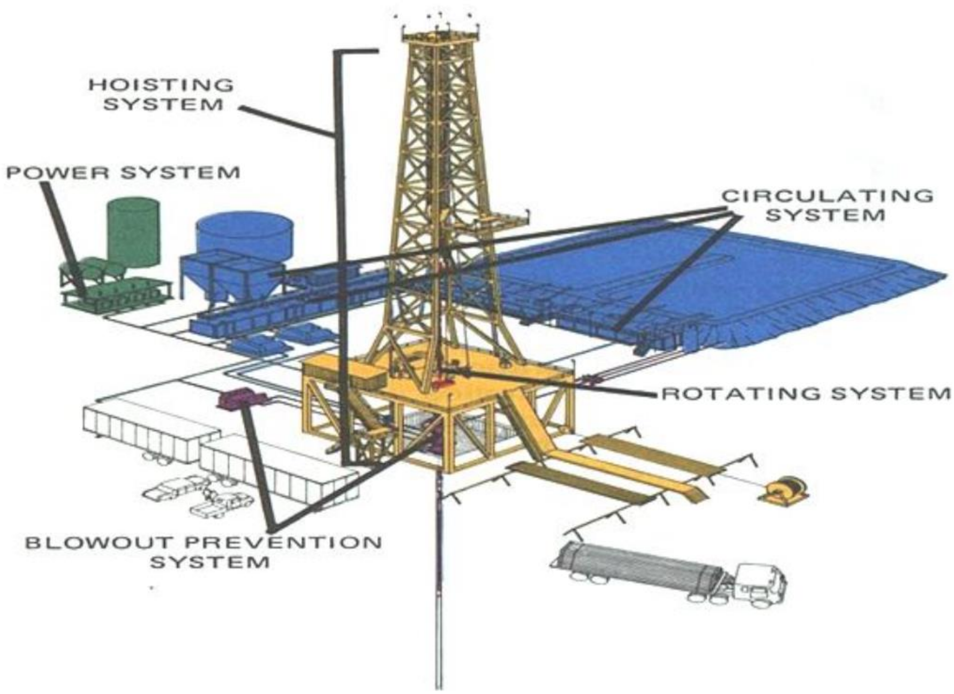


**Figure 21. Drilling Rig Systems [source: oil-gasportal.com]**

### 3.1.1 Power System

A power generation system is needed to operate the drilling rig. For this, internal combustion diesel engines or diesel-electric engines are used at the rig site. The total power requirement for most drilling rigs ranges between 1000 to 3000 hp and most of it is consumed by the hoisting system and the circulating system (Bourgoyne, et al., 1986). Belts, chains and drive shafts are used to transfer the power from the engines in a mechanical rig, whereas, in an electric rig, power is transferred in the form of DC electrical power. The performance of the power system is characterized by the output horse power, torque and efficiency.

### 3.1.2 Hoisting System

The function of the hoisting system is to raise or lower the drillstring, casing strings and other subsurface equipment into or out of the wellbore. The two routine functions performed using the hoisting system are: (i) making connection: this refers to the process of adding a length of drill pipe to the drillstring as the well deepens and, (ii) tripping: this is the process of pulling the drillstring out of the well and then running it back in. This is usually done to change a portion of the downhole assembly.

The three main components of the hoisting system are:

- Derrick and substructure: its function is to provide support and vertical height to raise and lower the drill pipes into the well.
- Block and tackle: the block and tackle provides mechanical advantage to allow easier handling of heavy loads.
- Drawworks: provides the braking and hoisting power needed to raise or lower the heavy drillstring.

### 3.1.3 Circulating system

While drilling a fluid called drilling mud/fluid is circulated down through the drillstring, through the nozzles in the drill bit, and up through the annular space between the wellbore and the drillstring. The main function of the drilling mud is to transport the rock cuttings from the bottom hole to the surface as drilling progresses. A circulating system has to be employed to serve this purpose. The main components of the circulating system are:

- mud pumps
- mud pits
- mud mixing equipment
- contaminant removal equipment

### 3.1.4 Rotary system

The rotary system on a drilling rig comprises of the equipment required to achieve drill bit rotation. This system can either be conventional or modern. In a conventional rotary system, also known as a kelly drive system, the rotational energy is imparted by a rotary table which is the revolving section of the drill floor. The kelly drive system is cheaper but is inefficient and unsafe. Modern rotary system, commonly known as top drive systems (TDS), use an electric or hydraulic motor to achieve drillstring rotation. The topdrive motor is installed along the vertical axis of the derrick and is suspended from a hook. This allows drilling with stands of pipes (three drill pipes), instead of single drill pipe, which results in saved time. Although TDS is comparatively expensive but it is much more efficient and safe compared to a kelly system.

The drillstring is an assembly of hollow pipes that extends from the surface to the bottom hole. It transfers the rotational energy to the bit and also permits circulation of the drilling fluid. The majority length of the drillstring is composed of the drill pipes. Normally a drill pipe is 30 ft in length and has special threaded ends which are used to connect them together as drilling progresses. The lower portion of the drillstring is the called the bottom hole assembly (BHA) which may have many different tubulars most of which is composed of drill collars. Drill collars are thick walled heavy steel tubulars which are used to apply weight on bit. Other tubulars that can be installed in the BHA depending on the complexity of the drilling operation are stabilizers, shock absorbers and drilling jars.

Finally, the drill bit is present below the BHA. Drill bits are chosen depending on the properties of the formation being drilled. Two types of drill bits are most commonly used: (i) roller cone bit and, (ii) PDC bit. The roller cone bits drill the formation by crushing or fracturing the rocks with tooth shaped cutters present on two or three cone shaped rolling elements/rotating cones rotating cones with each one rotating on its own axis during drilling. The PDC (polycrystalline diamond cutter) bits on the other have natural or synthetic diamond cutters which drill the formation by grinding or scraping the rock.


**Figure 22. Roller Cone Bit (left) and PDC Bit (right) [source: halliburton.com]**

### 3.1.5 Blowout prevention/well control system

The blowout prevention system or the well control system is a safety system that prevents the uncontrolled flow and release of high-pressure formation fluid. This uncontrolled flow is known as a kick or a blowout and is catastrophic. This system consists of blowout preventers (BOP) which is a stack of valves that are operated hydraulically. The BOP is present below the rig floor or on the seabed in some offshore wells and isolates the wells by stopping the fluid flow.

### 3.2 Experimental Setup

To conduct an experimental study on drilling vibrations, a laboratory scale drilling test rig equipped with several sensors and actuators was designed and built (Sharma et al., 2020). A National Instruments cDAQ data acquisition device was used to fetch real time data from the sensors and to control the actuators. The control system software was designed using National Instruments LabVIEW. A detailed description of the setup is presented in this section. A schematic overview of the setup overview is shown in figure 23.

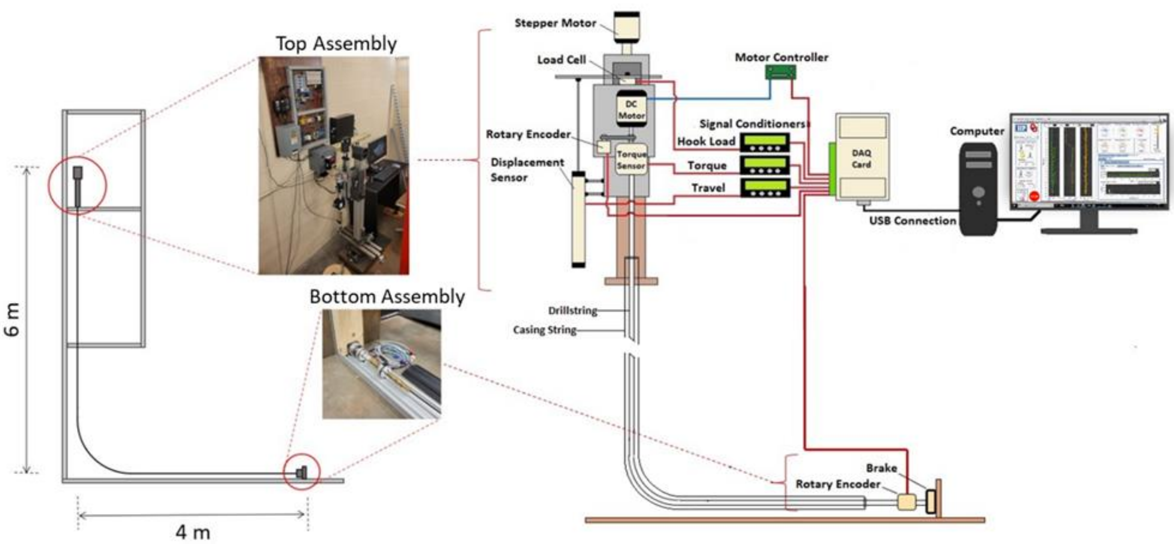


**Figure 23. Setup Overview**

Figure 24 shows a breakdown of the components of the setup. These components are described in the following sub-section.

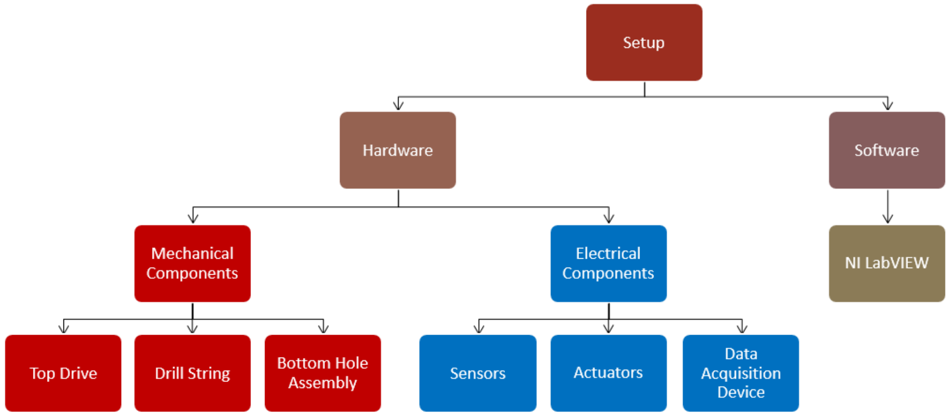


**Figure 24. Setup Components**

### 3.2.1 Mechanical Components

The mechanical components of the rig can be divided into three major parts, namely, top drive, drillstring and bottom hole assembly.

#### 3.2.1.1 Top Drive Assembly

The top drive assembly of the experimental setup consists of a 18V DC motor for providing rotational energy to the drillstring and a stepper motor with a lead screw mechanism for hoisting and weight on bit (WOB) control. The DC motor helps provide a constant voltage under a current limit for smooth torque output. Figure 25 shows the components of the top assembly. The sensors installed in the top drive assembly have been discussed at length in the electrical component section.

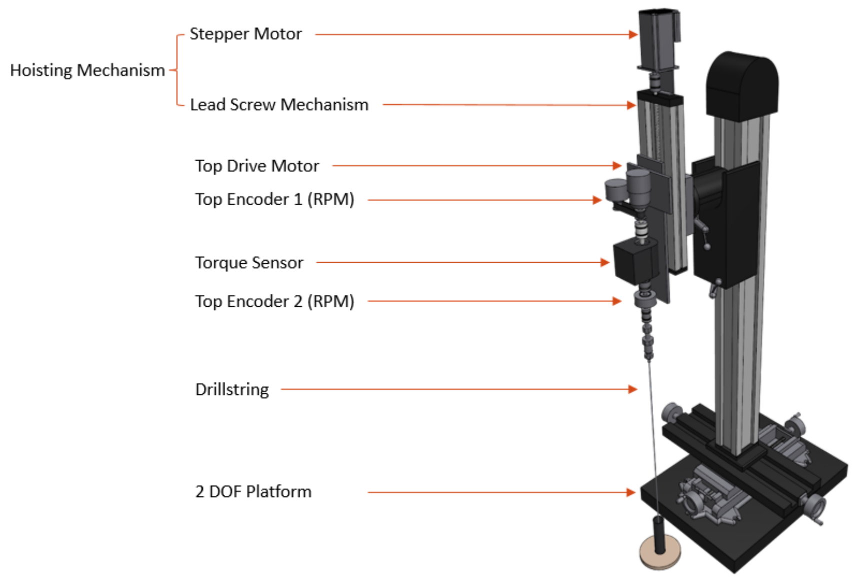


**Figure 25. Top Assembly**

3.2.1.2 Drillstring

The drillstring consists of a thin PVC pipe with an outer diameter of 1/8 inch and is approximately 40 ft in length. PVC is chosen in place of aluminum or steel for drill pipe material. Due to PVC's lower torsional stiffness, torsional vibrations are more readily generated in the setup.

To facilitate the testing of drilling dynamics in directional wells the setup is designed to be capable of simulating wells with vertical, curved and horizontal sections. For this, an actuation mechanism as shown in figure 26, is used to replicate various curved section geometries. Therefore, testing for vertical well configuration as well as direction well configuration can be carried out.

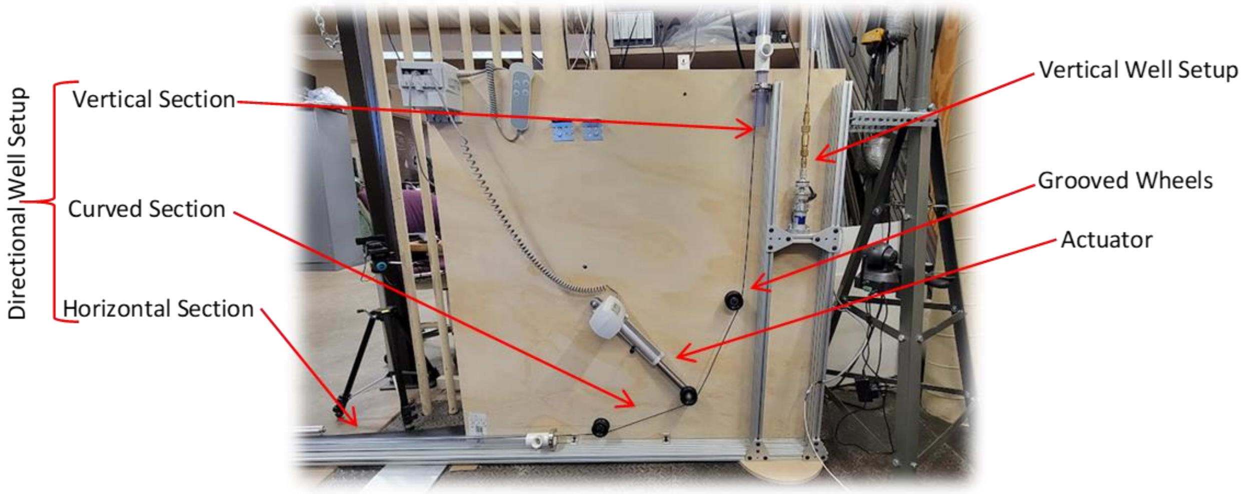


**Figure 26. Actuator mechanism to simulate different well geometries**

3.2.1.3 Bottom hole assembly

Torque is required to induce torsional vibrations in the drillstring. It can be generated by actual drilling of a rock sample or by a braking system. Considering how repeatability of results is a vital component of testing, the braking system is preferred. This system uses an electromagnetic brake to induce torque in the bottom hole assembly. The system further connects to a rotary encoder that measures precise angular movement during testing.

To simulate the bit-rock interaction a unique arrangement of electro-mechanical actuators and rotary encoders was designed and used in conjunction with a mathematical bit-rock model described in (Rudat & Dashevskiy, 2011). In this model the relationship between the applied weight on bit 'W', and the resulting torque on bit '$T$', at a given bit RPM '$\omega$' is as follows:

$$\mu = \frac{3T}{D_B W} \quad \ldots\ldots\ldots\ldots\ldots\ldots (25)$$

Here $'\mu'$ is the coefficient of friction at the bit-rock interface and $'D_B'$ is the diameter of the drill bit. The coefficient of friction can be represented as a function of the bit RPM by the following equation:

$$\mu(\omega) = a_1 + (a_2 - a_1)e^{-\frac{|\omega|}{a_3}} \quad \ldots\ldots\ldots\ldots\ldots\ldots (26)$$

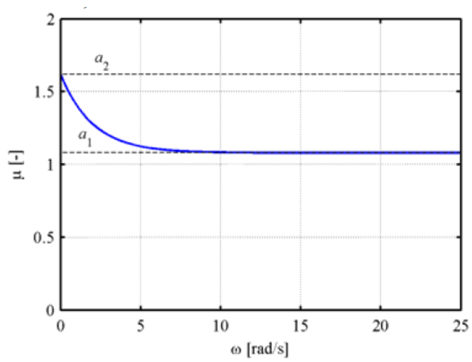


**Figure 27. Friction coefficient μ as a function of bit RPM ω (Rudat & Dashevskiy, 2011)**

where $a_1$, $a_2$ and $a_3$ represent the Coulomb friction, static friction and the slope of the decaying curve respectively. Changing the values translates to changing the type of formation being drilled. Using equations 25 and 26 the torque on bit can be calculated as:

$$T = \frac{\mu(\omega) D_B W}{3} \quad \ldots\ldots\ldots\ldots\ldots\ldots (27)$$

The above equation is implemented using LabVIEW, where a torque output is produced by an electro-mechanical brake in response to a RPM feedback generated by a rotary encoder. The torque output of the electro-mechanical brake is controlled by the current that is input to the brake, which follows a hysteresis function. The hardware implementation of the bit-rock model is shown in figure 28.

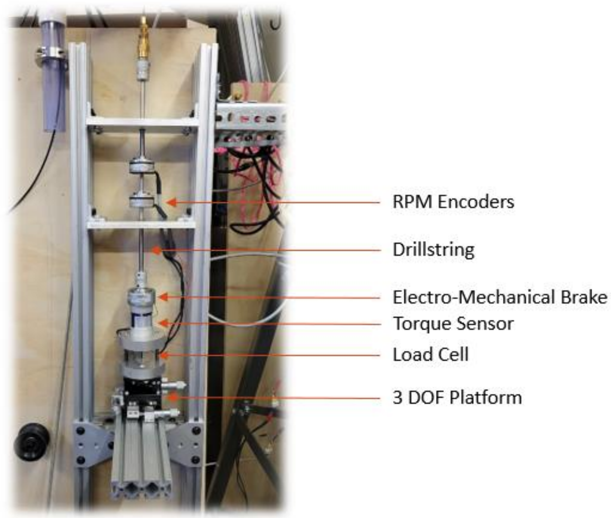


**Figure 28. Hardware implementation of the bit-rock model**

### 3.2.2 Electrical Components

The rig is equipped with several sensors and actuators that are described below.

3.2.2.1 Sensors

- *Load Cell*: The load cell used, is a strain gauge-based bridge transducer and is used to measure the hook load. The low magnitude voltage output signal from the load cell is amplified by a signal processor and is then fed to the DAQ device. Specifications include:

  - Make & Model: Omega LC201-25
  - Range: 0-25 lb.
  - Excitation: 10-15 Vdc
  - Output: 2 mV/V nominal
  - Accuracy: ±1.0% FSO linearity, hysteresis, repeatability combined

**Figure 29. Omega LC201-25 Load Cell**

- *Torque Sensor*: Like the load cell the torque sensor is also a strain gauge-based bridge transducer with a low magnitude voltage output signal. The output from this sensor must also be amplified by a signal processor before being fed to the DAQ device. It is placed just below the top drive and measures the torque on the drillstring. Specifications include:

    - Make & Model: Omega TCRT5000
    - Range: 0-1.41 N.m
    - Excitation: 20 Vdc maximum
    - Output at Full Scale: 2.0 mV/V nominal
    - Linearity: 0.10% FS
    - Hysteresis: 0.10% FS

**Figure 30. Omega TCRT5000 Torque Sensor**

- *Rotary Encoder*: Quadrature rotary encoders are used to measure the top (surface) and bottom (bit/BHA) RPM of the drillstring. Both the top and bottom encoders are 500 PPR i.e., they generate 500 digital pulses per revolution. Specifications include:

    - Make & Model: Encoder Products Company Model 15T
    - Excitation: 5-24 Vdc
    - PPR: 500
    - Max Shaft Speed: 8000 RPM

**Figure 31. Encoder Products Company Model 15T Rotary Encoder**

- *Displacement Sensor*: This is a potentiometer-based stroke pull rod linear position displacement sensor and is used to measure the vertical distance travelled. It can measure up to 300mm displacement. Specifications include:

  - Make & Model: Uxcell BWL300MM
  - Excitation: 5-24 Vdc
  - Resistance: 5K Ohm
  - Linearity: +/- 0.05%
  - Range: 0-300 mm

**Figure 32. Uxcell BWL300MM**

3.2.2.2 Actuators

- *DC motor*: A DC is used as the top drive motor for providing rotational energy to the drillstring. Specifications include:

  - Input Voltage: 0 to 18 V

- *Stepper Motor*: A programmable stepper motor is used for the hoisting mechanism. Specifications include:

  - Make & Model: NI ISM-7411
  - Input Voltage: 24-48 Vdc
  - Holding Torque: 0.88 N.m

- Steps/Rev: Programmable, set to 25000
- NEMA Size: 23

**Figure 33. National Instruments ISM-7411**

### 3.2.3 Data Acquisition and Software

This section talks about the hardware and software used to acquire and process the data collected from the setup.

3.2.3.1 National Instruments cDAQ-9178

The system design is based around the NI cDAQ-9178 data acquisition system which is a modular DAQ device that can be customized in terms of the I/Os to better fit the system design and application. The cDAQ chassis has eight slots where different C series I/O modules can be connected. The following I/O modules are used:

- NI 9201: Voltage input module
  - Voltage range: -10V to 10V
  - Analog input resolution: 12 bits
  - Maximum sampling rate: 500kS/s

- NI 9263: Voltage output module
  - Voltage range: -10V to 10V
  - Analog input resolution: 16 bits
  - Maximum sampling rate: 100kS/s

- NI 9361: Counter input module
  - Voltage range: 0V to 24V, 0V to 24V
  - Maximum sampling rate: 1000kS/s


**Figure 34. NI cDAQ-9178 and C series modules**

A control system panel shown in figure 35 was designed and built. This makes the control hardware setup modular, i.e., makes it much easier to make changes like changing or adding more sensors to the control system.

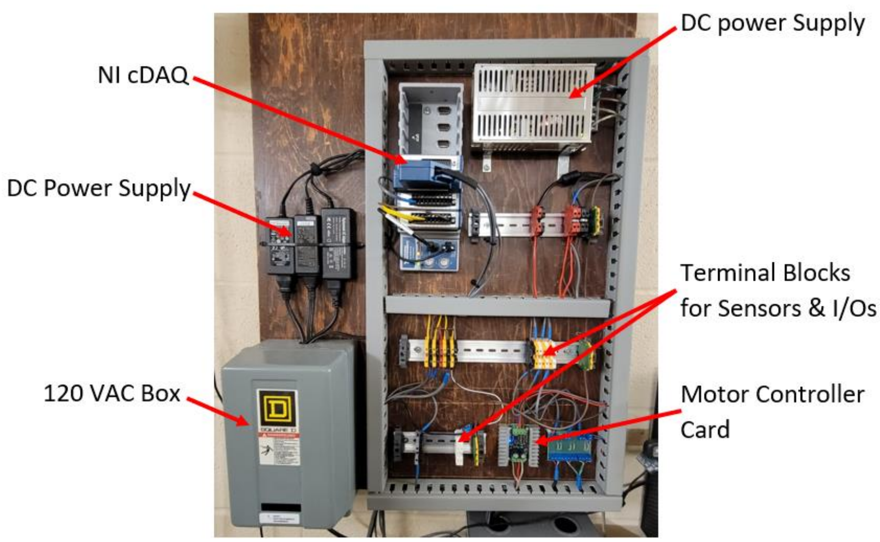


**Figure 35. Control Panel**

3.2.3.2 Process Meter/Signal Conditioner

The two strain-gauge based sensors: load cell and torque sensor have a signal output in millivolts(mV). Thus, a signal conditioner must be used for each of these sensors. The signal conditioner scales the output to the 0-10 V range which can be read by the data acquisition device.

Three process meters, with built in signal conditioners and programmable displays, are used in the setup. The raw output from the load cell, torque sensor and the displacement sensor is passed through the process meters before it goes to the data acquisition device. This allows for real time measurement of WOB, torque and displacement on the process meter display. Furthermore, in the case of the load cell and the torque sensor, it scales the output before it reaches the DAQ.

#### 3.2.3.3 National Instruments LabVIEW

LabVIEW is a system design platform developed by National Instruments which uses graphical programming language to design systems. It is widely used for data acquisition, instrumentation and control and automation, and is very easy to integrate with NI DAQ devices and many other data acquisition platforms. It supports various communication protocols to send and receive data.

LabVIEW has been used to control and monitor the setup and to develop the human machine interface (HMI). It collects data from the cDAQ-9178, processes it and then displays the process parameters on the HMI and provides the ability to control the setup. Screenshots of the code are shown in Appendix B.

### 3.2.4 Sensor Calibration

The load cell, torque sensor and the displacement sensor have a linear response to the input and were calibrated experimentally using known inputs and recording the respective voltage output responses to the inputs. Linear plots for the three sensors were generated and the equations of the trend line were used to derive the three physical quantities: hook load, torque and displacement. The equations are listed below:

Load cell equation:

$$y = 134.21x - 120.24 \quad \ldots\ldots\ldots\ldots\ldots\ldots (28)$$

Torque sensor equation:

$$y = 1.5935 - 1.4591 \quad \ldots\ldots\ldots\ldots\ldots\ldots (29)$$

Displacement sensor equation:

$$y = 125.85x - 250.57 \quad \ldots\ldots\ldots\ldots\ldots\ldots (30)$$

The plots generated for the three sensors are shown in figure 36, 37 and 38.

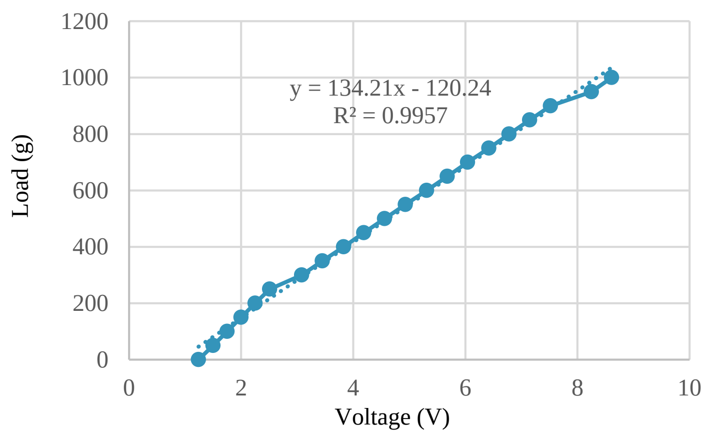


**Figure 36. Load Cell Calibration**

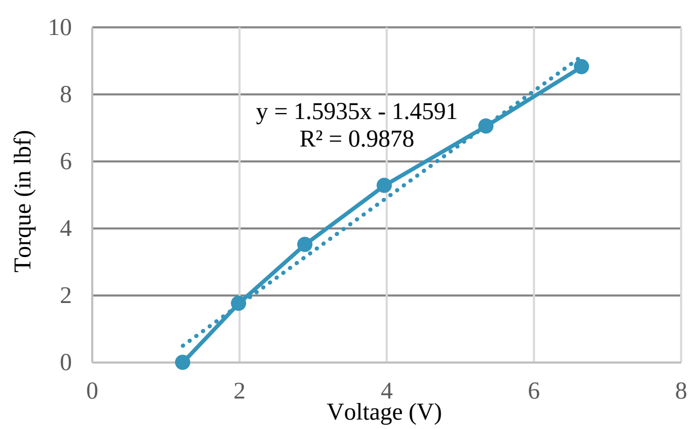


**Figure 37. Torque Sensor Calibration**

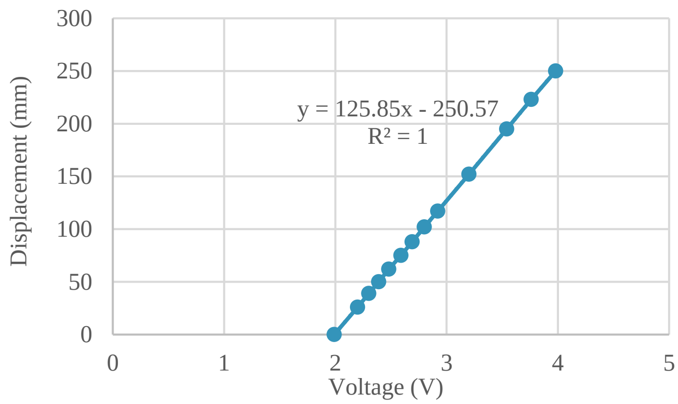

**Figure 38. Displacement Sensor Calibration**

### 3.2.5 Calculating RPM using Rotary Encoder data

A rotary encoder is an electro-mechanical device which coverts angular rotation of a shaft to an electrical signal. The rotary encoders used have a digital output, one complete rotation of the shaft generates 500 digital pulses. These digital pulses can be used to calculate the RPM with which the shaft rotates (Briz, et al., 1994). The method to derive RPM from the digital signal is described below.

$$\Delta p = p_{t2} - p_{t1} \quad \dots\dots\dots\dots\dots\dots (31)$$

where Δp is the change in the pulse count of the encoder from time ‘t1’ to time ‘t2’ (time in ms).

$$t = t2 - t1$$

$$PPR\ pulses \rightarrow\ 1\ revolution$$

PPR is the total number of pulses the encoder generates on completing one revolution of the shaft. Therefore,

$$1\ pulse \rightarrow \frac{1}{PPR}\ revolutions$$

$$\Delta p\ pulses \rightarrow \frac{\Delta p}{PPR}\ revolutions$$

$$t\ ms \rightarrow \frac{\Delta p}{PPR}\ revolutions$$

$$1\ min \rightarrow \frac{\Delta p \times 60000}{PPR \times t}\ revolutions$$

The left side of the equation is the RPM of the encoder shaft. Therefore,

$$RPM = \frac{\Delta p \times 60000}{PPR \times t}$$

$$RPM = \frac{\Delta p \times 60000 \times f}{PPR} \quad \ldots\ldots\ldots\ldots\ldots\ldots (32)$$

where,

$\Delta p$ is the total number of pulses generated in time 't' (in ms),
$PPR$ is the pulses per revolution of the encoder,
$f$ is the sampling frequency in Hz.

### 3.2.6 Human Machine Interface

The setup is monitored and controlled by a human machine interface (HMI) designed using LabVIEW. Figure 39 shows a screenshot of the HMI. The layout of the HMI is described in this section.

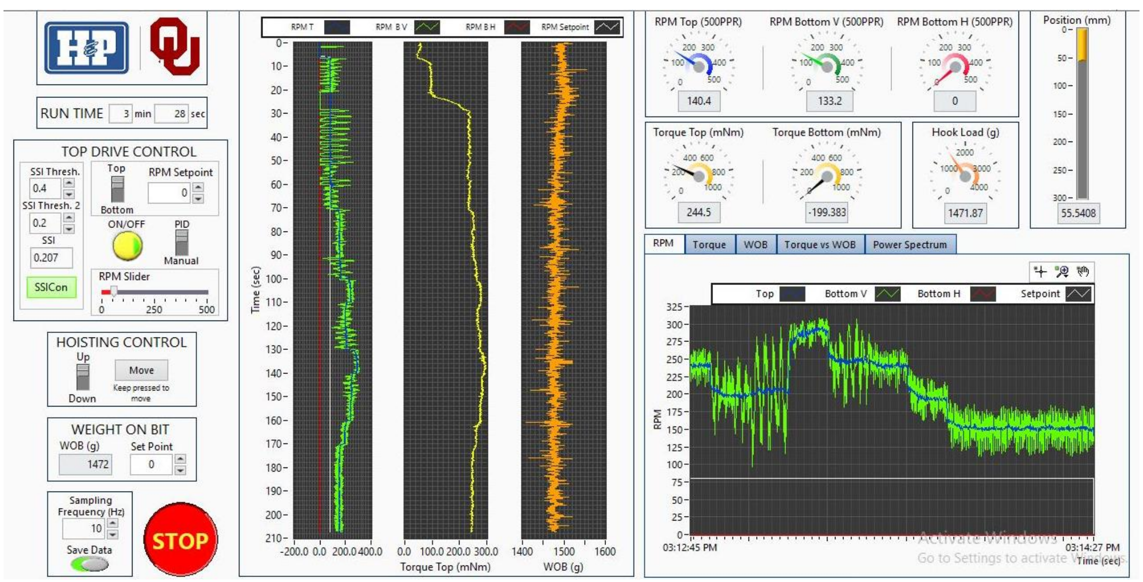


**Figure 39. Human machine interface**

On the right side of the HMI, the following setup controls are available:

- Top Drive Control: This is where the RPM of the top drive motor can be set. The RPM can be set by either an open-loop manual control or by a closed-loop. The RPM control is discussed in more detail in a later section.

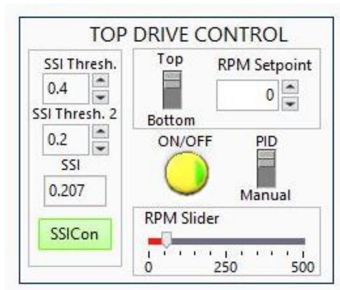


**Figure 40. Top drive control**

- Hoisting Control: The stepper motor, which is a part of the hoisting system, is controlled from here. Lead-screw mechanism, coupled with the stepper motor, moves the top assembly upwards with a clockwise motion of the stepper motor, thus increasing the hook-load. When the stepper motor is rotated counter-clockwise the top assembly moves downwards and the hook-load decreases.

- Sampling Frequency: Sampling frequency for data acquisition required for an experimental test run can be set here. An option to save or not save experimental data is also available.

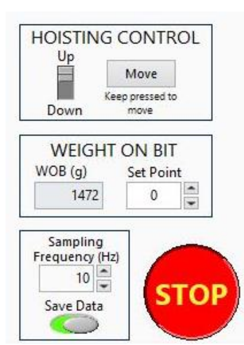


**Figure 41. Hoisting control and sampling frequency input**

The middle and the left section of the HMI is for data monitoring. This is where all the real-time data from different sensors and various dynamic drilling parameters can be observed.

- Vertical plots: the real-time RPM, torque and WOB (weight on bit) measurement are plotted vertically (time on y-axis), like the measurement plots on an actual driller's display in the field.

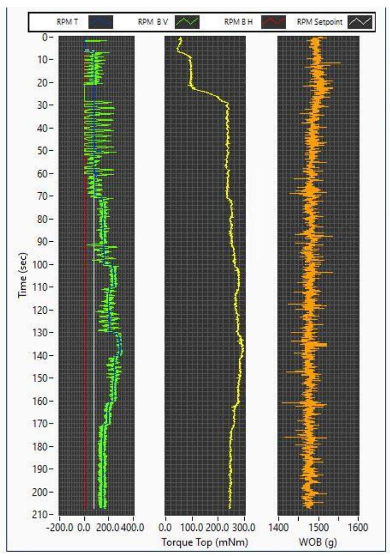


**Figure 42. Real-time data plots**

- Gauges: On the top right side the different drilling parameters are displayed with gauges and digital displays.

- Multiple tabs: Multiple tabs are available on the HMI, each of which focuses on a specific drilling parameters.

- Power spectrum/frequency domain plots: Real-time power spectrum/frequency domain plots of drilling parameters are also available on the HMI. This allows for frequency domain analysis for any of the drilling parameters and thus can be used to analyze the frequency components in the system. For example, the RPM power spectrum can be used to analyze the different vibration frequencies of the drillstring.

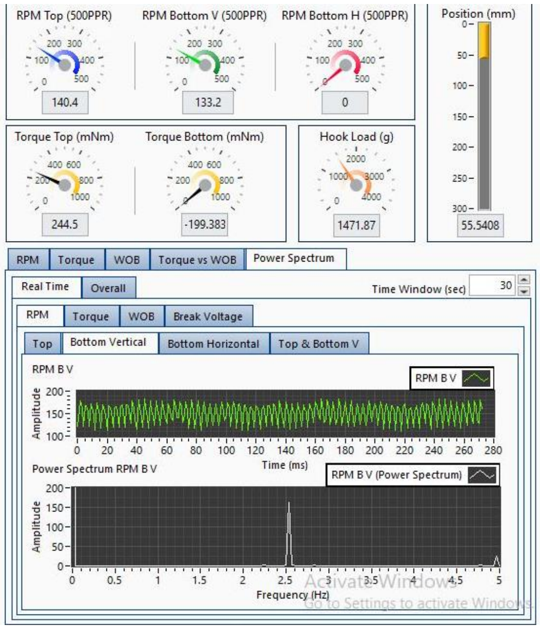


**Figure 43. Real-time data gauges, tabs and power spectrum**

The HMI for the bit-rock simulator is shown in figure 44. The parameters of the bit-rock models ($a_1$, $a_2$, $a_3$) can be changed using this HMI. The HMI also shows the coefficient of friction vs RPM plot for the set values of the bit-rock model in real-time.

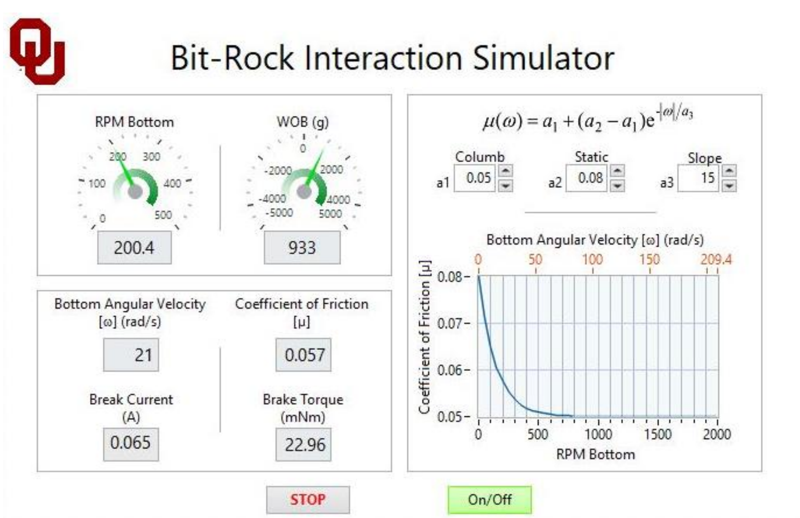


**Figure 44. Bit-rock simulator HMI**

### 3.3 Controlling the Experimental Setup

As described in section 3.1, there are several individual systems on a drilling rig that control the different aspects of the drilling process. Top drive/surface RPM and weight-on-bit/hook load are two important parameter that are controlled to optimize drilling (Wu et al., 2010). The experimental setup is capable of controlling the RPM and hook load. Control systems can be open-loop or closed-loop, as mentioned earlier. The hook load control for the setup is open loop, i.e., it has to be manually set and adjusted. To control the top drive RPM both, open-loop and the closed-loop, control systems were implemented. Firstly, a simple open-loop RPM control was designed followed by different closed-loop control strategies. This section describes the surface RPM control systems designed for the setup.

#### 3.3.1 Open-loop RPM Control

For the open-loop RPM control an analog output channel from the cDAQ output module was used. The voltage output from the module, set to an output range of 0V to 5V, was connected to a motor driver card which amplifies the control signal to run the motor. A block diagram of this control strategy is shown in figure 45. The input voltage from the analog output module (ranging between 0-5V) corresponds to a motor RPM. Experimental calibration of this system carried out to find a relationship between the input voltage and RPM is discussed in Appendix A.

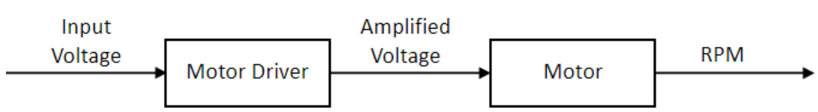


**Figure 45. Open-loop RPM control block diagram**

### 3.3.2 Feedback RPM Control

To implement a closed-loop control PID control algorithm was implemented. For the feedback signal the RPM of the top drive was used. Bottom-hole RPM, which is readily available in the setup, was also used as the feedback signal but because of excessive mechanical noise in the signal the controller response was not stable. Furthermore, it is not possible to get access to real-time bottom-hole RPM at high sampling frequencies in real world field applications. Because of this reason surface/top drive RPM signal was used as the feedback for the PID controller. Figure 46 shows the block diagram for this PID RPM controller.

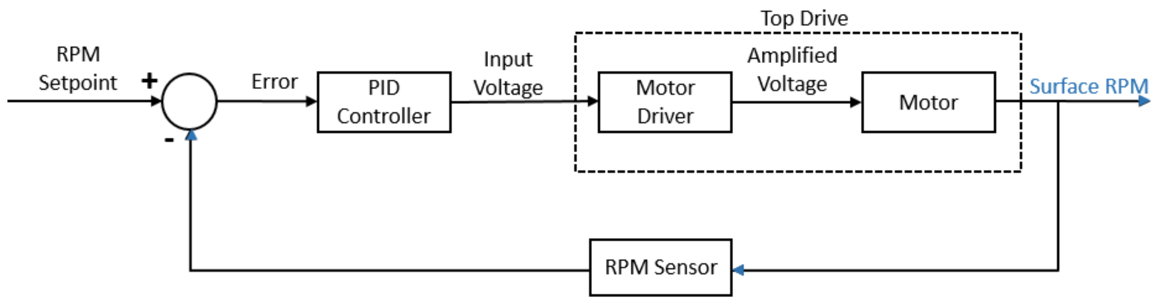


**Figure 46. Feedback RPM control**

The PID controller adjusts the input signal to the motor based on the feedback from the RPM sensor (rotary encoder) to keep the RPM as close to the setpoint as possible. With this a closed-loop feedback system for the surface RPM control was achieved. Tuning this controller is discussed in Appendix A.

### 3.3.3 Dual Feedback Control (Surface RPM and Surface Torque)

A second feedback control loop was added to the existing RPM feedback loop. In this second loop surface torque was used as the feedback signal with a proportional gain ($K_P$') controller. The response of the two loops was cascaded together and used as the control signal for the top drive. Figure 47 shows the block diagram for this controller.

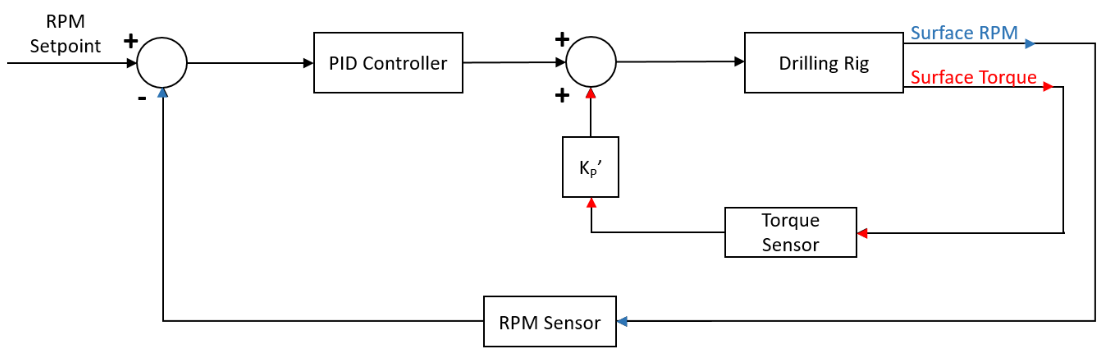


**Figure 47. Dual feedback control**

### 3.3.4 SSI-based Auto-tuning Control

To improve on the dual-feedback controller, an auto-tuning feature based on the stick-slip index (SSI) was incorporated in the control design. SSI, which is the most commonly used matric used to evaluate torsional oscillation severity, has been discussed in section 2.1.3. A downhole tool capable of measuring the bit RPM/angular velocity and calculating the SSI using equation 1 is required for this control strategy. The SSI computed downhole can be transmitted to the surface at a sampling frequency of 0.1 Hz or even lower using the existing MWD technology. Once the SSI measurement reaches the surface, the auto-tuning of the torque feedback loop gain ($K_P$') can be done using the decision tree shown in figure 49. This SSI feedback controller (SSIF controller) operates with an SSI range (between a low threshold value, 'SSI Low', and a high threshold value, 'SSI High') which can be adjusted. The algorithm block diagram for the SSI based auto-tuning is shown in figure 50.

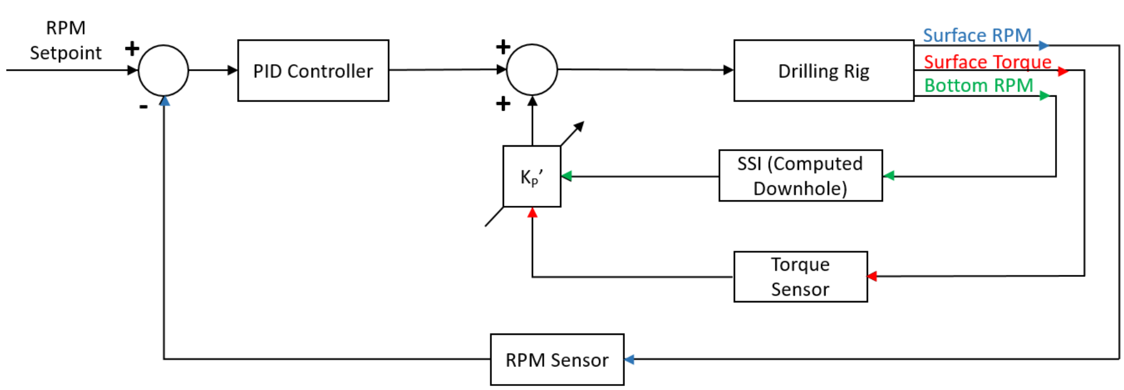


**Figure 48. SSI-based auto-tuning control**

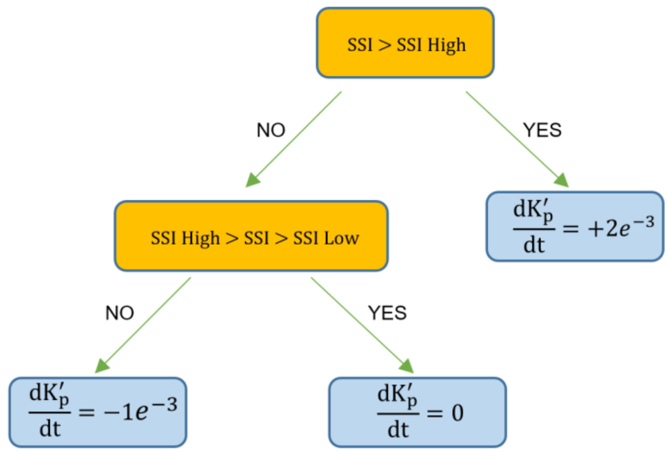


**Figure 49. Auto-tuning decision tree**

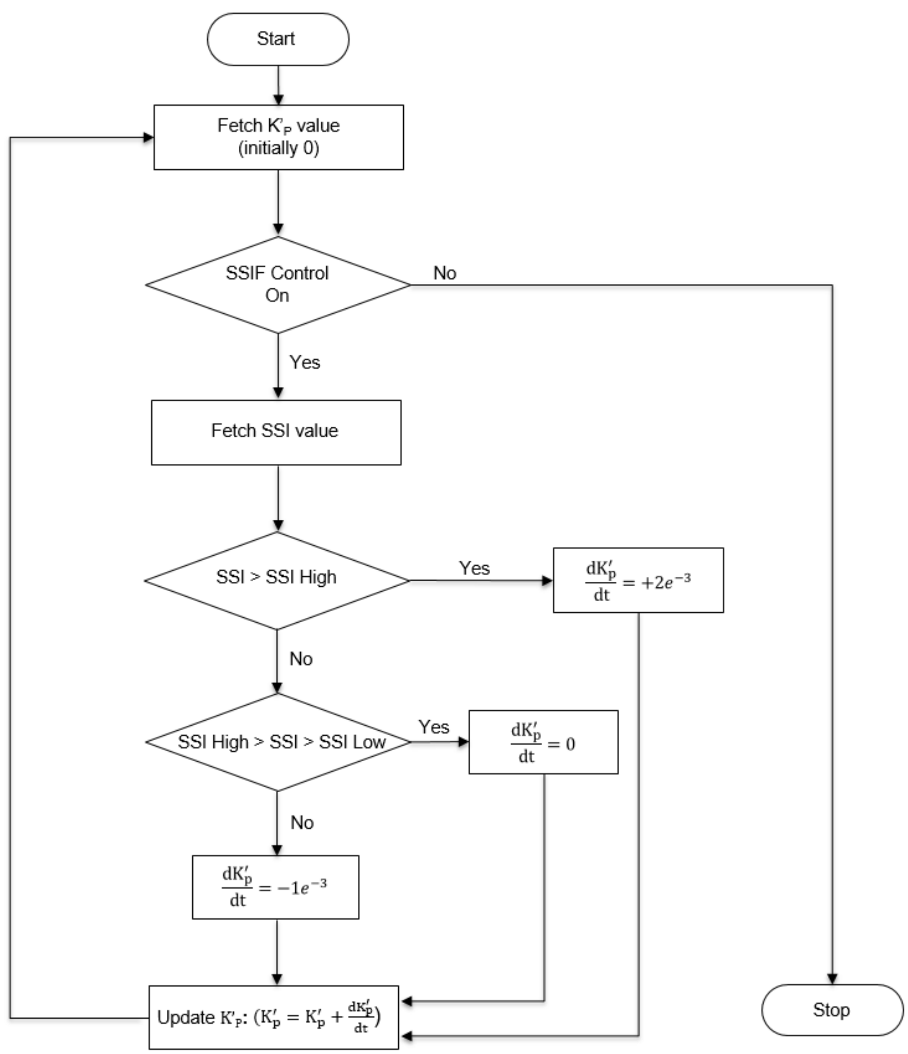


**Figure 50. Block diagram for auto tuning algorithm**

# Chapter 4: Results and Discussions

## 4.1 Design of Experiments

Extensive testing was conducted for calibrating and checking the hardware and software features that were added and updated continuously, and for tuning and analyzing the performance of the four RPM controllers (open-loop RPM control, feedback RPM control, dual feedback control and, SSI-based auto-tuning control). Out of all the tests that were conducted, data from over 700 reference tests was saved and analyzed. Table 6 shows a breakdown of the reference tests.

**Table 6. Breakdown of tests**

| Testing for | Number of tests |
|---|---|
| Hardware & Software Features | 258 |
| Open-loop Control | 123 |
| Feedback RPM Control | 167 |
| Dual feedback | 80 |
| SSI Feedback | 74 |
| **Total =** | **702** |

The four RPM control techniques were experimentally tested. The following system parameters and conditions were varied to conduct these tests.

- RPM: set manually or automatically by the controller
- Hook load: set manually
- Well configuration: vertical or directional
- Stick-slip inducing friction/force: mechanical friction or bit-rock model simulator

The design of experiment to test the controllers is graphically shown in figures 51 to 54.

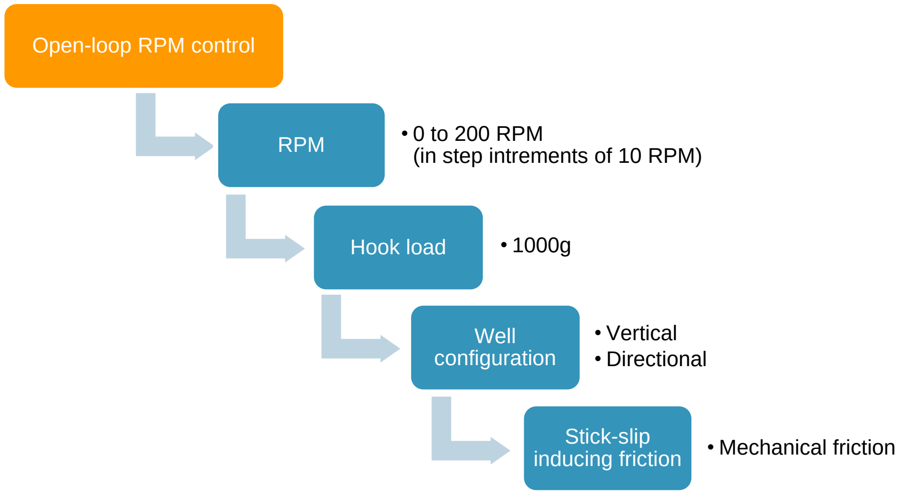


**Figure 51. Experiment design for open-loop RPM control**

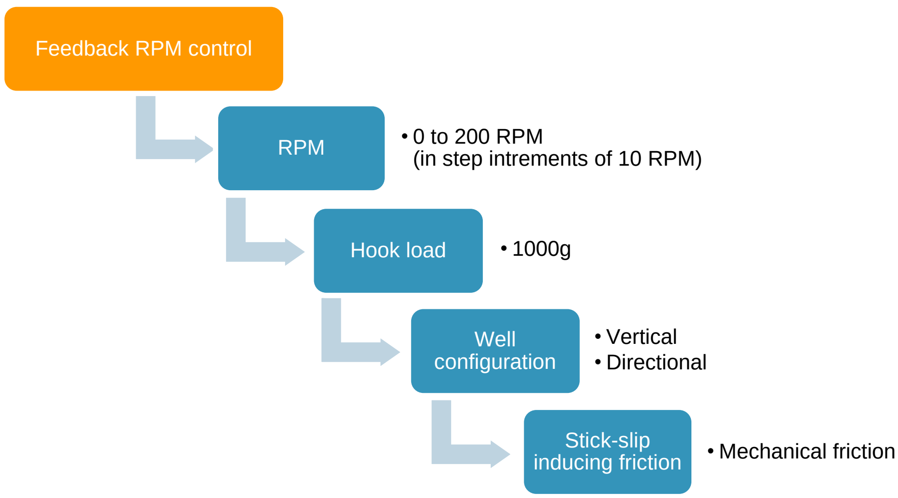


**Figure 52. Experiment design for feedback RPM control**

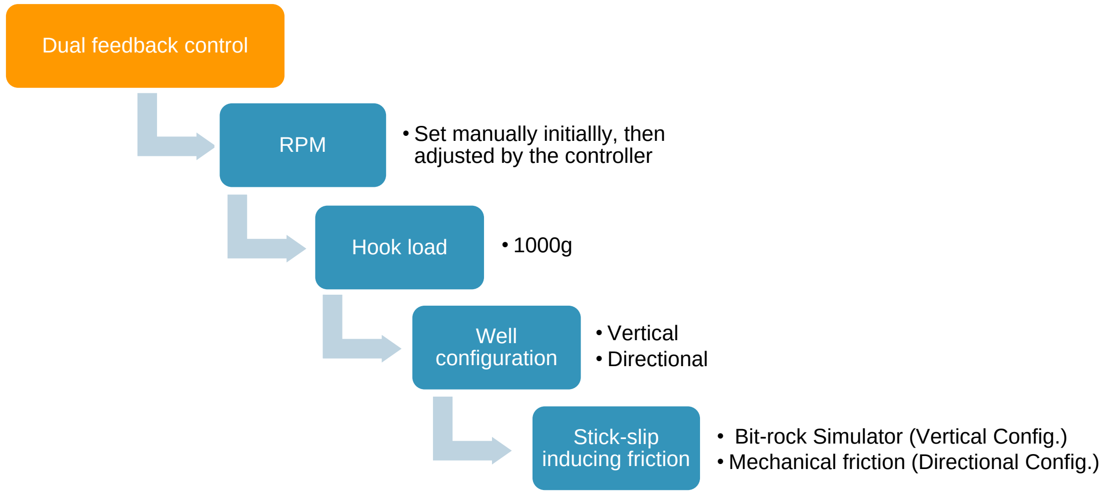


**Figure 53. Experiment design for dual feedback control**

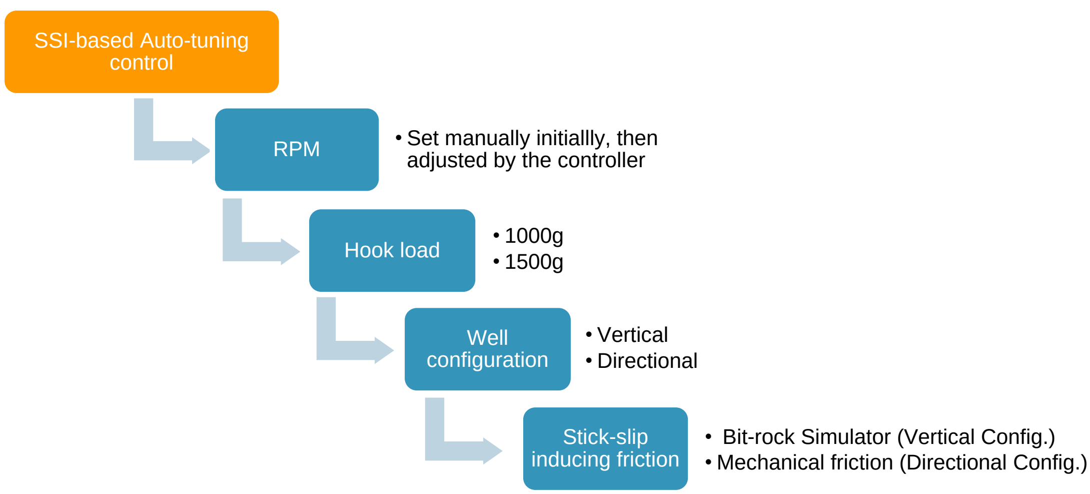


**Figure 54. Experiment design for SSI-based auto-tuning control**

### 4.2 Open-loop RPM Control

The first control strategy that was implemented on the setup was the open-loop RPM control. In this, the RPM is increased (or decreased) by increasing (or decreasing) the voltage input to the motor. This control strategy is still very common in drilling rigs around the world where the driller makes changes in the RPM to optimize the drilling process based on pure experience.

The open loop RPM control was tested on the experimental setup and the results obtained are shown in figures 55 and 56. Figure 55 shows the results for the vertical well configuration, whereas figure 56 shows the results for the directional well configuration. Both the tests were conducted at a hook load of 1000g. The bit-rock simulator was not used for these tests and the mechanical/contact friction in the system (present throughout the length of the drill-string) was sufficient to produce stick slip. The RPM was initially set to 40, and then incremented by 10 every 10 seconds. The RPM was set by moving the 'RPM Slider' control on the HIM (figure 40).

For the vertical well configuration test (figure 55), stick-slip can be observed from the start of the test till around the 160 seconds mark. The RPM of the BHA (in yellow) oscillates between 0 to as high as 250 during this time window. Even though the surface RPM is incremented up to 110, it is not sufficient to overcome stick-slip. After 160 seconds mark, stick-slip is removed from the system at 120 RPM and above.

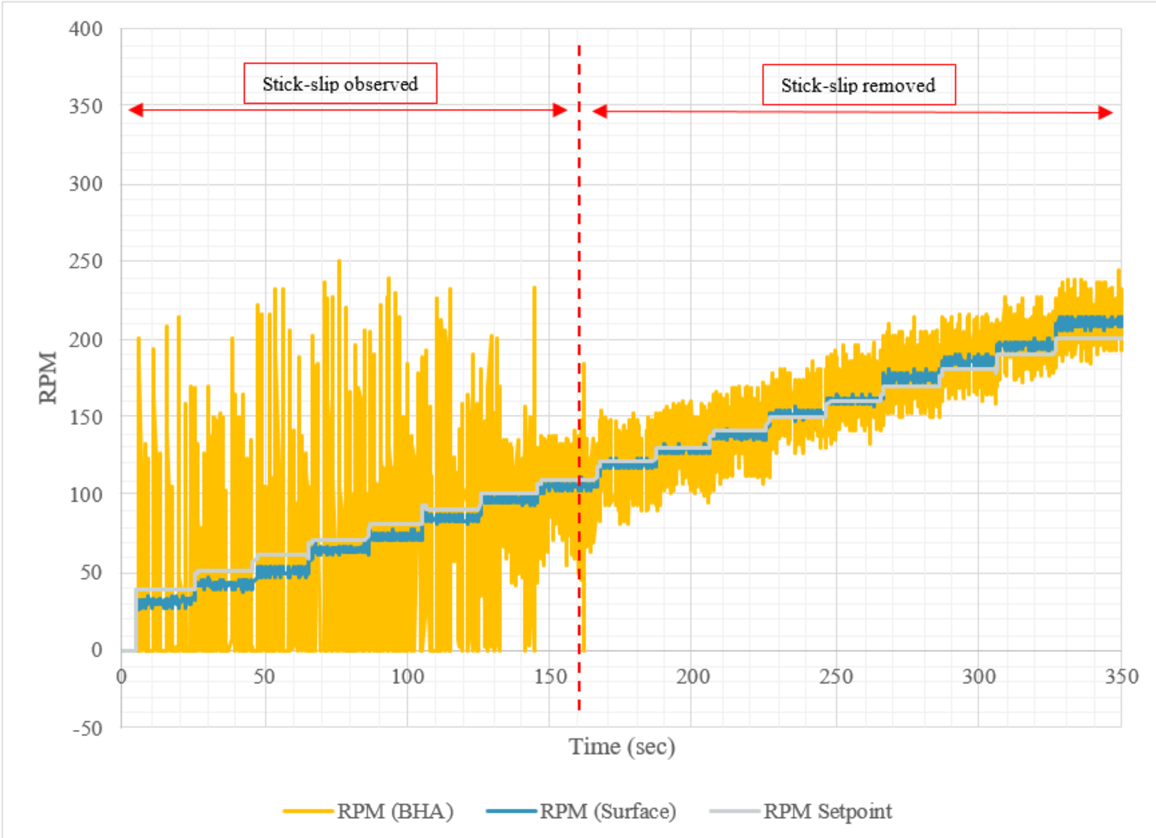


**Figure 55. Open-loop RPM control in vertical well configuration**

The same test was conducted again but this time for the directional well configuration (figure 56). In this case stick-slip is present till the 320 seconds mark. For RPM above 170 the stick-slip is removed but sever torsional oscillations are still present in the system. Because of a complex geometry, directional wells have much higher opposing friction in the well compared to a vertical well. Because of this reason a higher RPM value is needed in the directional well to overcome stick-slip.  The friction is also high enough to produce negative RPM in the drillstring as can be seen in figure 56.

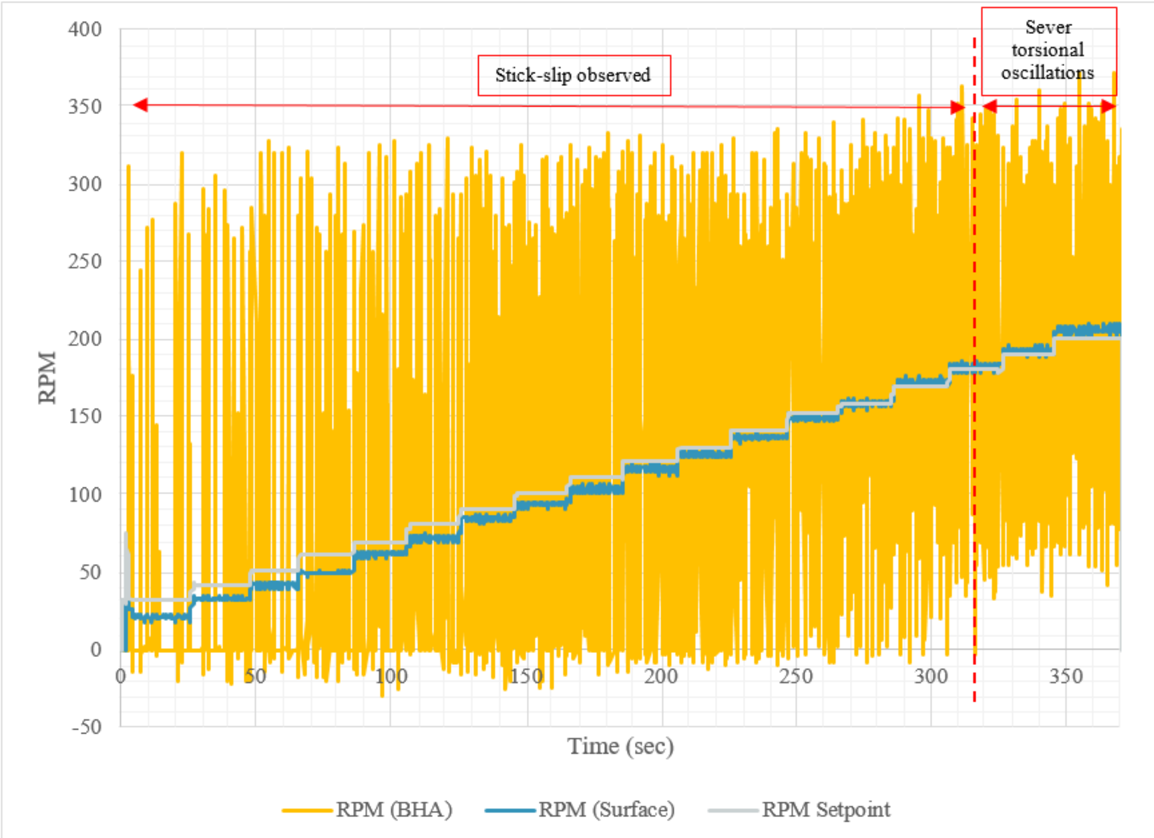


**Figure 56. Open-loop RPM control in directional well configuration**

Although the open-loop control is easy to implement, it has a drawback. Because of the absence of a feedback signal, the actual surface RPM changes based upon the torque acting on the drillstring for a constant value of input voltage. For example, at 2V the RPM should ideally be around 195 (based on calibrations shown in Appendix A) but if there is a higher torque acting on the drillstring the RPM will be lower. In this case the input voltage has to be increased manually to maintain an RPM of 195. Another thing that can be observed from the tests in figure 55 and 56 is that the open-loop control does not have a good set point tracking ability. These problems can be overcome by introducing a feedback loop in the system.

### 4.3 Feedback RPM Control

To overcome the shortcomings of the open-loop control, the PID control with a surface RPM feedback was used to implement a closed-loop RPM control. The testing conditions and procedure were same as that for the open loop control. The PID RPM control was used, and the RPM was incremented by 10 every 10 seconds.

Results for the vertical well configuration are shown in figure 57. Stick-slip is present for RPM below 100 and for RPM value of 100 and above stick-slip is mitigated.


**Figure 57. Feedback RPM control in vertical well configuration**

For the directional well test, higher friction in the system is noticed again. Stick-slip is observed RPM below 170 and for RPM values of 170 and greater stick-slip is removed but server torsional oscillations exist.


**Figure 58. Feedback RPM control in directional well configuration**

The feedback RPM control has much better set point tracking compared to the open-loop control. This is evident in figures 57 and 58 where the surface RPM (in blue) is much closer to the RPM set point (in grey) compared to figure 55 and 56.

Tests with the first two control strategies (open-loop control and feedback RPM control) conducted thus far, highlight the fact that with an increase in RPM stick-slip is eventually removed from the system. But with these controllers the RPM still has to be set manually. Surface RPM cannot be used to detect stick-slip at the bottom hole, therefore, just the surface RPM feedback cannot be used to design an automatic stick-slip controller. Torque data from the vertical and directional tests was analyzed and as seen in figures 59 and 60, it provides a better representation of stick-slip downhole. It can be observed in these plots that the torque (in black) oscillations and peaks match the downhole RPM (in yellow) oscillations and peaks. Based on this data, torque feedback was added to the next control strategy.

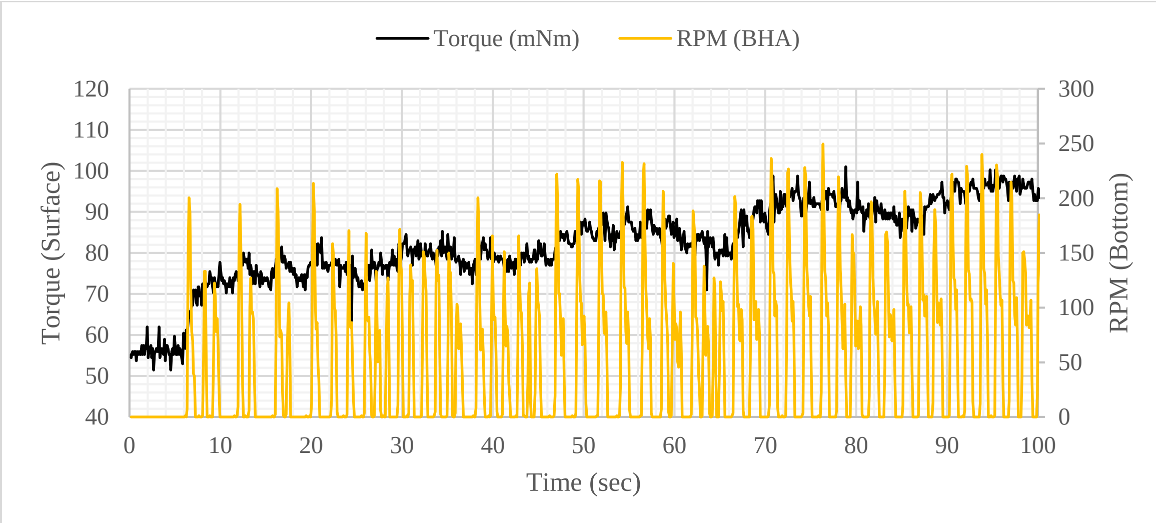


**Figure 59. Torque fluctuations in vertical well configuration**

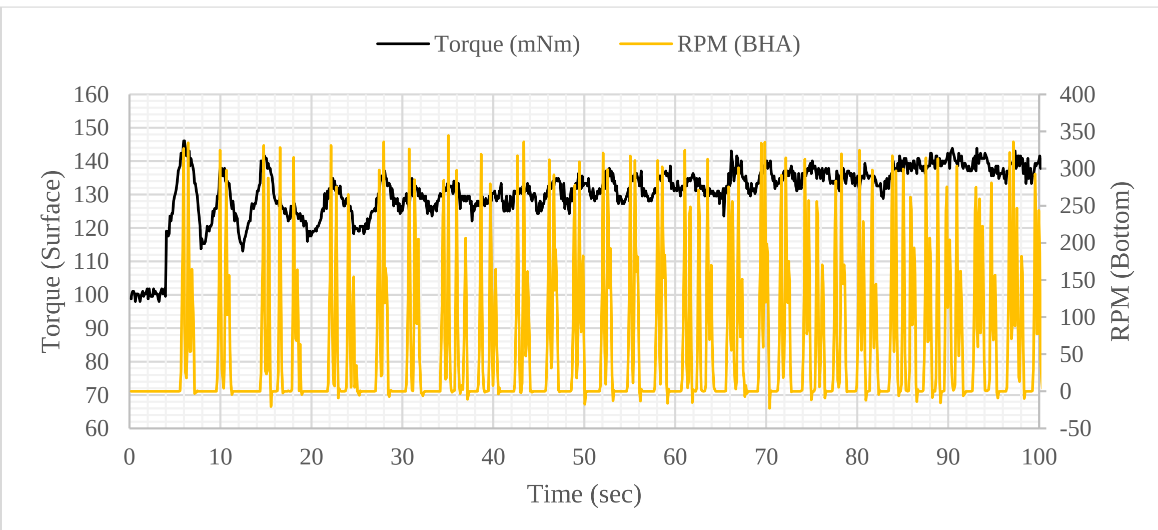


**Figure 60. Torque fluctuations in directional well configuration**

## 4.4 Dual Feedback Control

Since surface torque was found to better represent the downhole conditions, a surface torque feedback loop with a proportional gain ($K_p$') was added to the feedback RPM controller to form the dual feedback controller. This controller was tested for both the well configurations, i.e., vertical and directional at a hook load of 1000g. The testing procedure and results are described below.

The testing procedure for the vertical configuration is summarized in table 7 and the result is shown in figure 61. At 5 seconds the RPM was set to 80. From the bottom RPM data, it can be observed that a surface RPM of 80 was sufficient to avoid stick-slip. At 20 seconds the bit-rock simulator was turned on with the parameters set to: a1=0.05, a2=0.08, a3=15, which resulted in an increase in the downhole friction causing stick-slip. Around the 60 second mark, gain $K_p$', which was initially at zero, was set to 0.008. This increased the surface RPM to 240 and stick-slip was mitigated. At 90 seconds, to mimic an increase in the hardness of the rock formation being drilled, parameter a2 of the bit-rock model was increased to 0.1. Because of this, severe torsional oscillations were induced in the system. Gain $K_p$' was then increased to 0.009 and as a result torsional oscillations were reduced.

**Table 7. Testing procedure for Dual feedback control in vertical well configuration**

| Sec | Action |
|---|---|
| 5 | RPM set to 80 |
| 20 | Bit-Rock Sim. Parameters set to a1=0.05, a2=0.08, a3=15 |
| 60 | Gain Kp' set to 0.008 |
| 90 | Bit-Rock Sim. Parameters set to a1=0.05, a2=0.1, a3=15 |
| 110 | Gain Kp' set to 0.009 |

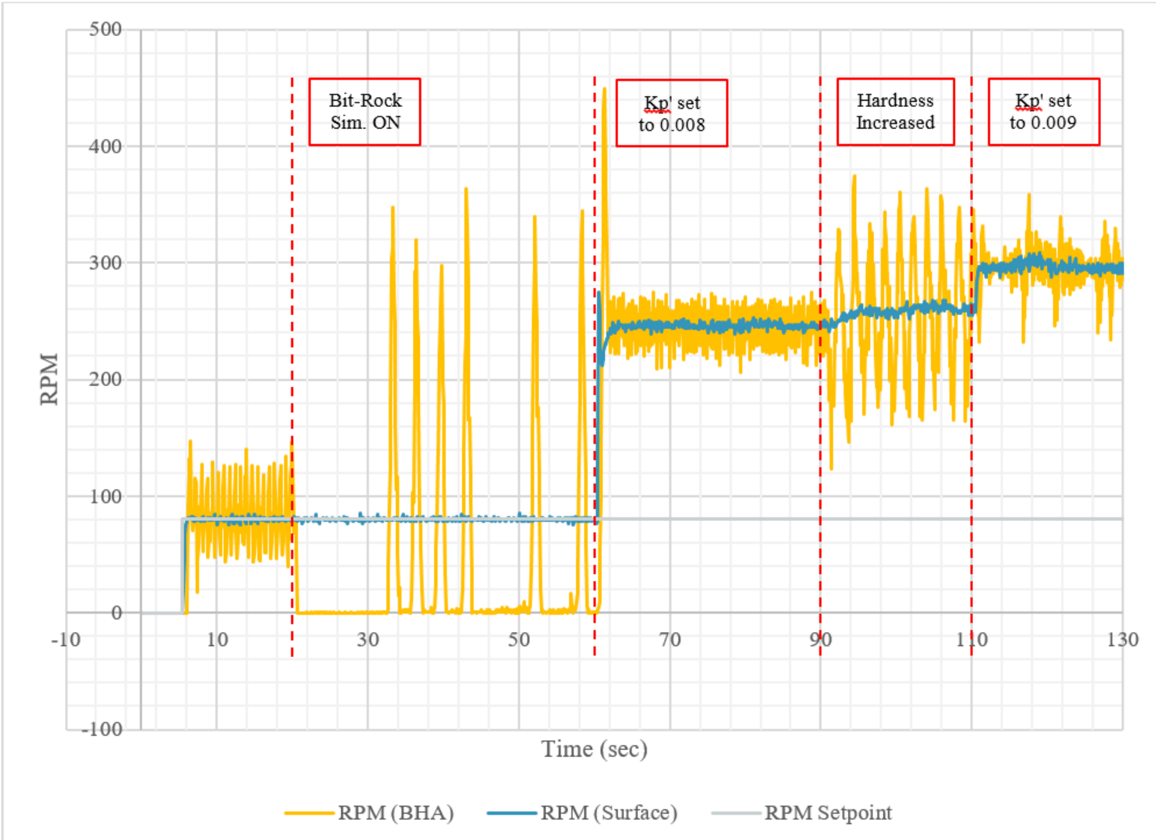


**Figure 61. Dual feedback control in vertical well configuration**

It must be noted here that the bit-rock interaction simulator has not yet been integrated with the directional well setup, and the stick-slip induced in this setup is purely a result of the mechanical friction in the system. Table 8 summarizes the testing procedure for the dual feedback controller in directional well configuration and the corresponding results are shown in figure 62. The test starts with an RPM setpoint of 40 at 5 seconds followed by setting the RPM to 80. Stick-slip can be observed at both these RPM levels. Gain $K_p'$ (initially at 0) was set to 0.008 at 50 seconds but stick-stick can still be noticed in the system. $K_p'$ was then increased by 0.001 after every 10 seconds starting at 70 seconds into the test. With increasing the gain, the surface RPM rises, and stick-slip is eventually mitigated.

**Table 8. Testing procedure for Dual feedback control in directional well configuration**

| Sec | Action |
| --- | --- |
| 5 | RPM set to 40 |
| 25 | RPM set to 80 |
| 50 | Gain Kp' set to 0.008 (initially at 0) |
| 70 | Gain Kp' set to 0.009 |
| 80 | Gain Kp' set to 0.010 |
| 90 | Gain Kp' set to 0.011 |
| 100 | Gain Kp' set to 0.012 |
| 110 | Gain Kp' set to 0.013 |

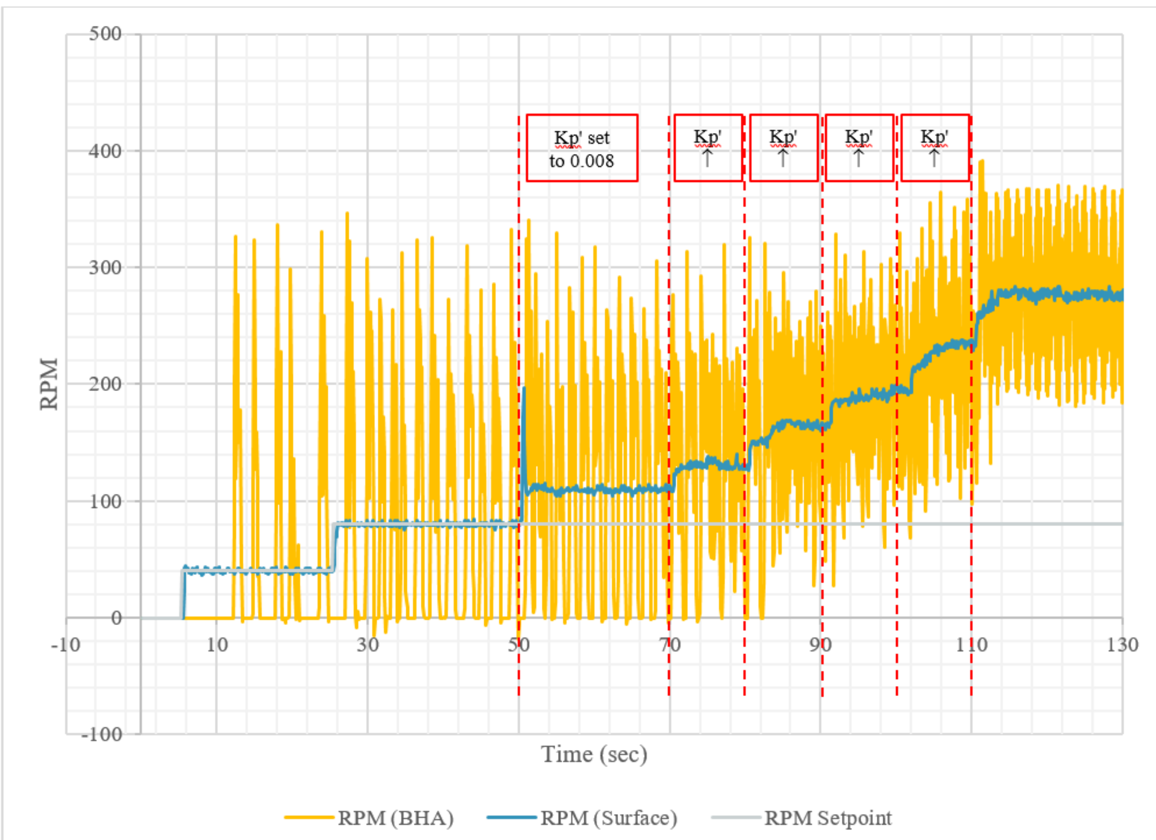


**Figure 62. Dual feedback control in directional well configuration**

These results showed that increasing the torque feedback loop gain ($K_p$') resulted in mitigation of stick. But the gain was manually increased.

### 4.5 SSI-based Auto-tuning Control

Since stick-slip was mitigated by manually changing the gain $K_p'$ of the dual feedback controller, a new technique had to be formulated to automatically adjust this gain. For this, an auto-tuning control based on the stick-slip index (SSI) was designed. As described in section 3.3.4, this controller requires a low and high threshold value for the SSI. Testing for this controller was conducted with three different sets of SSI threshold values (0.2-0.4, 0.3-0.5, 0.4-0.6) for vertical and directional well configuration. Also, the tests were conducted with two different hook load values (1000g and 1500g).

#### 4.5.1 Vertical well configuration

The SSI feedback control was tested on the vertical well setup with the bit-rock interaction simulator. Tables 9 and 10, list the steps followed in these tests. As mentioned, these tests were conducted for three sets of SSI threshold values and each test was done for two different hook load values. All tests described here follow the procedure listed in table 9, except for the test with SSI threshold 0.4-0.6 and hook load 1000g, which follows table 10. At 5 seconds the RPM is set to 80. Then 20 seconds into the test the bit-rock simulator is turned on with the parameters set to a1=0.05, a2=0.07, a3=15, and the SSI feedback control is turned on at 40 seconds. To mimic an increase in formation hardness parameter a2 of the bit-rock model is increased to 0.008 at 90 seconds. The hardness in increased again at 120 seconds by setting a2 to 0.009. At 150 seconds (170 seconds for one test) a softer formation is mimicked by setting the bit-rock simulator parameters to a1=0.05, a2=0.06, a3=15.

**Table 9. Testing procedure for SSIF controller in vertical well configuration**

| Sec | Action |
|---|---|
| 5 | RPM set to 80 |
| 20 | Bit-Rock Sim. Parameters set to a1=0.05.a2=0.07,a3=15 |
| 40 | SSI Feedback controller turned ON |
| 90 | Bit-Rock Sim. Parameters set to a1=0.05.a2=0.08,a3=15 |
| 120 | Bit-Rock Sim. Parameters set to a1=0.05.a2=0.09,a3=15 |
| 150 | Bit-Rock Sim. Parameters set to a1=0.05.a2=0.06,a3=15 |

**Table 10. Testing procedure for SSIF controller in vertical well configuration**

| Sec | Action |
|---|---|
| 5 | RPM set to 80 |
| 20 | Bit-Rock Sim. Parameters set to a1=0.05.a2=0.07,a3=15 |
| 40 | SSI Feedback controller turned ON |
| 90 | Bit-Rock Sim. Parameters set to a1=0.05.a2=0.08,a3=15 |
| 120 | Bit-Rock Sim. Parameters set to a1=0.05.a2=0.09,a3=15 |
| 170 | Bit-Rock Sim. Parameters set to a1=0.05.a2=0.06,a3=15 |

The different steps of the test procedure are marked with red markers on all the data plots. As before, the initial RPM set point is in grey, surface RPM in blue and the downhole RPM, i.e., the bit/BHA RPM is in yellow. Stick-slip index (SSI) is also plotted with respect to time for the corresponding test results.

- *SSI threshold: lower = 0.2, higher = 0.4 at hook load = 1000g*

The RPM is initially set to 80 and the bit-rock simulator is turned on at 20 seconds. Stick-slip is observed which is also characterized by high SSI values. To counter this, the SSIF controller is turned on 40 seconds. The controller takes around 30 seconds to adjust the gain and at the 70 second mark, the RPM set by the controller is sufficient to remove the stick slip. The controller to torsional oscillations in the system resulting from increasing formation hardness and adjusts the RPM to reduce the oscillations.


**Figure 63. SSIF controller response in vertical well configuration (0.2-0.4 SSI thresholds, 1000g hook load)**

- *SSI threshold: lower = 0.2, higher = 0.4 at hook load = 1500g*

The same testing procedure when followed with a hook load value of 1500g shows similar results. The controller is successful in combating stick-slip and torsional oscillations caused due to increasing formation hardness. The RPM set by the controller are lower in this case, specially towards the end when the hardness is reduced. The system can be observed to be stable at an RPM of 150, instead of 250 in the previous test, which is a result of increasing hook load.

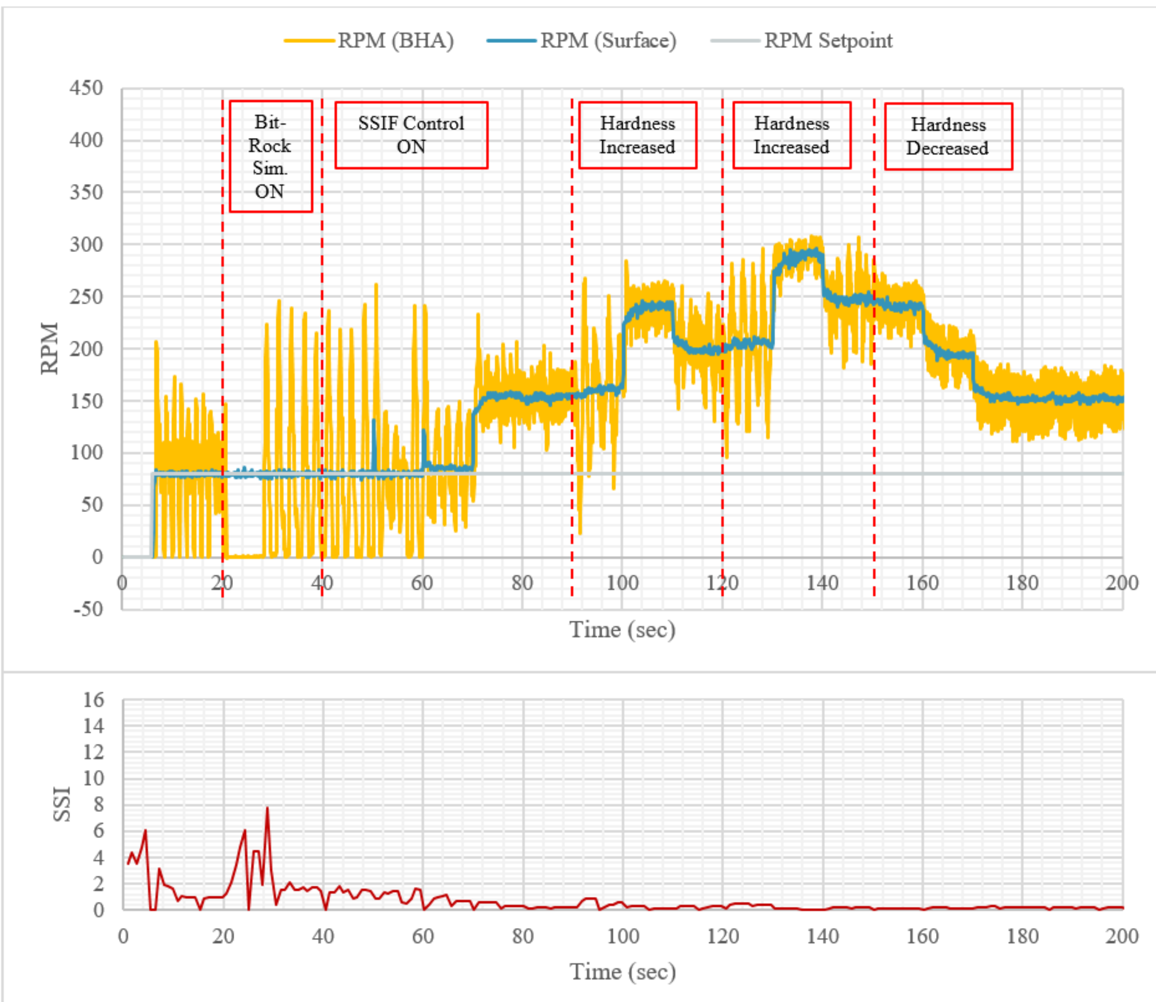


**Figure 64. SSIF controller response in vertical well configuration (0.2-0.4 SSI thresholds, 1500g hook load)**

- *SSI threshold: lower = 0.3, higher = 0.5 at hook load = 1000g*

The SSI threshold values were increased by 0.1 for this test. Stick-slip present in the system is again removed by the controller around 30 seconds after it is turned on. The RPM set by the controller at the hardest formation region (120-150 seconds) was around 280 and that for the softest formation region (150-200 seconds) was close to 110. The controller was again successful in combating stick-slip and torsional oscillations caused due to increasing formation hardness.


**Figure 65. SSIF controller response in vertical well configuration (0.3-0.5 SSI thresholds, 1000g hook load)**

- *SSI threshold: lower = 0.3, higher = 0.5 at hook load = 1500g*

With the hook load set to 1500g for this test, the same test procedure (table 9) was followed. The controller can again be observed to combat stick-slip and high amplitude torsional oscillations. For the hardest formation region (120-150 seconds) an RPM of approximately 225 was set by the controller which is less than that for the previous test.


**Figure 66. SSIF controller response in vertical well configuration (0.3-0.5 SSI thresholds, 1500g hook load)**

- *SSI threshold: lower = 0.4, higher = 0.6 at hook load = 1000g*

SSI thresholds were once again increased by 0.1 and the hook load was set to 1000g. For this test the procedure listed in table 10 was followed and the results are shown in figure 67. The controller response is as expected until the zone with the hardest formation, 120-170 seconds in this case, is reached. Severe sticking can be observed (downhole RPM going to zero for almost 25 seconds), meanwhile the controller ramps up the RPM and the stick-slip is finally removed. The RPM set for the hardest formation region (120-170 seconds) was around 300 and for the softest formation region (150-200 seconds) was close to 120.


**Figure 67. SSIF controller response in vertical well configuration (0.4-0.6 SSI thresholds, 1000g hook load)**

- *SSI threshold: lower = 0.4, higher = 0.6 at hook load = 1500g*

With the hook load set to 1500g the test procedure in table 9 was followed for an SSI threshold range of 0.04 to 0.06. The controller was successful in removing stick-slip form the system and also reacted as expected to the changes in formation hardness. It can be observed for the data in figure 68 that the amplitude of the oscillations produced by the set RPM values is higher in this test as compared to the previous tests. The RPM was set to approximately 200 for the hardest formation zone and to 85 for the softest formation zone.


**Figure 68. SSIF controller response in vertical well configuration (0.4-0.6 SSI thresholds, 1500g hook load)**

The test results shown and discussed above prove that the SSI based auto-tuning controller is successful in mitigating stick-slip from the system. The designed controller is also capable of doing so under changes in the formation hardness which are mimicked by changing the changing the parameters of the bit-rock simulator model. The controller when set to lower SSI threshold values (0.2 to 0.4) is more aggressive, i.e., the controller sets the RPM to higher values which results in less torsional oscillations in the drillstring. On the other hand, when the SSI threshold values are increased, the controller becomes more relaxed and sets the RPM to lower values resulting in torsional oscillations with comparatively higher amplitudes. The effect of increasing hook load in the vertical well configuration can also be seen in the results. Increase in hook load increases the torsional stiffness of the drillstring resulting in lower RPM set points set by the controller.

### 4.5.2 Directional well configuration

The SSI based auto-tuning was tested in the directional well configuration and the results of the tests are discussed in this section. Similar to the tests conducted for the vertical configuration, three sets of SSI threshold values (0.2-0.4, 0.3-0.5, 0.4-0.6) were tested with hook load set to 1000g and 1500g. Since the bit-rock simulator is not yet available for the horizontal setup, the tests were conducted using the inherent mechanical friction in the system which is capable of producing stick-slip. The testing procedure consists of just two steps as listed in table 11. Firstly, five seconds into the test, RPM is set to 40. Later at the 30 second mark the controller is turned on and the response is observed.

**Table 11. Testing procedure for SSIF controller in directional well configuration**

| Sec | Action |
|---|---|
| 5 | RPM set to 40 |
| 30 | SSI Feedback Controller turned on |

- *SSI threshold: lower = 0.2, higher = 0.4 at hook load = 1000g*

The RPM is initially set to 40 at 5 seconds and stick-slip in the system is evident from the data shown in figure 69. The controller is turned on at 30 seconds and stick-slip is removed after the 80 seconds mark, after the surface RPM is increased to a sufficient amplitude by the controller. The surface RPM ultimately stabilizes around an amplitude of 200.


**Figure 69. SSIF controller response in directional well configuration (0.2-0.4 SSI thresholds, 1000g hook load)**

- *SSI threshold: lower = 0.2, higher = 0.4 at hook load = 1500g*

The same test was performed with an increased hook load of 1500g and the results are shown in figure 70. The results can be observed to be very similar to the previous test. The surface RPM still stabilizes at 200. The one difference that can be observed in this test was that the stick-slip was removed after 70 seconds compared to 80 in the previous test.

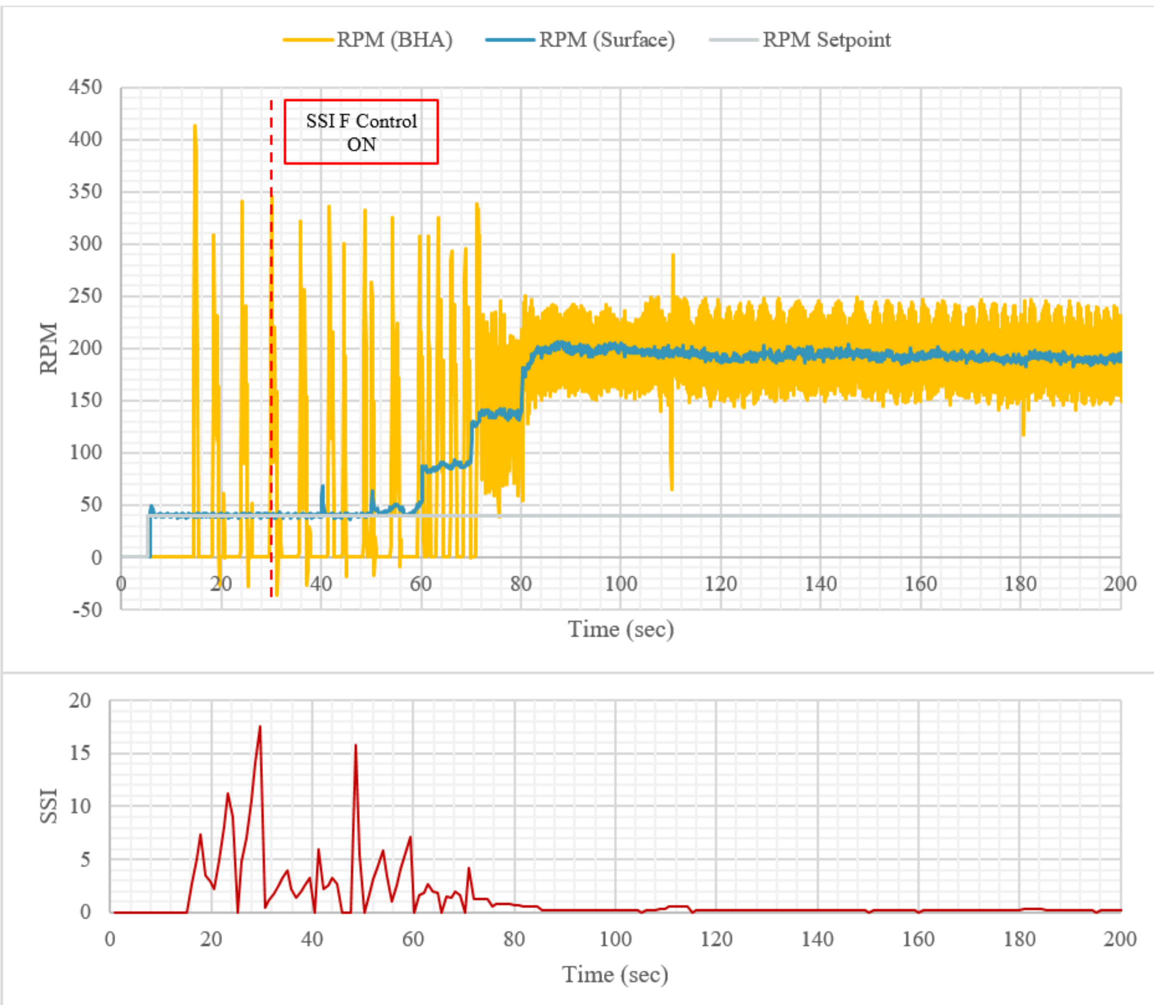


**Figure 70. SSIF controller response in directional well configuration (0.2-0.4 SSI thresholds, 1500g hook load)**

- *SSI threshold: lower = 0.3, higher = 0.5 at hook load = 1000g*

Figure 51 shows the results of the test when performed with SSI threshold values of 0.3 and 0.5, and hook load of 1000g. The initial set RPM of 40 is insufficient to overcome stick-slip and the controller, which is turned on at 30 seconds, removes the stick-slip at 80 seconds. The surface RPM stabilizes at approximately 150.


**Figure 71. SSIF controller response in directional well configuration (0.3-0.5 SSI thresholds, 1000g hook load)**

- *SSI threshold: lower = 0.3, higher = 0.5 at hook load = 1500g*

At a hook load of 1500g and SSI thresholds set to 0.3 and 0.5 the controller when turned on at 30 seconds mitigated the stick-slip at 70 seconds. The stable surface RPM value around 150. These results are shown in figure 72.


**Figure 72. SSIF controller response in directional well configuration (0.3-0.5 SSI thresholds, 1500g hook load)**

- *SSI threshold: lower = 0.4, higher = 0.6 at hook load = 1000g*

For the final set of tests, the SSI threshold was set to 0.4 and 0.6. The results of this test when conducted with 1000g hook load are shown in figure 73. Stick-slip is present for the initial RPM of 40, the controller is again turned on at 30 seconds and the stick-slip is removed at 80 seconds. After stick-slip is removed the surface RPM for the most time is around 140 but bounces between 130 and 180.


**Figure 73. SSIF controller response in directional well configuration (0.4-0.6 SSI thresholds, 1000g hook load)**

- *SSI threshold: lower = 0.4, higher = 0.6 at hook load = 1500g*

Figure 74 presents the results when tested with a hook load of 1500g. After around 70 seconds the stick-slip is removed in this case, the RPM is for most part stable around 130. The controller tries to shift to a higher RPM level but since the corresponding SSI values are outside of the threshold limits it is brought back to 130 RPM.


**Figure 74. SSIF controller response in directional well configuration (0.4-0.6 SSI thresholds, 1500g hook load)**

These results render the SSI based auto-tuning controller effective in mitigating stick slip. Similar to the results in the vertical configuration tests, lower SSI threshold values (0.2 to 0.4) for the controller result in a more aggressive. The RPM in this case is set to higher values consequential producing less torsional oscillations in the drillstring. For higher values of SSI threshold, the controller is more relaxed, thus, RPM is set lower values causing comparatively higher amplitude torsional oscillations. Changing the hook load is not as effective in increasing the torsional stiffness of the drillstring in the directional well configuration. This is because in a directional there are multiple points of contact between the wellbore and the drillstring, especially in the curved and horizontal sections. Because of these contact points the effect of increased hook load is greatly reduced. Therefore, no noticeable change in the RPM set by the controller is observed when comparing the results of tests at 1000g hook load with those at 1500g hook load. One difference that was noticed when changing the hook load was that with a hook load of 1000g the controller took around 50 seconds to remove stick-slip, whereas with 1500g hook load stick-slip was removed approximately 40 seconds after the controller was turned on.

Another set of tests was conducted to further analyses the performance of the SSI based auto tuning controller. The controller (SSIF) has been designed to operate only when the SSI goes outside of the set SSI threshold values. To validate this required behavior of the controller the SSIF controller was used in conjunction with the feedback RPM controller. With the hook load set to 1000g, these tests were conducted on both, vertical and directional, well configurations.

The test procedure followed for the vertical well is shown in table 12 and the corresponding results are plotted in figure 75. RPM is set to 80 at 5 seconds and bit-rock simulator is turned on at 20 seconds. Stick-slip can be observed during this time to counter which, the SSIF controller is turned on. After the 70 second mark stick-slip is mitigated. SSIF is turned off at 125 seconds, this shifts the control to the feedback RPM controller and the RPM goes to the original setpoint of 80. Stick-slip is again observed. Using the feedback RPM controller, the RPM is set to 150 at 140 seconds mark, this removes the stick-slip. The SIIF is turned back on at 160 seconds and since the torsional oscillations are within the acceptable range (i.e., SSI is within the thresholds), the SSIF does not make changes to the set RPM. Rock hardness is increased at 220 seconds, resulting in an increase in torsional oscillations. This is noticed by the SSIF controller, and it adjusts the RPM to bring the oscillations back to the desired range.

The testing procedure for the horizontal well configuration is listed in table 13 and the results are plotted in figure 76. At 5 seconds the RPM is set to 40 and stick-slip is observed. SSIF is then turned on at 30 seconds and stick-slip is mitigated by the 80 second mark. SSIF is turned off at 130 seconds, the RPM drops back to the original setpoint of 40 and stick-slip is observed again. Using the feedback RPM controller, the RPM is set to 150 at 160 seconds and stick-slip is mitigated. SSIF is turned back on at 180 seconds but since the oscillation are within the desired limit the controller does not make changes to the RPM setpoint.

These test results show that the SSIF controller only varies the RPM when the torsional oscillations are outside of the set range. With this control design the objective of automatic stick-slip detection and mitigation was also achieved. The controller was tested under various operational conditions and was successful in mitigating stick-slip and also in reducing the amplitude of the torsional oscillations in the drillstring.

**Table 12. SSIF and Feedback RPM control in vertical well configuration**

| Sec | Action |
|---|---|
| 5 | RPM set to 80 |
| 20 | Bit-Rock Sim. Parameters set to a1=0.05, a2=0.07, a3=15 |
| 40 | SSI Feedback controller turned ON |
| 130 | SSI Feedback controller turned OFF |
| 140 | RPM set to 160 |
| 160 | SSI Feedback controller turned ON |
| 220 | Bit-Rock Sim. Parameters set to a1=0.05, a2=0.08, a3=15 |

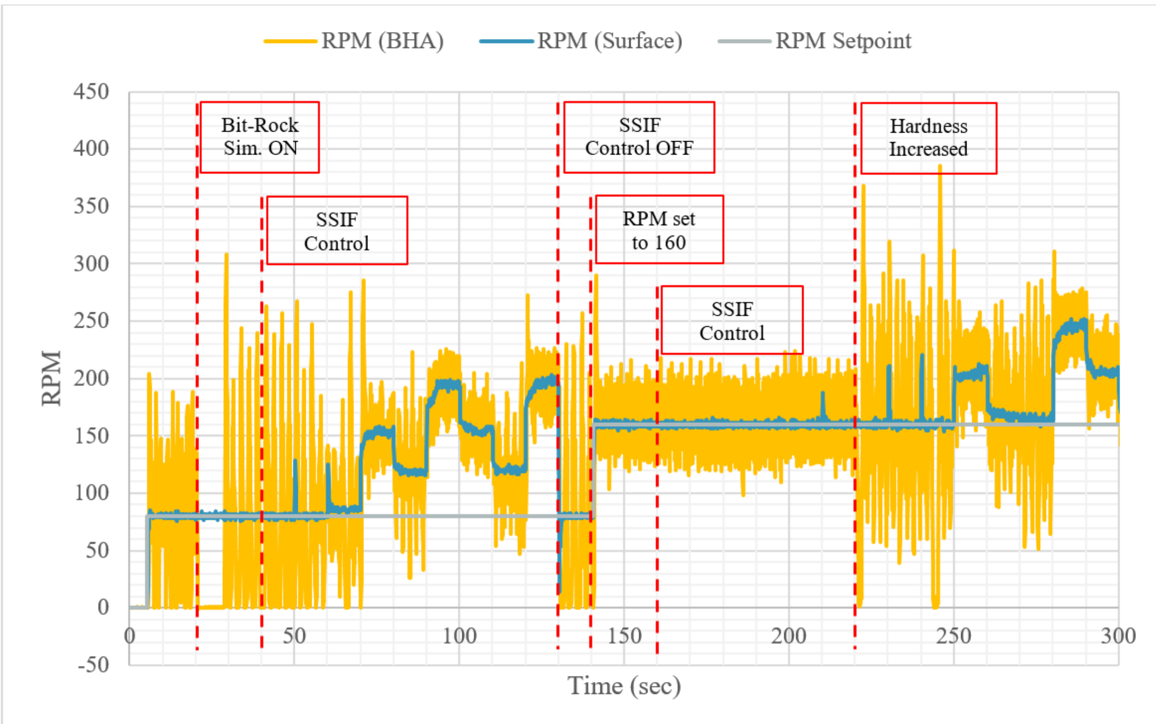


**Figure 75. SSIF controller and feedback RPM controller in vertical well configuration (0.3-0.5 SSI thresholds, 1000g hook load)**

**Table 13. SSIF and Feedback RPM control in directional well configuration**

| Sec | Action |
|---|---|
| 5 | RPM set to 40 |
| 30 | SSI Feedback controller turned ON |
| 130 | SSI Feedback controller turned OFF |
| 160 | RPM set to 150 |
| 180 | SSI Feedback controller turned ON |

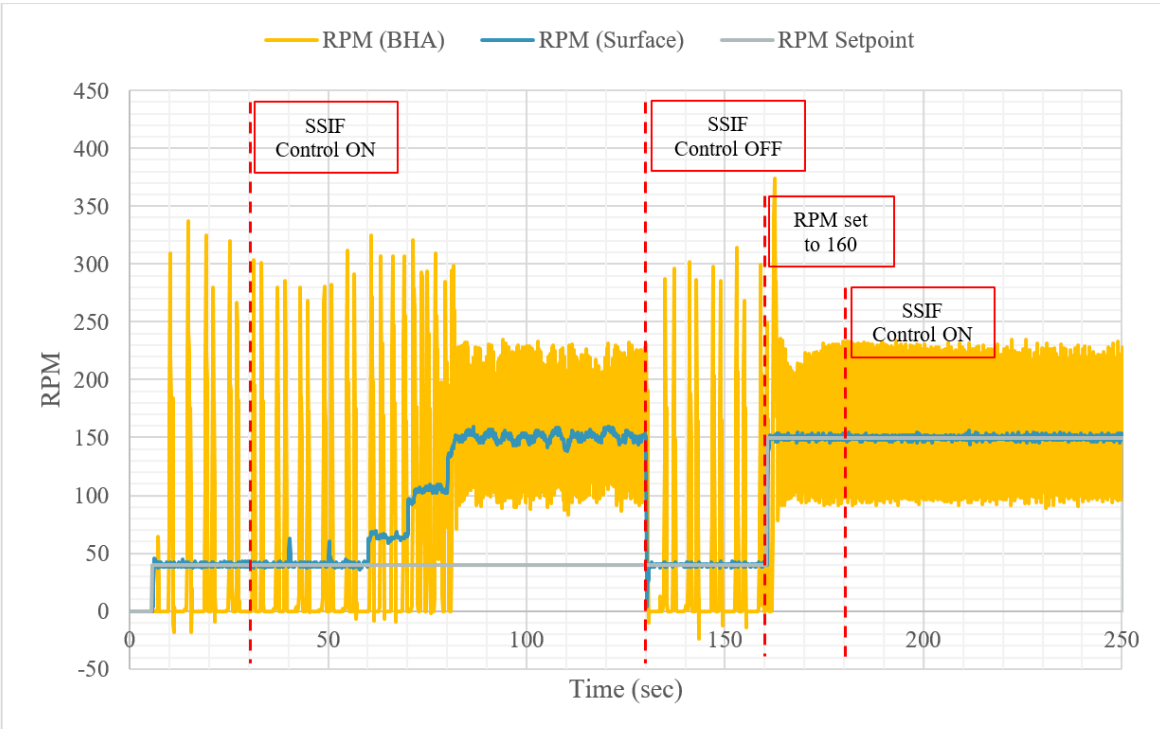


**Figure 76. SSIF controller and feedback RPM controller in directional well configuration (0.3-0.5 SSI thresholds, 1000g hook load)**

# Chapter 5: Conclusions and Recommendations

## 5.1 Conclusions

An experimental setup was designed and developed to mimic the process of rotary drilling. The setup consists of multiple sensors and actuators and is capable of simulating drilling dynamics in vertical and directional configuration. The software part of the setup was developed using National Instruments LabVIEW.

An electro-mechanical setup to simulate bit-rock interactions was also designed and developed. This system uses numerical bit-rock interaction models in conjunction with an electro-mechanical break and an RPM encoder to mimic the forces acting between a drill bit and the rock formation being drilled.

Open-loop RPM control and feedback RPM control was initially implemented. Testing conducted using these two control strategies showed that stick-slip in the drillstring can be overcome by the surface RPM to a sufficient level. These tests also showed the presence of a higher amount of mechanical/contact friction in a directional well compared to a vertical well.

Surface RPM alone cannot paint a clear picture of the downhole dynamics during stick-slip conditions. Surface torque data was analyzed, and it proved to be a much better indicator of the downhole dynamics. Therefore, surface torque feedback was added to the next control system.

A dual feedback controller, which uses surface RPM and surface torque feedback was designed. The controller was successful in mitigating stick-slip but the gain for the torque feedback had to manually adjusted. To automate the gain adjustments, a new strategy had to be devised.

Stick Slip Index (SSI) was used to design an auto-tuning controller. This controller, in addition to surface RPM and torque feedback, uses SSI values to automatically adjust the gain for the torque feedback. In actual field environment, the SSI calculations can be done in a downhole tool and the resultant SSI values can be sent to the surface using MWD techniques. For this reason, the SSI values were programed to be updated every 10 seconds (0.1Hz) in the experimental setup.

This new control approach was tested under different conditions. Three different sets of SSI thresholds were tested for vertical and directional well configurations under 1000g and 1500g hook load set point. The results prove the controller to be successful in mitigating stick-slip automatically.

It can also be concluded that the surface parameters alone are not sufficient to design a robust stick-slip mitigation system. Access to downhole data can play a crucial role in development of such a control system. Even downhole data sampled at low frequencies can aid in control and mitigation of stick-slip vibrations.

## 5.2 Recommendations

In this section some recommendations for future work are listed.

- As of now the bit-rock model simulator is only available for vertical well setup. It can also be incorporated with the directional well setup to better mimic the bottom hole conditions.
- The numerical bit-rock model current used in the setup only has a bottom RPM feedback. In literature, numerical models which relate the forces acting on the bit to bottom RPM and weight on bit are available. To implement these numerical models in the electro-

mechanical bit-rock setup, weight on bit feedback from a load cell can be integrated in the system. This will make the system more accurate.

- At present the experimental setup is capable of simulating torsional vibrations with some lateral vibrations. An actuation system can be added to the system to induce axial vibrations in the drillstring. Doing this will enable the setup to simulate coupling between the different vibration modes.
- More testing can be conducted for the SSI-based auto-tuning controller where the sampling frequency of the SSI feedback can be less than 0.1Hz.

## References


Aarrestad, T. V., Tonnesen, H., & Kyllingstad, A. (1986). Drillstring Vibrations: Comparison Between Theory and Experiments on a Full-Scale Research Drilling Rig. *IADC/SPE Drilling Conference*. Dallas, Texas.

Aarsnes, U. J., di Meglio, F., & Shor, R. (2018). Benchmarking of Industrial Stick-Slip Mitigation Controllers. *IFAC-PapersOnLine, 51*(8), 233-238.

Abbas, R. K. (2018). A review on the wear of oil drill bits (conventional and the state of the art approaches for wear reduction and quantification). *Engineering Failure Analysis, 90*, 554-584.

Abbassian, F., & Dunayevsky, V. (1998). Application of Stability Approach to Torsional and Lateral Bit Dynamics. *SPE Drilling & Completion, 13*(2), 99-107.

Abdulgalil, F., & Siguerdidjane, H. (2005). Backstepping design for controlling rotary drilling system. *Proceedings of 2005 IEEE Conference on Control Applications* (pp. 120-124). IEEE.

Albdiry, M. T., & Almensoury, M. F. (2016). Failure analysis of drillstring in petroleum industry: A review. *Engineering Failure Analysis, 65*, 74-85.

Al-Hiddabi, S., Samanta, B., & Seibi, A. (2003). Non-linear control of torsional and bending vibrations of oilwell drillstrings. *Journal of Sound and Vibration*, 401-415.

Antunes , J., Axisa , F., & Hareux, F. (1992). Flexural vibrations of rotors immersed in dense fluids Part II: Experiments. *Journal of Fluids and Structures, 6*(1), 23-38.

Arevalo, Y., & Fernandes, A. (2012). Quantification of Drillstring-Integrity-Failure Risk Using Real-Time Vibration Measurements. *SPE Drilling & Completion, 27*(2), 216–222.

Armstrong-Hélouvry, B., Dupont, P., & De Wit, C. C. (1994). A survey of models, analysis tools and compensation methods for the control of machines with friction. *Automatica, 30*(7), 1083-1138.

Bailey, J., & Finnie, I. (1960). An Analytical Study of Drill-String Vibration. *Journal of Engineering for Industry, 82*(2), 122-127.

Bailey, J., & Remmert, S. (2010, November 11). Managing Drilling Vibrations Through BHA Design Optimization. *SPE Drill & Compl , 25*(04), 458-471.

Bailey, J., Biediger, E., Gupta, V., Ertas, D., Elks, W., & Dupriest, F. (2008). Drilling Vibrations Modeling and Field Validation. *IADC/SPE Drilling Conference.* Orlando, Florida, USA.

Basturk, H. I. (2017). Observer-Based Boundary Control Design for the Suppression of Stick–Slip Oscillations in Drilling Systems With Only Surface Measurements. *Journal of Dynamic Systems, Measurement, and Control , 139*(10).

Bavadiya, V. A., Alsaihati, Z., Ahmed, R., & Gustafson, K. (2017). Experimental Investigation of the Effects of Rotational Speed and Weight on Bit on Drillstring Vibrations, Torque and Rate of Penetration. *Abu Dhabi International Petroleum Exhibition & Conference.* Abu Dhabi, UAE.

Bayliss, M., Panchal, N., & Whidborne, J. (2012). Rotary Steerable Directional Drilling Stick/Slip Mitigation Control. *IFAC Proceedings Volumes*, 66-71.

Berlioz, A., Hagopian, J. D., Dufour,, R., & Draoui,, E. (1996). Dynamic Behavior of a Drill-String: Experimental Investigation of Lateral Instabilities. *ASME. J. Vib. Acoust., 118*(3), 292–298.

Besselink, B., Vromen, T., Kremers, N., & van de Wouw, N. (2016). Analysis and Control of Stick-Slip Oscillations in Drilling Systems. *IEEE Transactions on Control Systems Technology, 24*(5), 1582-1593.

Bilgesu, H., Cox, Z., Elshehabi, T., Smith, C., Idowu, G., & Florence, F. (2017). A Real-Time Interactive Drill-Off Test Utilizing Artificial Intelligence Algorithm for DSATS Drilling Automation University Competition. *SPE Western Regional Meeting.* akersfield, California.

Bourgoyne, A. T., Millheim, K. K., Chenevert, M. E., & Young, F. S. (1986). *Applied Drilling Engineering.* Society of Petroleum Engineers.

Bresch-Pietri, D., & Krstic, M. (2014). Adaptive output feedback for oil drilling stick-slip instability modeled by wave PDE with anti-damped dynamic boundary. *2014 American Control Conference* (pp. 386-391). Portland, OR: IEEE.

Brett, J. (1992). The Genesis of Torsional Drillstring Vibrations. *SPE Drill Eng 7*, 168–174.

Briz, F., Cancelas, J. A., & Diez, A. B. (1994). Speed measurement using rotary encoders for high performance AC drives. *20th Annual Conference of IEEE Industrial Electronics* (pp. 538-542 vol.1). Bologna, Italy: IEEE.

Bu, F., & Dykstra, J. (2014). Indirect Adaptive Robust Controller Design for Drilling Rotary Motion Control. *Dynamic systems and control conference. 46186*, p. V001T09A001. San Antonio, Texas, USA: ASME.

Canudas-de-Wit, C., Rubio, F., & Angel Corchero, M. (2008). D-OSKIL: A New Mechanism for Controlling Stick-Slip Oscillations in Oil Well Drillstrings. *IEEE Transactions on Control Systems Technology*, *16*(6), 1177-1191.

Caponetto, R. (2010). *Fractional order systems: modeling and control applications.* (Vol. 72). World Scientific.

Cayeux, E., Sui, D., Akisanmi, O., & Alani, O. (2017). Challenges in the Automation of a Laboratory-Scale Drilling Rig and Comparison with the Requirements for Full Scale Drilling Automation. *SPE Bergen One Day Seminar.* Bergen, Norway.

Cayres, B., da Fonseca, C., Santos , A., & Weber , H. I. (2015). Analysis of Dry Friction-Induced Stick-Slip in an Experimental Test Rig Modeling a Drill String. *IFToMM International Conference on Rotor Dynamics.*

Challamel, N. (2000). Rock destruction effect on the stability of a drilling structure. *Journal of sound and vibration, 233*(2), 235-254.

Chen, S., Blackwood, K., & Lamine, E. (2002). Field Investigation of the Effects of Stick-Slip, Lateral, and Whirl Vibrations on Roller-Cone Bit Performance. *SPE Drill & Compl, 17*(1), 15–20.

Cheng, J., Wu, M., Wu, F., Lu, C., Chen, X., & Cao, W. (2020). Modeling and Control of Drill-String System With Stick-Slip Vibrations Using LPV Technique. *IEEE Transactions on Control Systems Technology*, 718-730.

Christoforou, A., & Yigit, A. (2001). Active control of stick-slip vibrations: The role of fully coupled dynamics. *SPE Middle East Oil Show.* Manama, Bahrain: SPE .

Cunningham, R. (1968). Analysis of Downhole Measurements of Drill String Forces and Motions. *Journal of Engineering for Industry*, ASME.

Derbal, M., Gharib, M., Refaat, S., Palazzolo, A., & Sassi, S. (2021). Fractional-order controllers for stick-slip vibration mitigation in oil well drill-strings. *Journal of Low Frequency Noise,*, 1571–1584.

Dong, G., & Chen, P. (2016). A Review of the Evaluation, Control, and Application Technologies for Drill String Vibrations and Shocks in Oil and Gas Well. *Shock and Vibration, 2016* .

Dufeyte, M.-P., & Henneuse, H. (1991). Detection and Monitoring of the Slip-Stick Motion: Field Experiments. *SPE/IADC Drilling Conference.* Amsterdam, Netherlands: SPE/IADC.

Dyson, F. (2004, January). A meeting with Enrico Fermi. *Nature*, p. 297. doi:10.1038/427297a

Efteland, F., Creegan, A., Jordan, L., & Caraway, C. (2015). The Significance of Pro-active Online Monitoring with Stick-slip Mitigation. *bu Dhabi International Petroleum Exhibition and Conference.* Abu Dhabi, UAE: SPE.

Esmaeili, A., Elahifar, B., Fruhwirth, R. K., & Thonhauser, G. (2012). Laboratory Scale Control of Drilling Parameters to Enhance Rate of Penetration and Reduce Drill String Vibration. *SPE Saudi Arabia Section Technical Symposium and Exhibition.* Al-Khobar, Saudi Arabia.

Fear, M., Abbassian, F., Parfitt, S., & McClean, A. (1997). The Destruction of PDC Bits by Severe Slip-Stick Vibration. *SPE/IADC drilling conference.* Amsterdam, Netherlands: SPE/IADC.

Feng, T., Zhang, H., & Chen, D. (2017). Dynamic programming based controllers to suppress stick-slip in a drilling system. *2017 American Control Conference (ACC)* (pp. 1302-1307). Seattle, WA, USA: IEEE.

Forster, I. (2011). Axial Excitation as a Means of Stick Slip Mitigation - Small Scale Rig Testing and Full Scale Field Testing. *SPE/IADC Drilling Conference and Exhibition.* Amsterdam, The Netherlands.

Forster, I., Macfarlane, A., & Dinnie, R. (2010). Asymmetric Vibration Damping Tool - Small Scale Rig Testing and Full Scale Field Testing. *IADC/SPE Drilling Conference and Exhibition.* New Orleans, Louisiana, USA.

Franca, L. F. (2010). Drilling action of roller-cone bits: modeling and experimental validation. *J., 132*(4), 043101-043110.

Fu, M., Zhang, P., Li, J., & Wu, Y. (2019). Observer and reference governor based control strategy to suppress stick-slip vibrations in oil well drill-string. *Journal of Sound and Vibration*, 37-50.

Ghasemloonia, A., Rideout, D., & Butt, S. D. (2014). Analysis of multi-mode nonlinear coupled axial-transverse drillstring vibration in vibration assisted rotary drilling. *Journal of Petroleum Science and Engineering, 116*, 36-49.

Ghasemloonia, A., Rideout, D., & Butt, S. D. (2015). A review of drillstring vibration modeling and suppression methods. *Journal of Petroleum Science and Engineering, 131*, 150-164.

Halsey, G., Kyllingstad, A., & Kylling, A. (1988). Torque Feedback Used to Cure Slip-Stick Motion. *SPE Annual Technical Conference and Exhibition.* Houston, Texas: SPE .

Han, G., Lemesany, L., Azizov, A., & DeLeon, F. (2013). Bottomhole Assembly Result Analysis to Improve Drilling Performance in Pinedale Field, Wyoming, USA. *SPE Unconventional Resources Conference Canada.* Calgary: SPE.

Harris, M. W., Açıkmeşe, B., & van Oort, E. (2014). LMI Based Control of Stick-Slip Oscillations in Drilling. *Dynamic Systems and Control Conference. 46186*, p. V001T09A004. San Antonio, Texas, USA: ASME.

Hong, L., Girsang, I., & Dhupia, J. (2016). Identification and control of stick–slip vibrations using Kalman estimator in oil-well drill strings. *Journal of Petroleum Science and Engineering*, 119-127.

Huang, Z., Xie, D., Xie, B., Zhang, W., Zhang, F., & He, L. (2018). Investigation of PDC bit failure base on stick-slip vibration analysis of drilling string system plus drill bit. *Journal of Sound and Vibration, 417*(1), 97-109.

Jaggi, A., Upadhaya, S., & Chowdhury, A. R. (2007). Successful PDC/RSS Vibration Management Using Innovative Depth-of-Cut Control Technology: Panna Field, Offshore India. *SPE/IADC Drilling Conference.* Amsterdam, The Netherlands.

Jansen, J. (1991, May 22). Non-linear rotor dynamics as applied to oilwell drillstring vibrations. *Journal of Sound and Vibration, 147*(1), 115-135.

Jansen, J., & van den Steen, L. (1995). Active damping of self-excited torsional vibrations in oil well drillstrings. *Journal of Sound and Vibration, 179*(4), 647-668.

Janwadkar, S., Fortenberry, D., Roberts, G., Kramer, M., Trichel, D., Rogers, T., . . . Isbell, M. (2006). BHA and Drillstring Modeling Maximizes Drilling Performance In Lateral Wells of Barnett Shale Gas Field of N. Texas. *SPE Gas Technology Symposium.* Calgary, Alberta, Canada.

Jardine, S., Malone, D., & Sheppard, M. (1994). Putting a damper on drilling's bad vibrations. *Oilfield Review, 6*(1), 15-20.

Jianhong , F., Kexiong , S., Zhi, Z., Dezhi, Z., Fei, L., Xin , X., & Xin , Z. (2012). Stress Analysis on Drilling String Vibration in Gas Drilling. *Energy Procedia, 16*, 1264-1268.

Kabziński, J. (2017). Adaptive Control of Drillstring Torsional Oscillations. *IFAC-PapersOnLine, 50*(1), 13360-13365.

Kamel, M., Elkatatny, S., Mysorewala, M. F., Al-Majed, A., & Elshafei, M. (2018). Adaptive and Real-Time Optimal Control of Stick–Slip and Bit Wear in Autonomous Rotary Steerable Drilling. *Journal of Energy Resources Technology, 140*(3), 032908 (12 pages).

Kapitaniak, M., Hamaneh, V. V., Chávez, J. P., Nandakumar, K., & Wiercigroch, M. (2015). Unveiling complexity of drill–string vibrations: Experiments and modelling. *International Journal of Mechanical Sciences, 101-102*, 324-337.

Karkoub, M., Zribi, M., Elchaar , L., & Lamont, L. (2010). Robust μ-synthesis controllers for suppressing stick-slip induced vibrations in oil well drill strings. *Multibody System Dynamics, 23*(2), 191–207.

Khulief, Y., & Al-Sulaiman, F. (2009). Laboratory investigation of drillstring vibrations. *Journal of Mechanical Engineering Science, 223*(10), 2249-2262.

Knight, M. J., & Brennan, F. P. (1999). Fatigue life improvement of drill collars through control of bore eccentricity. *Engineering Failure Analysis, 6*(5), 301-319.

Kovalyshen, Y. (2014). Experiments on Stick-Slip Vibrations in Drilling with Drag Bits. *48th U.S. Rock Mechanics/Geomechanics Symposium.* Minneapolis, Minnesota.

Krama, A., Gharib, M., Refaat, S., & Palazzolo, A. (2021). Design and Hardware in-the-Loop Validation of an Effective Super-Twisting Controller for Stick-Slip Suppression in Drill-String Systems. *Journal of Dynamic Systems, Measurement, and Control, 143*(11), 111008 (12 pages).

Kriesels, P., Keultjes, W., Dumont, P., Huneidi, I., Owoeye, O., & Hartmann, R. (1999). Cost Savings through an Integrated Approach to Drillstring Vibration Control. *SPE/IADC Middle East Drilling Technology Conference.* Abu Dhabi, United Arab Emirates: SPE/IADC.

Kyllingstad, A. (2017). A Comparison of Stick-Slip Mitigation Tools. *SPE/IADC Drilling Conference and Exhibition.* The Hague, The Netherlands.

Kyllingstad, Å., & Nessjøen, P. J. (2009). A New Stick-Slip Prevention System. *SPE/IADC Drilling Conference and Exhibition.* Amsterdam, The Netherlands: SPE.

Kyllingstad, Å., & Nessjøen, P. J. (2010). Hardware-In-the-Loop Simulations Used as a Cost Efficient Tool for Developing an Advanced Stick-Slip Prevention System. *IADC/SPE Drilling Conference and Exhibition.* New Orleans, Louisiana, USA: IADC.

Laib, A., Talbi, B., Krama, A., & Gharib, M. (2022). Hybrid Interval Type-2 Fuzzy PID+I Controller for a Multi-DOF Oilwell Drill-String System. *IEEE Access, 10*, 67262-67275.

Ledgerwood, L., Hoffmann, O. J., Jain, J. R., El Hakam, C., Herbig, C., & Spencer, R. W. (2010). Downhole Vibration Measurement, Monitoring, and Modeling Reveal Stick/Slip as a Primary Cause of PDC-Bit Damage in Today. *SPE Annual Technical Conference and Exhibition.* Florence, Italy.

Liao, C.-M., Balachandran, B., Karkoub, M., & Abdel-Magid, Y. L. (2011). Drill-String Dynamics: Reduced-Order Models and Experimental Studies. *J. Vib. Acoust., 133*(4), 041008 (8 pages).

Lin, T., Zhang, Q., Lian, Z., Xiao, Z., Wang, T., Li, G., & Ding, J. (2018). Experimental study on vibrational behaviors of horizontal drillstring. *Journal of Petroleum Science and Engineering, 164*, 311-319.

Lin, Y., Qi, X., Zhu , D., Zeng , D., Zhu, H., Deng , K., & Shi, T. (2013). Failure analysis and appropriate design of drill pipe upset transition area. *Engineering Failure Analysis, 31*, 255-267.

Lin, Y.-Q., & Wang, Y.-H. (1991). Stick-Slip Vibration of Drill Strings. *Journal of Engineering for Industry, 113*(1), 38-43.

Liu, Y. (2015). Suppressing stick-slip oscillations in underactuated multibody drill-strings with parametric uncertainties using sliding-mode control. *IET Control Theory & Applications, 9*(1), 91-102.

Loeken, E. A., Trulsen, A., Holsaeter, A. M., Wiktorski, E., Sui, D., & Ewald, R. (2018). Design Principles Behind the Construction of an Autonomous Laboratory-Scale Drilling Rig. *IFAC-PapersOnLine, 51*(8), 62-69.

Lu, H., Dumon, J., & Canudas-de-Wit, C. (2009,). Experimental study of the D-OSKIL mechanism for controlling the stick-slip oscillations in a drilling laboratory testbed. *IEEE Control.* St. Petersburg: IEEE.

MacLean, J., Vaziri, V., Aphale, S., & Wiercigroch , M. (2021). Feedback control method to suppress stick-slip in drill-strings featuring delay and actuation constraints. *The European Physical Journal Special Topics*, 3627-3642.

Macpherson, J., Mason, J., & Kingman, J. (1993). Surface measurement and analysis of drill-string vibrations while drilling. *SPE/IADC Drilling Conference.* Amsterdam, Netherlands.

Mahyari, M., Behzad, M., & Rashed, G. (2010). Drill string instability reduction by optimum positioning of stabilizers. *Journal of Mechanical Engineering Science, 224*(3), 647-653.

Marquez, A., & Teodoriu, C. (2017). A Novel Drillstring Dynamics Experimental Setup to Be Integrated Into Hardware in the Loop Capable Drilling Simulators. *ASME 2017 36th International Conference on Ocean, Offshore and Arctic Engineering.* Trondheim, Norway.

Márquez, M. B., Boussaada, I., Mounier, H., & Niculescu, S.-I. (2015). *Analysis and Control of Oilwell Drilling Vibrations: A Time-Delay Systems Approach.* Springer.

Melakhessou, H., Berlioz, A., & Ferraris, G. (2003). A Nonlinear Well-Drillstring Interaction Model. *ASME. J. Vib. Acoust. January, 125*(1), 46–52.

Mihajlovic, N., van de Wouw, N., Hendriks, M. P., & Nijmeijer , H. (2006). Friction-induced limit cycling in flexible rotor systems: An experimental drill-string set-up. *Nonlinear Dynamics, 46*, 273–291.

Mitchell, R., & Allen, M. (1987). Case Studies of BHA Vibration Failure. *SPE Annual Technical Conference and Exhibition.* Dallas, Texas.

Moradi, S., & Ranjbar, K. (2009). Experimental and computational failure analysis of drillstrings. *Engineering Failure Analysis, 16*(3), 923-933.

Navarro-López, E. (2009). An alternative characterization of bit-sticking phenomena in a multi-degree-of-freedom controlled drillstring. *Nonlinear Analysis: Real World Applications*, *10*(5), 3162-3174.

Navarro-López, E. M., & Cortés, D. (2007). Sliding-mode control of a multi-DOF oilwell drillstring with stick-slip oscillations. *American control conference.* New York, NY, USA: IEEE.

Navarro-López, E., & Licéaga-Castro, E. (2009). Non-desired transitions and sliding-mode control of a multi-DOF mechanical system with stick-slip oscillations. *Chaos, Solitons & Fractals*, 2035-2044.

Nessjøen, P. J., Kyllingstad, Å., D'Ambrosio, P., Fonseca, I. S., Garcia, A., & Levy, B. (2011). Field Experience with an Active Stick-Slip Prevention System. *SPE/IADC Drilling Conference and Exhibition.* Amsterdam, The Netherlands: SPE.

Nicholson, J. (1994). An Integrated Approach to Drilling Dynamics Planning, Identification, and Control. *IADC/SPE Drilling Conference.* Dallas, Texas: IADC/SPE.

Omojuwa, E., Osisanya, S., & Ahmed, R. (2011a). Dynamic Analysis of Stick-Slip Motion of Drillstring While Drilling. *Nigeria Annual International Conference and Exhibition.* Abuja, Nigeria: OnePetro.

Omojuwa, E., Osisanya, S., & Ahmed, R. (2011b). Measuring and Controlling Torsional Vibrations and Stick-Slip in a Viscous-Damped Drillstring Model. *International Petroleum Technology Conference.* Bangkok, Thailand: OnePetro.

Ortiz, B., Casallas, C., & Parra, H. (1996). Improved Bit Stability Reduces Downhole Harmonics (Vibrations) . *SPE/IADC Asia Pacific Drilling Technology*. Kuala Lumpur, Malaysia.

Patil, P. A., & Teodoriu, C. (2013). A comparative review of modelling and controlling torsional vibrations and experimentation using laboratory setups. *Journal of Petroleum Science and Engineering, 112*, 227-238.

Pavone, D., & Desplans, J. (1994). Application of High Sampling Rate Downhole Measurements for Analysis and Cure of Stick-Slip in Drilling. *SPE Annual Technical Conference and Exhibition.* New Orleans, Louisiana: SPE.

Pehlivantürk, C., Chen, D., & van Oort, E. (2017). Torsional Drillstring Vibration Modelling and Mitigation with Feedback Control. *SPE/IADC Drilling Conference and Exhibition.* The Hague, The Netherlands: OnePetro.

Pires, I., Cayres, B. C., & Weber, H. I. (2019). Friction-Induced Vibrations in a Drill-String Experimental Set-Up. *XVIII International Symposium on Dynamic Problems of Mechanics.* Rio de Janeiro, Brazil.

Plácido, J. C., Santos, H. M., & Galeano, Y. D. (2002). Drillstring Vibration and Wellbore Instability. *J. Energy Resour. Technol. , 124*(4), 217-222.

Puebla, H., & Alvarez-Ramirez, J. (2008). Suppression of stick-slip in drillstrings: A control approach based on modeling error compensation. *Journal of Sound and Vibration, 310*(4-5), 881-901.

Raymond, D. W., Elsayed, M. A., Polsky, Y., & Kuszmaul, S. S. (2008). Laboratory Simulation of Drill Bit Dynamics Using a Model-Based Servohydraulic Controller. *J. Energy Resour. Technol., 130*(4), 043103 (12 pages).

Real , F., Lobo, D., Ritto, T., & Pinto, F. A. (2018). Experimental analysis of stick-slip in drilling dynamics in a laboratory test-rig. *Journal of Petroleum Science and Engineering, 170*, 755-762.

Reckmann, H., Jogi, P., Kpetehoto, F., Chandrasekaran, S., & Macpherson, J. (2010). MWD failure rates due to drilling dynamics. *IADC/SPE Drilling Conference and Exhibition.* New Orleans, Louisiana, USA.

Rector , J., & Marion, B. (1991). The use of drill-bit energy as a downhole seismic source. *Geophysics*, 598-730.

Riane, R., Doghmane, M. Z., Kidouche, M., & Djezzar, S. (2022a). Observer-Based H∞ Controller Design for High Frequency Stick-Slip Vibrations Mitigation in Drill-String of Rotary Drilling Systems. *Vibration, 5*(2), 264-289.

Riane, R., Doghmane, M. Z., Kidouche, M., Tee, K. F., & Djezzar, S. (2022b). Stick-Slip Vibration Suppression in Drill String Using Observer-Based LQG Controller. *Sensors, 22*(16), 5979.

Rivas, M. A., Ramirez, A. A., Al-Zahrani, B. S., & Abouelnaaj, K. K. (2021). Mitigating Twist-Offs While Drilling with the Help of BHA Dynamics Software. *SPE/IADC Middle East Drilling Technology Conference and Exhibition.* Abu Dhabi, UAE.

Robnett, E., Hood, J., Heisig, G., & Macpherson, J. (1999). Analysis of the Stick-Slip Phenomenon Using Downhole Drillstring Rotation Data. *SPE/IADC Drilling Conference.* Amsterdam: SPE.

Rudat, J., & Dashevskiy, D. (2011). Development of an Innovative Model-Based Stick/Slip Control System. *SPE/IADC Drilling Conference and Exhibition.* Amsterdam, The Netherlands: SPE.

Sagert, C., Di Meglio, F., Krstic, M., & Rouchon, P. (2013). Backstepping and flatness approaches for stabilization of the stick-slip phenomenon for drilling. *IFAC Proceedings Volumes, 46*(2), 779-784.

Saldivar, B., Boussaada, I., Mounier, H., Mondié, S., & Niculescu, S. I. (2014). An Overview on the Modeling of Oilwell Drilling Vibrations. *IFAC Proceedings Volumes, 47*(3), 5169-5174.

Saldivar, B., Mondié, S., Niculescu, S. I., Mounier, H., & Boussaada, I. (2016). A control oriented guided tour in oilwell drilling vibration modeling. *Annual reviews in Control, 42*, 100--113.

Sananikone, P., Kamoshima, O., & White, D. (1992). A Field Method for Controlling Drillstring Torsional Vibrations. *IADC/SPE Drilling Conference.* New Orleans, Louisiana: SPE.

Serrarens, A., van de Molengraft, M., Kok , J., & van den Steen, L. (1998). H∞ control for suppressing stick-slip in oil well drillstrings. *IEEE Control Systems Magazine*, 19-30.

Sharma, A., Srivastava, S., & Teodoriu, C. (2020). Experimental Design, Instrumentation, and Testing of a Laboratory-Scale Test Rig for Torsional Vibrations—The Next Generation. *Energies, 13*(18), 4750.

Sharma, A., Srivastava, S., Teodoriu , C., & Stan, M. (2021). Experimental Comparison of PID Based RPM Control for Long Horizontal vs. Vertical Drillstring. *Preprints* .

Shuttleworth, N., van Kerkoerle, E., Folmer, D., & Foekema, N. (1998). Revised Drilling Practices, VSS-MWD Tool Successfully Addresses Catastrophic Bit/Drillstring Vibrations. *IADC/SPE Drilling Conference.* Dallas, Texas: IADC/SPE.

Shyu, R.-J. (1989). Bending vibration of rotating drill strings. *Massachusetts Institute of Technology*.

Sotomayor, G. P., Placido, J. C., & Cunha, J. (1997). Drill string vibration: How to identify and suppress. *Latin American and Caribbean Petroleum Engineering Conference.* OnePetro.

Srivastava, S., & Teodoriu, C. (2019). An extensive review of laboratory scaled experimental setups for studying drill string vibrations and the way forward. *Journal of petroleum Science and Engineering, 182*, 106272.

Srivastava, S., Sharma, A., & Teodoriu, C. (2023). Optimizing Sampling Frequency of Surface and Downhole Measurements for Efficient Stick-Slip Vibration Detection. *Petroleum,*.

Sugiura, J., & Jones, S. (2019). A Drill Bit and a Drilling Motor With Embedded High-Frequency (1600 Hz) Drilling Dynamics Sensors Provide New Insights Into Challenging Downhole Drilling Conditions. *SPE Drilling & Completion, 34*(3), 223-247.

Tang, L., Guo, B., Zhu, X., Shi , C., & Zhou, Y. (2020). Stick–slip vibrations in oil well drillstring: A review. *Journal of Low Frequency Noise, Vibration and Active Control, 39*(4), 885-907.

Tian, J., Wei, L., Yang, L., Dai, L., Zhang, T., & Liu, H. (2020b). Research and experimental analysis of drill string dynamics characteristics and stick-slip reduction mechanism. *Journal of Mechanical Science and Technology, 3*(34), 977-986.

Tian, J., Zhou, Y., Yang, L., & Hu, S. (2020a). Analysis of stick-slip reduction. *Journal of Multi-Body Dynamics, 1*(234), 82-94.

Tucker, R. W., & Wang, C. (1999). On the Effective Control of Torsional Vibrations in Drilling Systems. *Journal of Sound and Vibration, 224*(1), 101-122.

Ullah, F. K., & Bohn, C. (2018). Dynamic Surface Control for the Reduction of Torsional Vibrations in a Scaled Experimental Drillstring Setup. *2018 UKACC 12th International Conference on Control (CONTROL).* Sheffield, UK.

Vaziri, V., Kapitaniak, M., & Wiercigroch, M. (2018). Suppression of drill-string stick–slip vibration by sliding mode control: Numerical and experimental studies. *European Journal of Applied Mathematics,* 805-825.

Vaziri, V., Oladunjoye, I., Kapitaniak, M., Aphale, S., & Wiercigroch , M. (2020). Parametric analysis of a sliding-mode controller to suppress drill-string stick-slip vibration. *Meccanica*, 2475–2492.

Vogel, S., & Creegan, A. (2016). Case Study for Real Time Stick/Slip Mitigation to Improve Drilling Performance. *SPE/IADC Middle East Drilling Technology Conference and Exhibition.* Abu Dhabi, UAE: OnePetro.

Vromen, T., Dai, C.-H., van de Wouw, N., Oomen, T., Astrid, P., Doris, A., & Nijmeijer, H. (2019). Mitigation of Torsional Vibrations in Drilling Systems: A Robust Control Approach. *IEEE Transactions on Control Systems Technology, 27*(1), 249-265.

Vromen, T., Dai, C.-H., van deWouw, N., Oomen, T., Astrid, P., & Nijmeijer, H. (2015). Robust output-feedback control to eliminate stick-slip oscillations in drill-string systems. *IFAC-PapersOnLine, 48*(6), 266-271.

Vromen, T., van de Wouw, N., Doris, A., Astrid, P., & Nijmeijer, H. (2014). Observer-based output-feedback control to eliminate torsional drill-string vibrations. *53rd IEEE Conference on Decision and Control* (pp. 872-877). Los Angeles, CA, USA: IEEE.

Wang, R.-h., Zang, Y.-b., Zhang, R., Bu, Y.-h., & Li, H.-z. (2011). Drillstring failure analysis and its prevention in northeast Sichuan, China. *Engineering Failure Analysis, 18*(4), 1233-1241.

Wen, X., Guan, Z., Zhou, Y., & Zhang, B. (2018). Experimental Research on Lateral Vibration of Drill String in the Highly Deviated Well. *Offshore Technology Conference Asia.* Kuala Lumpur, Malaysia.

Westermann, H., Gorelik, I., Rudat, J., Moritz, C., Neubauer, M., Wallaschek, J., & Höhn, O. (2015). A New Test Rig for Experimental Studies of Drillstring Vibrations. *SPE Drill & Compl, 30*(2).

Wu, S. X., Paez, L., Partin, U., & Agnihotri, M. (2010). Decoupling Stick-Slip and Whirl to Achieve Breakthrough in Drilling Performance. *IADC/SPE Drilling Conference and Exhibition.* New Orleans, Louisiana, USA.

Yigit, A., & Christoforou, A. (1996). Coupled axial and transverse vibrations of oilwell drillstrings. *Journal of Sound and Vibration*, 617-627.

Yigit, A., & Christoforou, A. (2000). Coupled torsional and bending vibrations of actively controlled drillstrings. *Journal of Sound and Vibration*, 67-83.

Yigit, A., & Christoforou, A. (2006). Stick-Slip and Bit-Bounce Interaction in Oil-Well Drillstrings. *J. Energy Resour. Technol.*, 268-274.

Zamanian, M., Khadem, S., & Ghazavi, M. (2007). Stick-slip oscillations of drag bits by considering damping of drilling mud and active damping system. *Journal of Petroleum Science and Engineering*, 289-299.

Zarate-Losoya, E., Cunningham, T., El-Sayed, I., Noynaert, S., & Florence, F. (2018). Lab-Scale Drilling Rig Autonomously Mitigates Downhole Dysfunctions and Geohazards Through Bit Design, Control System and Machine Learning. *IADC/SPE Drilling Conference and Exhibition.* Fort Worth, Texas, USA.

Zhang, Q., & Xv, S. (2019). Stick-Slip Vibration Suppression of Drill String Based on Fractional Order PID. *International Conference on Computer Network, Electronic and Automation (ICCNEA)* (pp. 468-473). Xi'an, China: IEEE.

Zou, C., Yang, Z., Zhamg, G., Hou, L., Zhu, R., Tao, S., . . . Wu, N. (2014). Conventional and unconventional petroleum “orderly accumulation”: Concept and practical significance. *Petroleum Exploration and Development*, 14-30.

## Nomenclature

| | |
|---|---|
| NPT | Non-Productive Time |
| WOB | Weight-on-bit |
| BHA | Bottom hole assembly |
| RPM | Revolutions per minute |
| HFTO | High frequency torsional oscillation |
| V&S | Vibration and shocks |
| EDC | Equivalent circulation density |
| PDC | Polycrystalline diamond compact |
| TDS | Top drive systems |
| BOP | Blowout preventers |
| DOF | Degrees-of-freedom |
| MWD | Measure while drilling |
| LQR | Linear quadratic regulator |
| RLS | Recursive least squares |
| PDE | Partial differential equations |
| LMI | Linear matrix inequality |
| FEM | Finite element method |
| LTI | Linear time invariant |
| FOPID | Fractional order PID |
| LPV | Linear parameter varying |
| MICR | Modified integral resonant controller |
| VFD | Variable frequency drive |

| | |
|---|---|
| HIL | Hardware in loop |
| LQG | Linear quadratic Gaussian |
| IT2FC | Interval type-2 fuzzy logic controller |
| PSO | Particle swarm optimization |

# Appendix A: Calibrations and Tuning

## A.1 Open-loop controller Calibration

Experimental calibration of the open-loop RPM control system was carried out to find a relationship between the input voltage and RPM. The results of this calibration are shown in table A-1 and the corresponding plot is shown in figure A-1. The equation for the relationship between voltage and RPM is:

$$y = 107.14x - 11.19 \quad \ldots\ldots\ldots\ldots\ldots\ldots (A.1)$$

**Table A-1. Open-loop RPM control calibration**

| Voltage (V) | RPM |
|---|---|
| 0 | 0 |
| 1 | 90 |
| 2 | 195 |
| 3 | 305 |
| 4 | 420 |
| 5 | 530 |

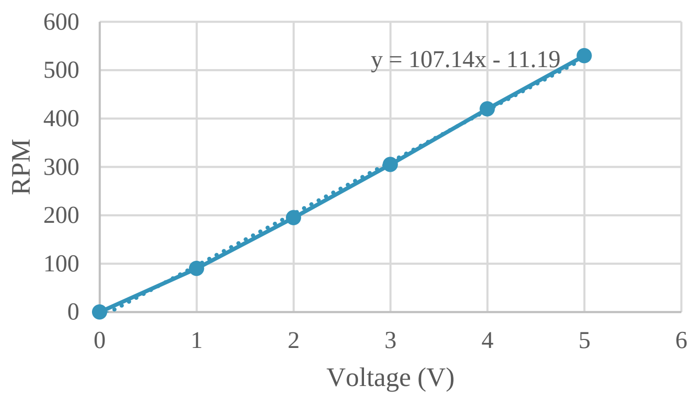


**Figure A-1. Voltage vs RPM plot**

## A.2 Feedback RPM Controller Tuning

LabVIEW PID toolset was used to design the PID control. It calculates the error i.e., the difference between the RPM setpoint and the RPM feedback and generates a control signal which is a 0-5V voltage signal from one of the analog outputs on the cDAQ data acquisition device. The control signal is fed to a motor driver, which takes in the 0-5V signal and produces a 0-18V output which is the driving voltage range for the DC motor.

To tune the PID controller, Ziegler-Nichols method and, trial-and-error method were used. Firstly, Ziegler-Nichols method was used to calculate the PID variables. Table A-2 shows the variables derived for a PI and a PID controller using this method. The controller response, as shown in figures x and y, was very oscillatory and had high overshoots. Figures A-2 shows the PID and PI response.

**Table A-2. PID variables calculated using Ziegler-Nichols method**

| Controller | $K_p$ | $T_i$ (min) | $T_d$ (min) |
|---|---|---|---|
| PI | 0.036 | 0.022222 | 0 |
| PID | 0.048 | 0.013333 | 0.003333 |

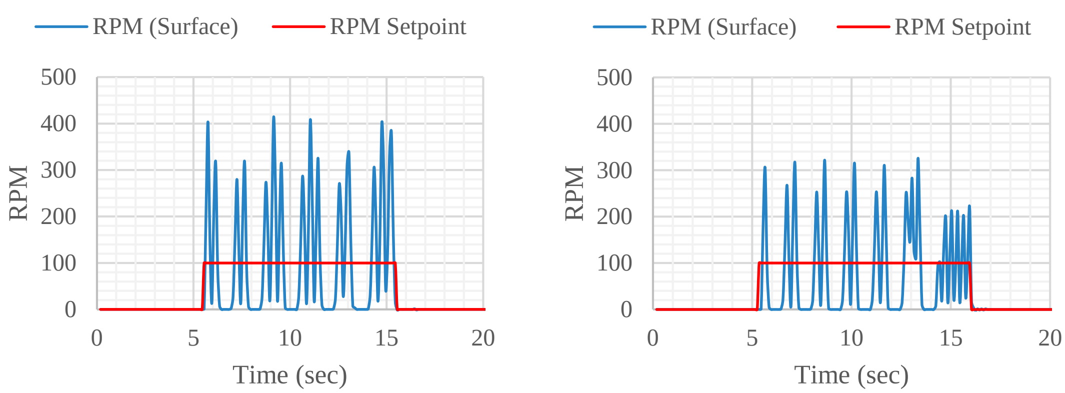


**Figure A-2. Response of the PI controller (left) and PID controller (right) derived using Ziegler-Nichols method**

Since the response of the controllers derived using Ziegler-Nichols method was not satisfactory, trial-and-error method was used. To tune a PID with using the trial-and-error method the first step is to set the proportional gain to a small value and the other two gains to zero.

The value of the proportional gain can then be increased until an acceptable response time is achieved. At this point there are oscillations in the system which can be reduced by setting integral gain. Again, a small value can be chosen to start with and then it can be increased to reduce the oscillations. Now if there is an overshoot in the system it can be fixed by using the derivative gain which can be set by using a similar approach. It must be mentioned here that the derivative gain must be kept very low or even avoided altogether if not needed. This is because the derivative gain is very sensitive to noise and can make the system unstable.

To tune the PID controller using the trial-and-error method, and get the desired response time, a little over 100 experimental tests with different values of the PID coefficients were conducted. PID response for three different RPM changes (0 to 100, 0 to 150 and 0 to 200) was recorded and analyzed. Following are the plots generated from three of these experiments with different PID coefficients (RPM setpoint is in red and surface RPM is in blue):

- $K_p$= 0.010, $T_i$= 0.006, $T_d$= 0.010

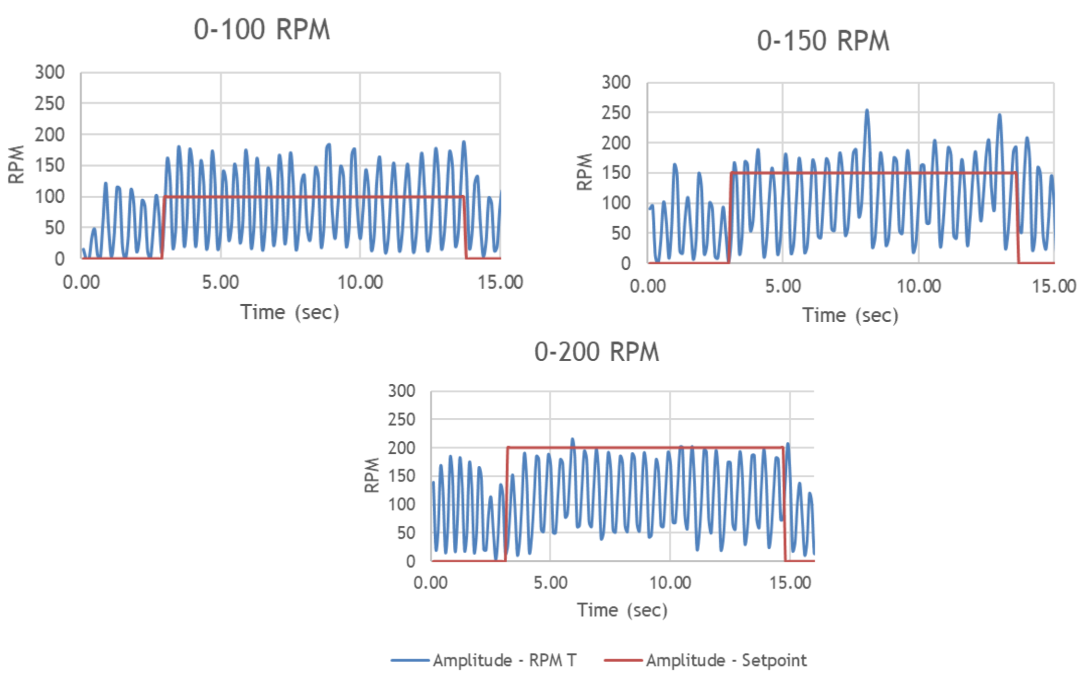


**Figure A-3. Tests at $K_p$= 0.010, $T_i$= 0.006, $T_d$= 0.010**

- $K_p$= 0.010, $T_i$= 0.003, $T_d$= 0.000

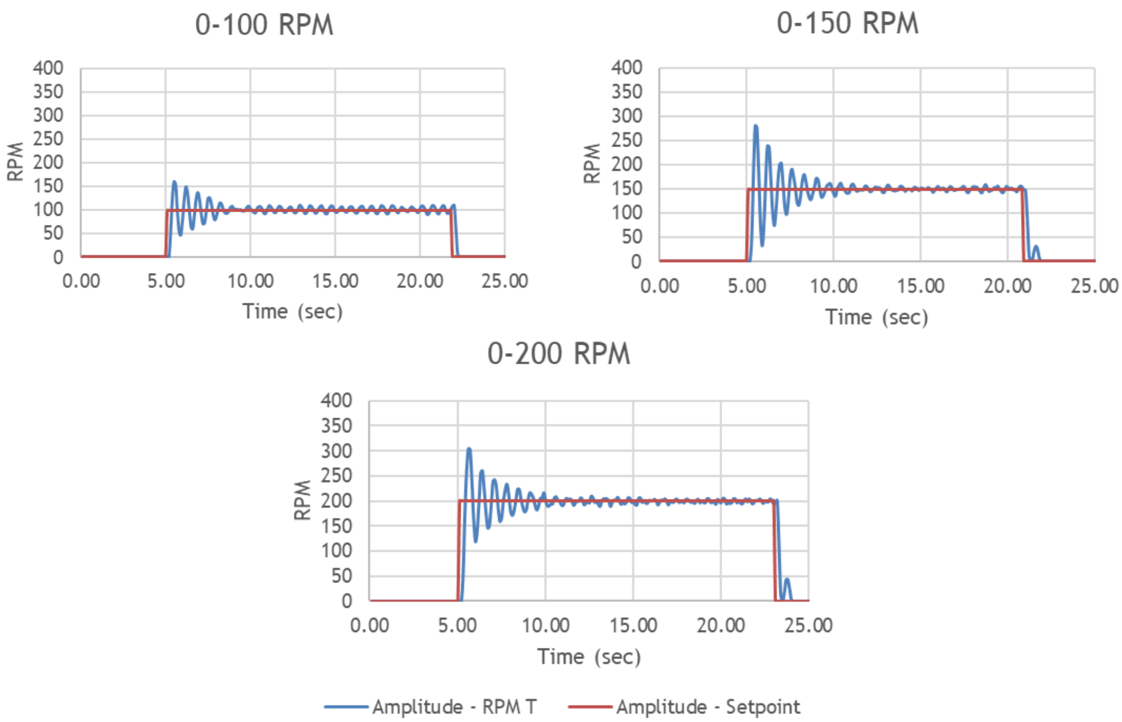


**Figure A-4. Tests at $K_p$= 0.010, $T_i$= 0.003, $T_d$= 0.000**

- $K_p$= 0.005, $T_i$= 0.003, $T_d$= 0.000

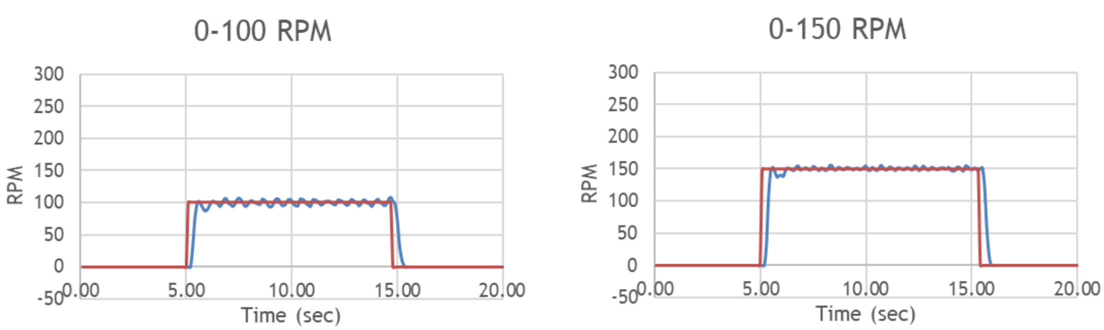

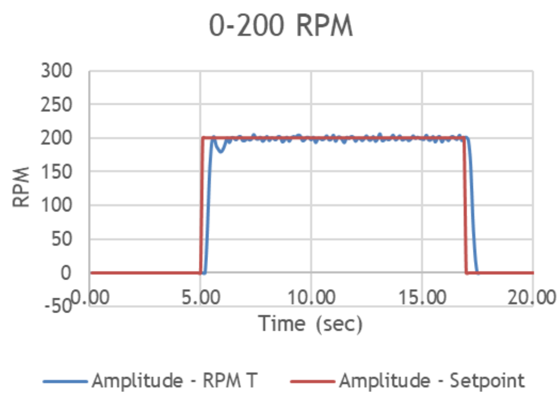


**Figure A-5. Tests at $K_p$= 0.005, $T_i$= 0.003, $T_d$= 0.000**

In case 1, ($K_p$= 0.010, $T_i$= 0.006, $T_d$= 0.010) excessive oscillations can be observed and the system is not stable. For case 2, ($K_p$= 0.010, $T_i$= 0.003, $T_d$= 0.000) an improved response can be observed, the RPM does stabilize but with big oscillations initially. The response time recorded for this set of PID variables was 5 second, which was slow. Finally, case 3 ($K_p$= 0.005, $T_i$= 0.003, $T_d$= 0.000) shows a much-improved response with minimal oscillations and a response time of under 0.5 second. These tests were conducted on the vertical setup. Similar tuning approach was applied on the directional setup and the PID variables when set to $K_p$= 0.004, $T_i$= 0.002, $T_d$= 0.001, provided a good controller response. A detailed discussion can be found in (Sharma, et al., 2021).

## Appendix B: LabVIEW Code

Screenshots of different parts of the LabVIEW code developed for the setup have been shown in this section.

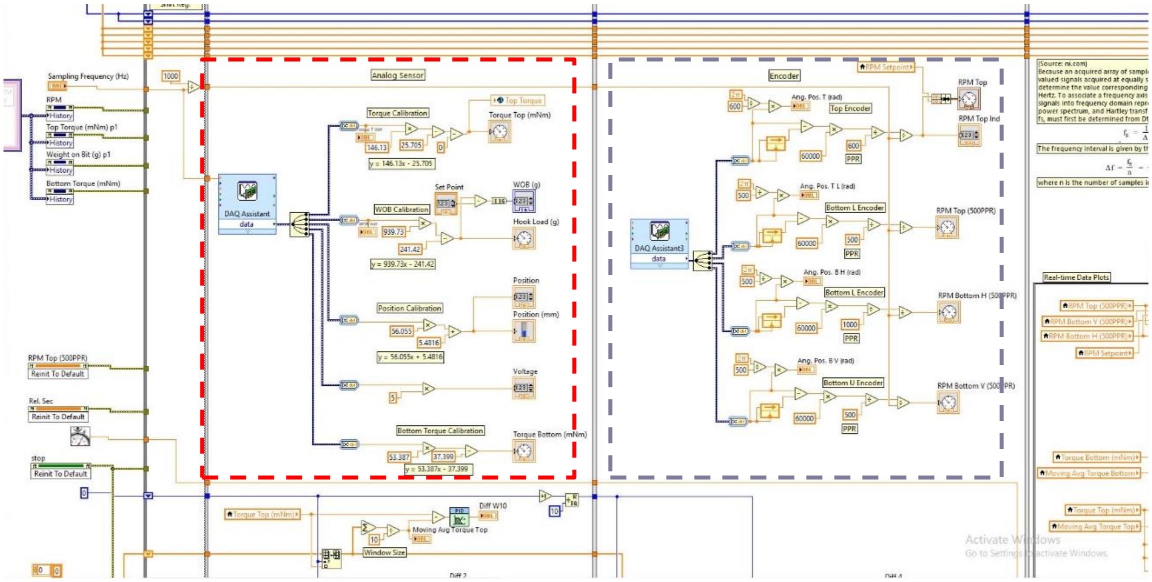


**Figure B-1. Analog (in red) and digital (in blue) data acquisition and calibration block diagram code**

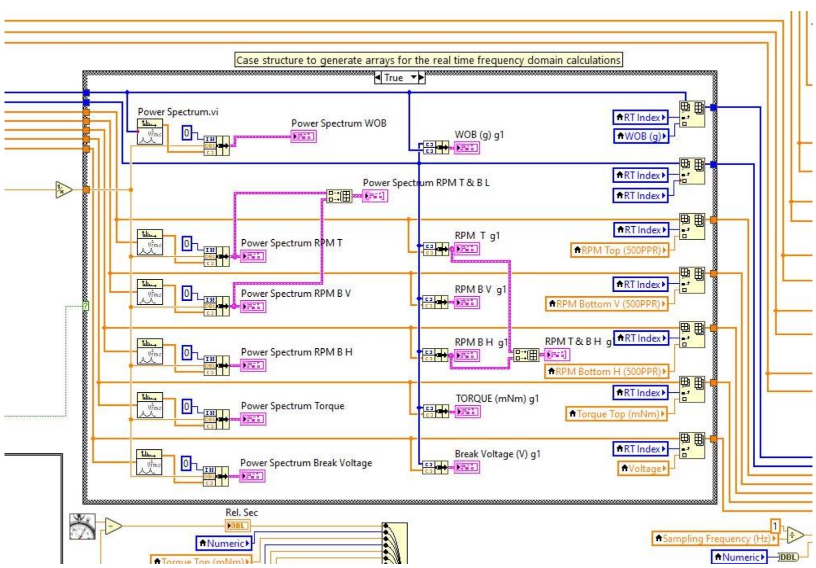


**Figure B-2. Code to generate power spectrum (for set time window)**

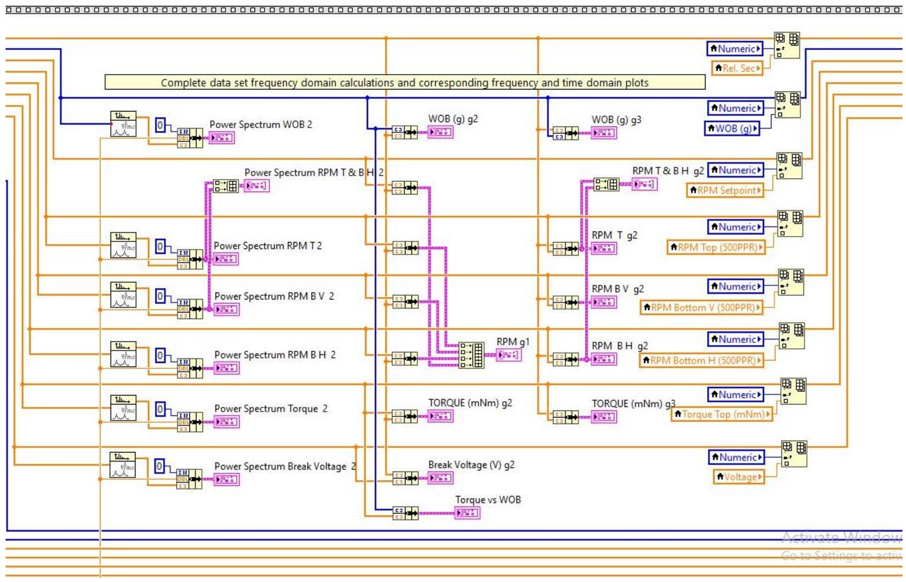


**Figure B-3. Code to generate power spectrum (for complete experimental test)**

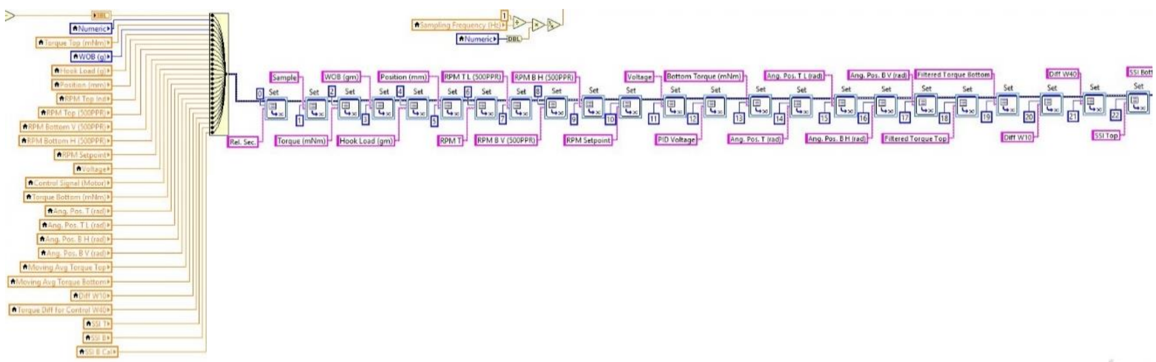

**Figure B-4. Code to save experimental data**

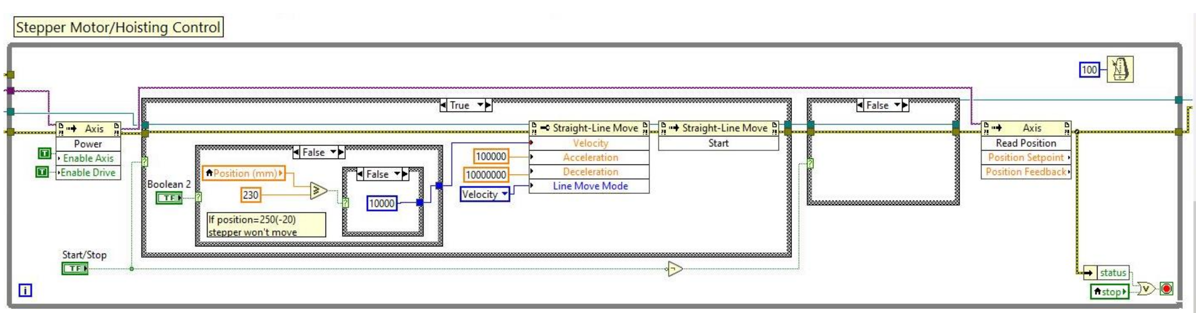


**Figure B-5. Hoisting system control loop**

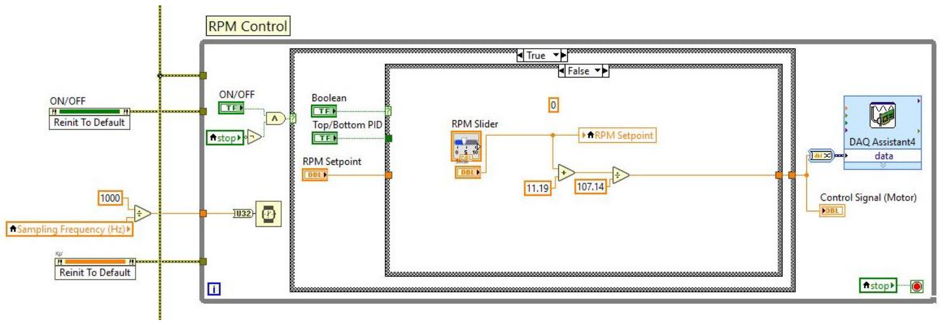


**Figure B-6. Open-loop RPM control loop**

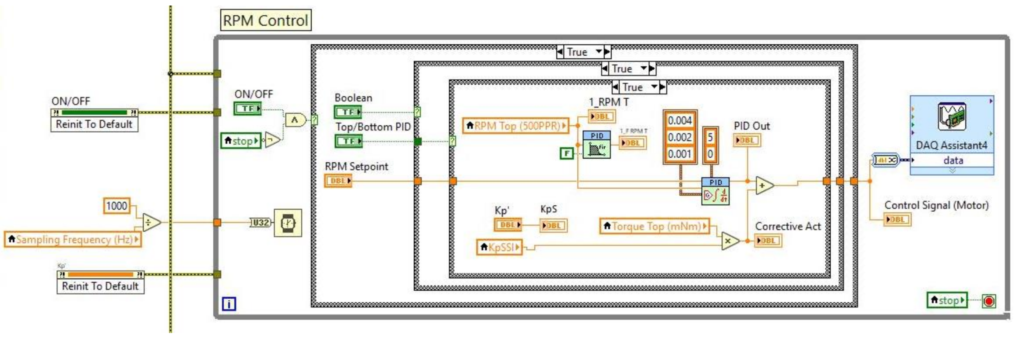


**Figure B-7. Feedback RPM control loop**

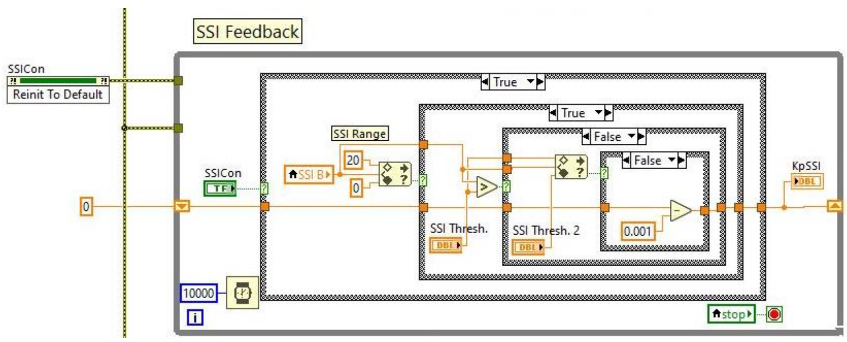


**Figure B-8. SSI feedback loop**